PROPAGATION OF PLANE ACOUSTIC NOISE OF FINITE AMPLITUDE

Frederick M. Pestorius

APPLIED RESEARCH LABORATORIES
THE UNIVERSITY OF TEXAS AT AUSTIN

ARL-TR-73-23
August 1973

Copy No.

PROPAGATION OF PLANE ACOUSTIC NOISE OF FINITE AMPLITUDE

Frederick M. Pestorius

AFOSR F44620-71-C-0015
ONR N00014-70-A-0166, Task 0004

ARL-TR-73-23
August 1973

PROPAGATION OF PLANE ACOUSTIC NOISE OF FINITE AMPLITUDE

Frederick M. Pestorius

Office of Naval Research
Contract N00014-70-A-0166 NR 386-503
Air Force Office of Scientific Research
Contract F44620-71-C-0015

APPLIED RESEARCH LABORATORIES
THE UNIVERSITY OF TEXAS AT AUSTIN
AUSTIN, TEXAS 78712

FOREWORD

This technical report is an adaptation of the author's Ph.D. Dissertation. A student in Electrical Engineering at the University of Texas, Mr. Pestorius was directly supported by the Naval Postgraduate School, Monterey, California, through the Junior Line Officer Scientific Education Program (Burke Program).

The research described herein was carried out at the Applied Research Laboratories and was sponsored by the Air Force Office of Scientific Research under Contract F44620-71-C-0015, by the Office of Naval Research under Contract N00014-70-A-0166-0004, and the Naval Ship Systems Commander under Contract N00024-72-C-1380. Technical monitors were Capt. W. H. Smith for AFOSR, Mr. R. E. Faires for ONR, and Mr. J. E. Neely for NAVSHIPS.

David T. Blackstock

Supervisor

ACKNOWLEDGEMENTS

I wish to thank the many persons on the staff of the Applied Research Laboratories who have assisted me in this research. Mr. Steven L. Watkins assisted with a significant portion of the computer programming, and Messrs. Ward M. Widener and Robert K. Goodnow provided equipment and experimental know-how. Drs. Thomas G. Muir and James C. Lockwood and Messrs. James J. Truchard and Jack A. Shooter offered stimulating ideas and encouragement. Mr. Solon B. Williams ably assisted me in all phases of this work. I wish to thank Dr. David T. Blackstock, who initially suggested this research, and who provided the major continuing direction and support necessary for a work of this nature. I also wish to thank my wife Eileen McGee Pestorius for her invaluable assistance in reviewing the manuscript.

This work was supported by the Air Force Office of Scientific Research under Contract F44620-71-C-0015, the Office of Naval Research under Contract N00014-70-A-0166-0004 and Naval Ship Systems Command under Contract N00024-72-C-1380-0007. It also is a pleasure to acknowledge the support of the Naval Postgraduate School under the auspices of the Junior Line Officer Scientific Education Program (Burke Program).

This work is dedicated to the memory of Professor Frederick Vinton Hunt, who first interested me in the study of acoustics.

ABSTRACT

We investigate the propagation in air of plane finite-amplitude noise waves. The reported research is both theoretical and experimental, and the results obtained are valid both before and after shock formation. In the theoretical portion of the work, a new model called modified weak-shock theory is discussed. In this model the effects of ordinary weak-shock theory and Kirchhoff tube wall attenuation and dispersion are combined. The inclusion of tube wall effects is necessary because the experimental work is done in a pipe. The modified weak-shock theory is implemented in a computer algorithm.

Our theoretical model is novel in that it is applicable both before and after shock formation, it contains the effects of nonlinear distortion as well as tube wall attenuation and dispersion, and it is applicable for input waveforms of arbitrary shape. Previous theories do not include all of these features.

We use a plane wave tube in our experiments. The tube is 96 ft long, has a circular cross section, and is terminated in such a way that the reflected wave is 40 dB lower in sound pressure level than the incident wave. The acoustic source is a 75 W horn driver that is mounted at one end of the pipe. The passband of this source is 700 Hz to 2200 Hz and it can generate a sound pressure level of 160 dB at the source. We use a microphone and an oscilloscope to observe the finite-amplitude wave as a function of distance.

In the developmental testing of this new model we investigate the propagation of sawtooth waves in a pipe. Asymmetric waveforms, reported by previous researchers, are observed and compared to predictions made using the new theory. We obtain excellent agreement between theory and experiment over the frequency range 500 to 3500 Hz and the sound pressure level range 142 to 160 dB re 0.0002 μbar.

We then investigate high intensity (155 to 160 dB) noise pulses and we observe that they undergo significant distortion as a function of distance. In particular, the observed pulses simplify because the shock fronts merge and minor waveform irregularities are fed into the shocks. The waveform at the source is used as an input to the computer algorithm. Waveform predictions, obtained via the algorithm, are compared to the observed waveforms and excellent agreement is found.

Computed and observed noise spectra as a function of distance are then obtained. The spectra show significant shaping due to nonlinear effects. The spectra obtained at locations remote from the source are broader in frequency content than the source spectrum and in fact the remote spectra actually cross over the source spectrum. In this work we observe a high frequency crossover at about 5500 Hz and a low frequency crossover at about 350 Hz. Hence, we arrive at the very important conclusion that nonlinear propagation can cause a net gain in energy at frequencies above the high frequency crossover and below the low frequency crossover.

We conclude this work with a discussion of the physical effects that give rise to the observed nonlinear waveform changes and spectral

shaping. We also include a discussion of the role of dispersion in the propagation of finite-amplitude waves in pipes.

TABLE OF CONTENTS

TABLE OF CONTENTS (Cont'd)

TABLE OF CONTENTS (Cont'd)

TABLE OF CONTENTS (Cont'd)

LIST OF TABLES

LIST OF FIGURES

LIST OF FIGURES (Cont'd)

GLOSSARY OF IMPORTANT SYMBOLS

c_o small-signal sound speed

c sound speed

h specific enthaply

H_s sensitivity relative to 1 V/μbar

j $\sqrt{-1}$

k wavenumber $(=\omega/c_o)$

P absolute pressure. In the study of sawtooth waves P_2=P at the peak and P_1=P at the trough

P_o absolute pressure at x=0

Pr Prandtl number

R pipe internal radius

S the curve described by $d(1/\delta)/d(x/\lambda)$

s specific entropy

$\hat{s}$ Riemann invariant for incoming waves in a compound wave field

t time

t' retarded time, $(=t-x/c_o)$

u particle velocity

u_o peak particle velocity at x=0

$\bar{V}$ shock velocity $\left[= c_o + \frac{\beta}{2}(u_2+u_1)\right]$

x distance

$\bar{x}$ shock formation distance

α attenuation coefficient $\left[= \frac{1}{R}\sqrt{\frac{\nu\omega}{2c_o^2}}\left(1 + \frac{\gamma-1}{\sqrt{Pr}}\right)\right]$

α_o fundamental frequency value of α

β $\frac{\gamma+1}{2}$ in air; $1 + \frac{\beta}{2A}$ in a liquid, where B and A are constants that depend upon the liquid being considered

γ ratio of specific heats

δ dimensionless pressure used in the study of sawtooth waves, $\left(= \frac{P_2 - P_1}{P_1} \right)$

δ_o value of δ at $x=0$

Δ boundary layer thickness $[= 2.2838 \, (2\nu/\omega)^{1/2}]$

ϵ the acoustic Mach number $(=u_o/c_o)$

λ wavelength

ν kinematic viscosity

ρ density

σ a dimensionless distance $(=\beta\epsilon kx)$

φ a parameter used to indicate the time that a wavelet left the origin

ω angular frequency

CHAPTER 1 INTRODUCTION

The general subject of this dissertation is the propagation of plane, finite-amplitude sound waves of arbitrary waveform. We are especially interested in finite-amplitude noise. Our approach to the subject matter is both experimental and theoretical, and the results obtained are valid both before and after shock formation.

We restrict our attention to plane waves, even though most practical problems involve nonplanar waves. The rationale behind the plane wave restriction is quite simple. We wish to check experimentally our theoretical results and plane waves are easily generated in a tube. A secondary benefit is a simplification of the mathematical analysis. The problem solution technique that we use is implemented in a computer algorithm that utilizes existing theoretical results.

Examples of high intensity sound occur in many industrial and military situations. Ribner (1969) states that a Saturn V rocket radiates 0.2 billion acoustic watts and generates a sound pressure level of 110 dB* ten miles from the launch site. Webster (1971) reports sound pressure levels as high as 140 to 150 dB measured on the flight deck of an aircraft carrier 50 ft from a jet airplane. In both of these examples the noise source is broadband in frequency content.

The preceding examples are examples of high intensity sound, but are they examples of the type of sound to be considered in this work? To answer this question, we must carefully define what we mean

*Throughout this work, sound pressure levels are referred to 0.0002 microbar.

when we use the term finite-amplitude distortion. The equations that describe the propagation of sound are nonlinear and, in general, cannot be solved. If the magnitude of the nonlinear terms in the equations is small, however, the equations can be linearized and solved. The applicability of linear theory is amply illustrated by the fact that the use of linear theory gives adequate results for the vast majority of acoustic problems. We are, however, interested in acoustic problems that require the retention of the nonlinear terms. We further restrict our interest to those problems wherein the main effect of nonlinearity is a cumulative distortion of the waveform. To be sure, there are important problems in which the primary nonlinear effects are local rather than cumulative; but in the wave propagation problems we shall consider, noncumulative nonlinear effects are minor in comparison to the cumulative ones. Henceforth in this dissertation the term finite-amplitude distortion should be considered synonymous with the term cumulative distortion. Now, before we can consider the question posed at the beginning of this paragraph, we must identify the factors that affect finite-amplitude distortion.

The magnitude of finite-amplitude distortion depends on three factors: the frequency (or frequencies) of the disturbance, the local amplitude of the disturbance, and the propagation distance of interest. The sound wave is distorted over each wavelength propagated and the total amount of distortion is the sum of the distortion that occurs in each wavelength (whence the term "cumulative" used above). Without going into detail, inappropriate in an introductory chapter, we cannot say with certainty whether the sound waves in the examples discussed

earlier will exhibit appreciable finite-amplitude distortion. We can, however, state that the two examples appear to be very strong candidates for examples of the type of sound wave in which we are interested.

The specific objective of this research then is to investigate the propagation of plane, finite-amplitude noise. The noise waveforms of interest are broadband in frequency content and intense enough that the first shocks in the wave develop within a short distance from the noise source. In support of this objective we develop a computer algorithm that can be used to predict the distortion of a wave whose waveform at the source is arbitrary. In this algorithm we calculate, via weak-shock theory, the distortion suffered by a wave in nonlinearly propagating a short distance. The distorted wave is then corrected for tube wall attenuation and dispersion and another short distortion step is taken. The waveform for any value of propagation distance may be computed in this fashion. Predictions obtained by use of the algorithm are then compared to experimental measurements made using a plane wave tube.

CHAPTER 2 REVIEW OF THE LITERATURE

1. Introduction

In this chapter we have two specific objectives. The first is to review the development of the theoretical ideas that provide the basic underpinning for the computer methods we shall develop. The second objective is to briefly consider the results of other researchers who have worked on problems similar to those considered here and, where applicable, to comment on how their ideas have helped to shape and influence our own.

2. Background of the Basic Theory

We call the analytic method that is developed in this dissertation modified weak-shock theory. In this theory three factors are combined to form a formal method for considering the propagation of a finite-amplitude sound wave in a tube. These factors are as follows:

a. The distortion of a continuous sound wave due to nonlinear effects. The formal method that we shall use to calculate this distortion is called the Earnshaw (1860) solution.

b. Once the sound wave is no longer continuous (i.e., shocks form) the Earnshaw solution must be supplemented by a relation that describes the shock motion. The combination of the Earnshaw solution with the shock motion relation is called weak-shock theory.

c. Since our experimental work will be done using a plane wave tube, it is necessary to account for the effects of

attenuation and dispersion due to the tube wall boundary layer. We shall modify weak-shock theory in an iterative fashion to account for the tube wall effects.

Each of these factors will now be briefly described.

a) The Earnshaw Solution

Poisson (1808) derived the classic result for plane sound waves of finite amplitude,

$$\psi_x = f[x \mp (a \pm \psi_x)t] \quad , \tag{2-1}$$

where

ψ = the velocity potential,

ψ_x = the derivative of ψ with respect to distance x,

t = time, and

a = the speed of sound in a process that obeys Boyle's law.

In Eq. (2-1) the upper signs apply to outgoing waves, the lower signs to incoming waves. As Blackstock (1969) points out, Poisson missed the importance of his result. Poisson recognized that the propagation velocity dx/dt, which is obtained from Eq. (2-1), depends upon ψ_x. But because such a result had never been observed experimentally, he concluded, "... that the original disturbance is transmitted uniformly and with a speed equal to a ...." We now recognize that most acoustic wave propagation is isentropic and that a is properly replaced by c, where

$$c^2 \equiv \left.\frac{\partial P}{\partial \rho}\right)_s \tag{2-2}$$

and

P = absolute pressure,

ρ = density, and

s = entropy.

Thus the more general form of "Poisson's solution" is Eq. (2-1) with a replaced by c.

We shall be concerned here with simple, or unidirectional, waves. For a simple wave in air the relation between the local sound speed c and the particle velocity u is [see, for example, Courant and Friedrichs (1948)]

$$c = c_o \pm 1/2\ (\gamma-1)u \quad , \tag{2-3}$$

where

c_o = the small-signal sound speed, and

γ = ratio of specific heats.

In Eq. (2-3) the upper signs are used when considering outgoing waves and the lower signs when considering incoming waves. Substituting Eq. (2-3) into Eq. (2-1) and recognizing that $\psi_x=u$, we obtain the propagation velocity

$$\left.\frac{dx}{dt}\right)_{u=\text{const}} = \beta u \pm c_o \quad , \tag{2-4}$$

where $\beta=(\gamma+1)/2$ for gases. Equations (2-3) and (2-4) may be generalized to apply to liquids by using the relation

$$\beta = 1 + B/2A \quad , \tag{2-5}$$

where B and A are constants that depend upon the liquid being considered [see, for example, Beyer (1960)]. The dependence of the propagation velocity upon the particle velocity, as described by use of Eq. (2-4), is the basic physical phenomenon causing the cumulative distortion discussed in Chapter 1. A much more complete discussion of Eq. (2-4) appears in Chapter 3.

Earnshaw (1860) considered the problem of the lossless propagation of a plane wave in a tube. He was aware of the variable propagation velocity implicit in Poisson's result. Earnshaw's solution, which we postpone giving until Chapter 3, relates the shape of any continuous wave at some field point (x,t) to the shape of that wave at the source. Hence, the Earnshaw result can be used to describe the progressive distortion of a simple plane sound wave.

b) Weak-Shock Theory

The Earnshaw solution provides an adequate method for calculating distortion so long as the sound wave remains continuous. In general, however, the Earnshaw solution leads to multivalued waveforms. Multivaluedness signals the presence of shocks in the waveform.

An analytic method called weak-shock theory, which is basically an extension of the Earnshaw solution, enables one to proceed with the calculation of waveform distortion when shocks are present, provided the shocks are not strong. By use of the Rankine-Hugoniot shock relations, we obtain an equation that describes the velocity of the shock front in a simple wave. The propagation velocity and attendant distortion in the remainder of the wave is calculated using the Earnshaw relation.

Several researchers contributed to the development of weak-shock theory; foremost among them were Landau (1945), Friedrichs (1948), and Whitham (1952 and 1956). Blackstock (1966) stated the theory in the form used here. The adjective "weak" refers to simplifying assumptions concerning the shock amplitude made in the theoretical development.

c) Tube Wall Effects

The experimental observations reported here were made using a plane wave tube. As we shall see later, attenuation and dispersion caused by the presence of the tube wall boundary layer are significant effects and must be considered in our calculations. The only attenuative effect that is accounted for in weak-shock theory is dissipation at the shock. We shall calculate attenuation and dispersion in the remaining portions of the wave using the classical theory first derived by Kirchhoff (1868). The Kirchhoff theory is a "small-signal" theory. Nonetheless, it can be combined with weak-shock theory to form what we shall call modified weak-shock theory.

3. The Contributions of Other Researchers

In this section the results of other researchers who have worked on problems similar to the subject of this study are briefly reviewed. The emphasis in this review is on the relation that these other studies have to our own. The section is organized by subjects as follows:

a. General studies of finite-amplitude propagation in rigid tubes.

b. Attenuation of sawtooth waves in a tube.

c. Computational schemes.

d. Propagation of finite-amplitude noise.

e. The "Burgers Turbulence" model.

a) General Studies of Finite-Amplitude Propagation in Tubes

The problem of propagation in tubes has attracted the attention of a number of previous researchers. We shall discuss in chronological order those research efforts which we consider to be the most significant.

Nearly 40 years ago Thuras, Jenkins, and O'Neil (1935) investigated the propagation of an initially sinusoidal tone in a pipe. The amplitude and frequency of the tone were such that only the planar mode was excited and shocks did not form in the pipe. Using a lossless wave equation in Lagrangian coordinates, Thuras et al. found ordinary differential equations for the change in amplitude of the second and third harmonics of the fundamental as a function of distance from the source. The differential equation for the second harmonic was then corrected for the attenuative effect (but not the dispersive effect) of the tube wall boundary layer by postulating that both the fundamental and second harmonic decrease in amplitude at a rate proportional to the amount of that frequency component present. The differential equation proposed was

$$\frac{dP_2}{dx} = KP_o^2 e^{-2\alpha_1 x} - \alpha_2 P_2 \quad , \qquad (2\text{-}6)$$

where

P_2 = the second harmonic pressure amplitude,

P_o = the fundamental pressure amplitude at x=0,

α_1 and α_2 = attenuation coefficients at the fundamental and second harmonic frequencies respectively, and

K = a constant.

Predictions obtained using Eq. (2-6) were compared with experimentally observed second harmonic levels. For the propagation distances considered, the second harmonic grew linearly with distance. Agreement between theory and experiment was good with the exception of a constant 3 dB discrepancy. Geertsen (1951), Blackstock (1962b), and Cruikshank (1966) reported similar experiments in which good agreement between theory and experiment was found. It seems likely that the "missing 3 dB" of Thuras, Jenkins, and O'Neil was a calibration error.

Using a perturbation analysis, Blackstock (1962b) demonstrated that dispersion as well as attenuation should be included in the analysis of the second harmonic. Although predictions obtained from his expression agreed well with his experimental data, the effect of dispersion was quite small for the conditions of his experiment.

Burns (1966a)* continued Blackstock's perturbation analysis, greatly expanding its scope. He calculated the change with distance of the fundamental through the fourth harmonic. His theoretical results include the effects of nonlinear distortion as well as tube wall attenuation and dispersion but are limited to propagation distances that preclude shock formation. Unfortunately, however, assumptions made to simplify the analysis impose a further limitation on the propagation distance over which his theory can be used. A secondary result of these assumptions is to deemphasize the effect of dispersion on the various harmonic components. However, the effects of dispersion are small over the

*For a shorter and more accessible reference, see Burns (1966b).

limited distances that were considered. Hence, the deemphasis of the role of dispersion led to no significant errors. If much longer propagation distances were to be considered, however, Burns' treatment of dispersion would require modification. Burns conducted experiments meant to verify his theory. The propagation distances used in the experiments were limited to seven wavelengths, or distances less than the experimental shock-formation distance, whichever came first. These distances were far too short for dispersion to be significant. The agreement between theory and experiment is good within a few wavelengths of the source, but only fair at larger distances.

McKittrick, Blackstock, and Wright (1967) presented experimental results that clearly showed wave propagation phenomena that had not been previously reported. Oscillograms of shock waves formed by the nonlinear distortion of sinusoids showed rounded peaks and sharply angled troughs rather than the expected symmetric sawtooth shape. The authors showed that the asymmetry of the waveform was probably due to the influence of dispersion, caused by the tube wall boundary layer, on the propagating wave.

Pernet and Payne (1969)* also considered the problem of the propagation of finite-amplitude waves in pipes. The analytic method employed is very similar to that used by Thuras, Jenkins, and O'Neil.

---

*The 1969 report appears in a shorter but more accessible paper, Pernet and Payne (1971a). Unfortunately, the paper does not contain the discussion of dispersion and waveform asymmetry given in the 1969 report.

Formulae describing the change in amplitude as a function of distance for the fundamental through the seventh harmonic of an initially sinusoidal wave were derived. Results obtained from the formulae for the fundamental through fourth harmonic were experimentally verified by comparison with experimental results obtained using a source wave of moderate (i.e., no shock formation) intensity. We emphasize here that Pernet and Payne's analytic methods are only applicable for distances prior to shock formation.

Pernet and Payne mention that oscillograms of high intensity waves (e.g., 160 dB) show the type of asymmetry described earlier. Like McKittrick et al. they conclude that dispersion is the cause of the asymmetry. Although they do not present any theory applicable to waves of high intensity they do present some experimental measurements. In Chapter 6 of the present work we make a comparison between their high intensity experimental data and predictions based on modified weak-shock theory. Excellent agreement is obtained. Incidentally, Burns' theory does not agree with Pernet and Payne's experimental results, nor should it, since the propagation distances considered by Pernet and Payne far exceed the distance limits built into Burns' theory.

An entirely different approach from those presented above has been proposed by Blackstock (1972). In this work the author argues that the proper wave equation describing the propagation of finite-amplitude waves in a pipe of circular cross section is

$$\frac{\partial u}{\partial x} - \beta c_o^{-2} u \frac{\partial u}{\partial t'} = \frac{1}{R}\sqrt{\frac{\nu}{\pi c_o^2}}\left[1 + \frac{\gamma - 1}{\sqrt{Pr}}\right]\int_o^\infty \frac{\partial u(x,t'-\lambda)}{\partial t'}\frac{d\lambda}{\sqrt{\lambda}} \quad , \tag{2-7}$$

where

ν = the kinematic viscosity,

R = the pipe internal radius,

Pr = the Prandtl number, and

$t' = t - x/c_o$, a retarded time.

The right side of Eq. (2-7) represents the effects of attenuation and dispersion caused by the boundary layer and the $u\,\partial u/\partial t'$ term represents the effects of nonlinear distortion. It is not clear at this time whether Eq. (2-7) could be used alone or whether use of the Rankine-Hugoniot relations would also be necessary. In either case, it appears that solving Eq. (2-7) would be an ideal way to approach the problem of finite-amplitude propagation in a pipe. However, the analytic solution of Eq. (2-7), even for very simple source functions, has not been found. An alternative approach would be a numerical solution of Eq. (2-7) obtained by means of a computer. This path has not been pursued either.

Coppens (1971) authored the last paper that we shall consider in this section. He started with the nonlinear one-dimensional wave equation developed by Coppens and Sanders (1968). Coppens' equation is different from Eq. (2-7) in form but similar in content. The equation is solved using both pertubation techniques and Fourier expansion. The latter method is amenable to computer implementation and provides the major portion of Coppens' analytic results. The work reported is purely theoretical and is limited to the region before shocks form. Coppens' computed waveforms clearly exhibit the asymmetry previously

reported by McKittrick et al. (1967) and Pernet and Payne (1969). Coppens attributes this asymmetry to the effects of dispersion.

The studies just reviewed are of value here for the theoretical and experimental background they provide, rather than for any specific method or technique. The exception to this statement is the apparent necessity of including the effects of dispersion in our analysis. The necessity might be regarded as questionable, since Thuras, Jenkins, and O'Neil (1935), Geersten (1951), and Pernet and Payne (1969) ignored dispersion and nonetheless got good agreement between theory and experiment. We shall include dispersion in our analysis, and in our concluding remarks in Chapter 7 indicate why dispersion is important in some analyses but may be ignored in others.

b) Attenuation of Sawtooth Waves in a Tube

A major portion of the study of finite-amplitude sound in pipes has been directed at the specific problem of the attenuation of sawtooth-shaped plane waves. The various theoretical analyses of this problem have concluded with predictions of the attenuation per wavelength propagated. In the several analyses that we shall review all of the authors took account of attenuation due to irreversible compression that the fluid medium experiences during the passage of a shock. Additionally all of the authors save two took account of attenuation due to the boundary layer. The dependent variable commonly used in studies of sawtooth wave decay is [see Rudnick (1952) or Medwin (1964)]

$$\delta \equiv \frac{P_2 - P_1}{P_1} \quad , \tag{2-8}$$

where

P_2 = the total pressure at the wave peak, and

P_1 = the total pressure at the wave trough.

The value of δ at the space origin is denoted by the symbol δ_o. The independent variable is the dimensionless distance x/λ, where λ is the wavelength of the sawtooth. It has been common to present the experimental data by plotting δ^{-1} versus x/λ. Then a convenient quantity that describes the relationship between δ^{-1} and x/λ is the slope S, given by

$$S \equiv \frac{d(1/\delta)}{d(x/\lambda)} \quad . \tag{2-9}$$

Rudnick (1952) derived the value, which we shall call S_1,

$$S_1 = \frac{\gamma + 1}{2\gamma} \quad . \tag{2-10}$$

Equation (2-10) may also be derived using weak-shock theory. Fay (1956) proposed a new value of S, viz.,

$$S_2 = \frac{\gamma + 1}{3\gamma} \quad , \tag{2-11}$$

but later withdrew this result, and affirmed the value of S derived by Rudnick, S_1 [see Fay (1962)].

Westervelt (1960) concluded that the proper value of S is given by

$$S_3 = \frac{\gamma + 1}{2\gamma^2} \quad . \tag{2-12}$$

Temkin (1969) included the attenuative effects of the tube wall directly in his value of S and obtained

$$S_4 = \frac{\gamma + 1}{2\gamma} + \frac{3}{2}\,\alpha\left(\frac{1}{\delta} + \frac{1}{2}\right) \quad , \tag{2-13}$$

where α=the tube wall attenuation coefficient for the fundamental. Rudnick (1952), on the other hand, included tube wall attenuation in his analysis by adjusting his experimental data in such a fashion that tube wall attenuation losses are removed. This adjustment is accomplished using a correction term based upon the attenuation coefficient of the fundamental. The correction term is commonly referred to as "Rudnick's zero-order correction." Westervelt ignored tube wall attenuation entirely in his analysis. None of the above researchers considered the effects of dispersion.

Both Temkin and Rudnick gave the limits on the applicability of their analyses. Temkin stated that his result S_4 is valid for values of $\delta_o < 0.1$, whereas Rudnick said simply that his expression S_1 is valid for "δ of order 0.1." Westervelt did not mention a limit to the applicability of S_3. The maximum value of δ is an important limit in our analysis because it can be used to identify the largest sound pressure level that can be accurately investigated using weak-shock theory. Our analysis of this limit appears in Appendix E.

Hence, at present, there are at least three distinct values of S(i.e., S_1, S_3, and S_4) supported by theoretical arguments. Unfortunately, conclusive experimental confirmation does not exist for any of these values.

Using a 10 in. plane wave tube, Rudnick (1952) with experimental assistance from Leonard and Wilson (1952) investigated the attenuation of intense (0.076 to 0.25 atm peak acoustic pressure), low frequency (30 to 200 Hz) sawtooth waves. The peak pressures corresponded to a range of δ_o of

$$0.167 < \delta_o < 0.667 \quad . \tag{2-14}$$

Rudnick found that the observed value of S was less than that given by Eq. (2-10). In other words, the amplitude of the observed sawtooth waves decreased at a slower rate than predicted. Adjustment of the data using the zero-order correction was accomplished but the effect was slight, since for Rudnick's experimental conditions the correction terms are very small. Rudnick formed ratios of the observed values of S and S_1. With a single exception, these ratios fell between 0.5 and 1.0, with the majority near 0.7. It is noteworthy that the ratios appeared to tend towards 1.0 as the value of δ_o decreased toward 0.1, thereby suggesting that the value S_1 is valid only for values of $\delta_o \leqq 0.1$. Rudnick's experimental methods were extended to other frequency and peak pressure ranges, other gases, and other pipe sizes by Werth and Delsasso (1954) and Medwin (1964). In general the results reported are similar to Rudnick's. That is, the observed values of S were less than S_1 even after correction for tube wall losses. Although Werth et al. and Medwin extended the range of measured results, with a single exception all of their reported data was gathered using sawtooth waves for which $\delta_o > 0.1$. The exception is a portion of the data reported by Medwin (1964) in his Fig. 4. Temkin (1969) compared his predicted value S_4 to this data and obtained favorable agreement. Medwin also

reported that some results obtained in air and argon confirm Westervelt's value S_3, but measurements obtained using other gases fail to confirm either S_1 or S_3.

A piece of evidence in support of validity of the value S_1 has been reported by Shin (1963). Shin recast the Rudnick theory in spherical coordinates, calculated the rate of change of δ^{-1} with distance, and adjusted this calculation for spherical spreading. The resultant theoretical value S_1 was then compared to experimental values of S observed in an anechoic medium. Shin obtained excellent agreement between theory and experiment. The range of values of δ_o, measured at the point of sawtooth wave formation, was

$$0.027 < \delta_o < 0.047 \quad . \tag{2-15}$$

In Appendix E we have attempted to improve on Rudnick's computation of the quantity $d(1/\delta)/d(x/\lambda)$ by using the exact expression for the entropy change across any shock.* On the basis of our improvement of Rudnick's result we conclude that the weak-shock value S_1 is accurate only if $\delta_o < 0.1$. For cases where $\delta_o > 0.1$, terms ignored in Rudnick's original derivation become significant and must be considered. Implicit in both Rudnick's derivation and ours is the assumption of simple wave flow. However, for values of $\delta_o > 0.1$ reflections from the shock may cause one to challenge seriously the validity of this assumption. Therefore, our result should not be considered a complete correction of

---

*Rudnick used a one-term approximation, namely the first term in Eq. (3-17).

Rudnick's theory but rather a working limit on the range of applicability of weak-shock theory. We have, nonetheless, compared both our three-term result and numerical integration result (see Appendix E) with Rudnick's (1952) experimental data and obtained generally good agreement.

c) Computational Schemes

The theory developed in this dissertation has been implemented by means of a computer algorithm. Hence, it is appropriate that we review briefly earlier computational schemes. Fox and Wallace (1954) investigated the distortion of an initially sinusoidal wave in a dissipative (but not dispersive) medium for propagation distances prior to the formation of shocks. Their analytic method was an iterative numerical scheme wherein a separate difference equation was used for each harmonic. The significance of their work in relation to the present work is that we have also used an iterative procedure wherein we correct the computed waveform for attenuation and dispersion after each incremental propagation step. A procedure not limited to distances that preclude shock formation was developed by Cook (1962). A parametric integration method similar to that used to generate the Bessel-Fubini solution [see Blackstock (1962a)] was used. The basic procedure was iterative with absorption (but not dispersion) introduced after each incremental distance step. An extension of Cook's method to nonsinusoidal deterministic waves was formulated by Van Buren and Breazeale (1968) in their study of the reflection of finite-amplitude waves. In both these algorithms dissipative effects such as viscosity are relied upon to prevent the waveform from becoming multivalued. There is no guarantee that pipe wall effects are sufficient by themselves to prevent

multivaluedness during propagation in a pipe. Hence, Cook's method would have to be significantly modified to be applicable to our problem. A second difficulty with Cook's method is that it does not contain any provision for relative motion of shocks within the waveform. We will see in Chapter 3 that in an arbitrarily shaped wave shocks exhibit relative motion with respect to one another and with respect to the continuous portion of the wave.

A computer model wherein relative motion of the shocks is allowed has been formulated by Hawkings (1970). An initial waveform that is sawtoothed with one or more of the sawtooth peaks larger than the rest is postulated. The model is based on plane wave weak-shock theory, and the waveform is simplified by representing it in straight line segments. Of all the computer models of finite-amplitude propagation of which we are aware, Hawkings' model is the most similar to ours. The major differences between our model and Hawkings' are the straight line representation, which we do not require, and our inclusion of explicit attenuation and dispersion effects, which are ignored by Hawkings.

d) The Propagation of Finite-Amplitude Noise

There have been only a few reported research efforts devoted to the investigation of finite-amplitude noise propagation. Burnett and Ackerman (1960) considered 1/2 octave wide bands of noise, and claim validity for their theoretical analysis for propagation distances insufficient for the formation of shocks. The authors arbitrarily imposed a maximum propagation limit of 3 meters. Using this limit, Burnett and Ackerman were able to define frequency-source amplitude

regions in which 1) small-signal approximations are valid, 2) difference frequency signals are important, 3) sum and difference frequency signals are important, 4) the proposed theory failed. Their analysis may be useful for very short ranges and source conditions that preclude shock formation within these ranges but is not useful for the present study. The results of Burnett and Ackerman's theoretical study were investigated experimentally by Oda and Ackerman (1960). Oda and Ackerman claim to have verified Burnett and Ackerman's theory in regions 1 and 2.

In a portion of the previously mentioned work by Pernet and Payne (1969), and in a later paper by the same authors [Pernet and Payne (1971b)], finite-amplitude noise propagation in tubes was considered. In both papers the authors obtained theoretical results and described verifying experiments. In the first paper the authors compared pure tones to narrow bands of noise centered at the frequency of the tone. The energy content of the two signals was equal. The harmonics of the pure tone were calculated. Since the amplitude peaks in a narrowband noise signal have a Rayleigh distribution [see, for example, Horton (1969)], Pernet and Payne were able to modify their theory and calculate the statistical amplitude distribution of the second through seventh harmonics of the finite-amplitude primary band. Over the distances considered, it was shown that noise harmonic bands grew more quickly with propagation distance than did pure tone harmonics. The theoretical predictions were experimentally verified. As in the analysis of pure tones, Pernet and Payne's noise theory is limited to distances that preclude shock formation. In the second paper the authors utilized the fact that the amplitude of the second harmonic is proportional to the squared amplitude

of the fundamental. This quadratic relation was analyzed using the mathematics of the square-law detector. The derived expression for the second harmonic is valid for distances before the formation of shocks. The theory was experimentally verified. Since we want to consider broadband noise and are interested in a solution valid both before and after shock formation, we require more general methods than those proposed by Pernet and Payne. Therefore, we shall not make specific use of their analytic results.

Kuznetsov (1970) studied the spectra of high intensity noise. The basis for his theoretical results was the Fourier transform of the Earnshaw relation. For large values of frequency Kuznetsov computed an approximate form of the spectrum. Although Kuznetsov does not mention it, his result is also applicable for large values of distance. The results are somewhat perplexing, however, because Kuznetsov's theory is only applicable for distances at which there is no shock formation.

There are, of course, other studies wherein the authors deal with finite-amplitude noise [see, for example, Jones (1971) or Pickett (1971)] but no researchers that we are aware of, other than those commented on above, have dealt directly with the analysis of the propagation of intense random noise.

e) The "Burgers Turbulence" Model

Burgers (1948) proposed a mathematical model to describe turbulence. Using this model, we may consider the development of some initial value turbulent velocity field as functions of a space

coordinate x and time t. The ranges of the independent variables in the case in which we are interested are $0 \rightarrow \infty$. The equation is

$$u_t + uu_x = \nu u_{xx} \quad , \tag{2-16}$$

where ν represents the frictional effects. In a later paper by Burgers (1972) solutions of Eq. (2-16) for which the initial velocity field $u(x,0)$ is random and ν vanishingly small are considered. Under these circumstances the solution of Eq. (2-16) for large values of t assumes the form of a series of discontinuities in velocity separated by straight line sections whose slope is t^{-1}. We shall refer to such a solution as a "random sawtooth" [see Fig. (2-1)].

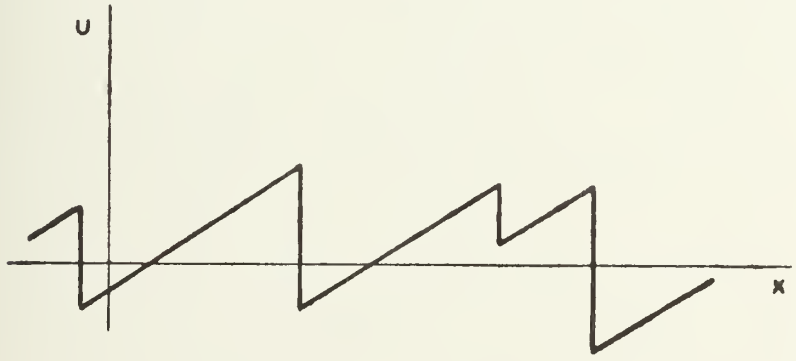

Figure 2-1
A sawtooth pattern as the asymptotic solution of $u(x, t)$ for large t and υ vanishingly small.

Although Burgers' results were originally meant to apply to turbulence, Morfey (1973), and Pelinovskii and Fridman (1973) have noted that they apply equally well to acoustic noise waveforms because Burgers' equation is also a model for finite-amplitude wave propagation. In the papers to which we shall refer in the remainder of this section the authors were interested in turbulence but their results, because they are based upon Burgers' equation, may also be construed as applying to finite-amplitude noise.

Kraichnan (1968) noted that for the case of very small values of ν (Kraichnan used the term "very large Reynolds number") that the random sawtooth pattern changes with time because discontinuities (shocks) coalesce. In addition, fluid elements travel at constant velocity until they meet a shock whereupon they disappear into the shock. This behavior indicates that the turbulent field should simplify with time. Because of the shock coalescence, the spectrum should show a shift of energy to lower wave numbers [the same prediction was made earlier by Ffowcs Williams (1965)]. We will see in Chapter 6 that the simplification of the particle velocity field is as described by Kraichnan. In addition, we will see that there is cascading of energy to both the high and low ends of the noise spectrum, the downward cascading being as described by Kraichnan.

The random sawtooth waveforms predicted by Burgers, and the merging of shocks, waveform simplification, and downward shifting of energy predicted by Kraichnan will be confirmed later in this work. However, our analytical tool is weak-shock theory, not Burgers' equation. The fact that use of weak-shock theory will produce results equivalent to asymptotic solutions of Burgers' equation is not surprising, since

it is known that the Burgers' equation approach and weak-shock theory are equivalent for the case of $\nu \to 0$ [see, for example, Lighthill (1956)].

Burgers' results have been extended by Tatsumi and Kida (1972) in a paper devoted primarily to the statistical properties of Burgers' model of turbulence. Two results produced by Tatsumi and Kida are equations for the number of shocks and the mean interval between shocks as functions of time. These relations are

$$N = N_o\left(\frac{t_o}{t}\right)^{\xi} \tag{2-18}$$

and

$$\ell = \ell_o\left(\frac{t}{t_o}\right)^{\xi} \quad , \tag{2-19}$$

where

ℓ = the mean interval between shocks,

ℓ_o = the mean interval between shocks at $t=t_o$,

N = the number of shocks,

N_o = the number of shocks at $t=t_o$, and

ξ = a constant, ξ/t is the number of shock collisions per unit time.

Via statistical arguments, Tatsumi and Kida show that $\xi=1/2$ corresponds to the condition of maximum randomness and is therefore the value most likely to occur in real turbulence. A numerical calculation of the energy of Burgers turbulence was carried out by Crow and Canavan (1970). Tatsumi and Kida extrapolated the value of ξ from the Crow and Canavan

data for the condition of very large Reynolds number and obtained the value 1/2.

Burgers' equation is convenient for initial value problems. For boundary value problems the roles of "space" and "time" in the Burgers' equation are reversed [see, for example, Blackstock (1972)]. Recasting Eq. (2-18) so that it applies in a boundary value problem, we obtain

$$N = N_o\left(\frac{x_o}{x}\right)^{\xi} \quad . \tag{2-20}$$

where x_o is a reference distance. Utilizing some of our experimental results obtained using noise waves, we attempted to verify Tatsumi and Kida's asymptotic value of ξ. The results of this attempt are reported in Chapter 6.

As we shall see in Chapter 6, we are unable to verify Tatsumi and Kida's predicted value of ξ by using waves of initial strength suitable for analysis via weak-shock theory. In addition the asymptotic results that form the basis of the work of Burgers, Tatsumi and Kida, and Kraichnan appear to require very strong initial disturbances. Hence, in light of the experimental results in Chapter 6 and the analysis in Appendix E, we question whether weak-shock theory can be applied to disturbances of the strengths required to obtain the asymptotic results discussed here.

CHAPTER 3 THEORY

1. Introduction

The basic weak-shock theory used in this dissertation is well known and has been available in the literature for many years [see, for example, Whitham (1956), or Blackstock (1966) and (1972)]. The basic equations of the theory are briefly derived and explained in this chapter in order that the present work be complete and clear. The application of weak-shock theory is then demonstrated in two example problems. Results similar to those found for the second example problem are then presented for a generalized plane shock propagation problem. The results of the generalized problem illustrate that analytical solutions of even fairly simple problems are quite complex. This complexity suggests that a computer method may be more useful than an analytic method for the analysis of complicated waveforms. The results of the generalized problem serve a second purpose. In Chapter 2 we discussed some of the results that have been obtained using the Burgers model of turbulence. In this chapter we shall show that equivalent results may be obtained from the asymptotic forms of the results of the generalized problem.

Our theory is cast in terms of particle velocity, but we actually measure pressure. In Section 4 of this chapter we develop the necessary relations between pressure and particle velocity. Next, we consider in greater detail the effects of the tube wall. The chapter is concluded with a discussion of modified weak-shock theory.

2. Weak-Shock Theory*

a) The Earnshaw Solution

Consider a continuous plane sound wave propagating in an otherwise quiescent medium. We assume that simple wave flow exists, that the thermodynamic processes involved are isentropic, and that the medium is a perfect gas.

At this point it is convenient to introduce the term "wavelet." A wavelet is a specific point on a waveform; associated with this point is a specific particle velocity u. If more than one point on the wave has the same particle velocity, each point is still a different wavelet.

The propagation velocity of a wavelet of particle velocity u is given by Eq. (2-4). Restricting Eq. (2-4) to apply to only outgoing waves, we obtain

$$\left.\frac{dx}{dt}\right)_{u=\text{const}} = c_o + \beta u \quad . \tag{3-1}$$

Equation (3-1) may be integrated to yield the Earnshaw solution once we have specified appropriate boundary conditions.** Let us assume that a plane sound wave of arbitrary shape is being observed in a tube by use of a microphone sensitive to particle velocity. We will consider the microphone location the origin x-0 and assume that the wave propagation is lossless.

---

* Blackstock (1972) considers waves of SPL of 174 dB or below as weak. Temkin (1969), in a more detailed analysis, estimates the upper limit of weak-shock theory as 165 dB or below. We will restrict our analysis to SPL's of 165 dB or less.

** Earnshaw (1860) used a piston as the wave source. The piston then represented a moving boundary condition and introduced into the integral solution of Eq. (3-1) a term proportional to the piston displacement. Our solution, since it is formed using a stationary boundary, does not contain a source displacement term. In any event, for propagation distances large compared to the piston displacement, the piston displacement term contributes negligibly to the solution.

The source velocity, i.e., the velocity at x=0, is given by g(t). The value of particle velocity at the source for a particular wavelet is then

$$u = g(t) \quad . \tag{3-2}$$

We will solve Eq. (3-1) subject to the condition that u remain constant. Identifying the parameter φ as the time that the wavelet of particle velocity u left the origin, we may write

$$u = g(\varphi) \quad , \tag{3-3}$$

and

$$\int_o^x dx' = \int_\varphi^t (c_o+\beta u)dt'' \quad . \tag{3-4}$$

Substituting Eq. (3-3) into Eq. (3-4) and performing the integration, we obtain the result

$$x = [c_o + \beta g(\varphi)](t-\varphi) \quad . \tag{3-5}$$

Equations (3-3) and (3-5) are the Earnshaw solution. The Earnshaw solution is more useful if Eq. (3-5) is recast in an approximate form. Substituting the retarded time $t'=t-x/c_o$ into Eq. (3-5), we obtain

$$\begin{aligned} t' &= \varphi + \frac{x}{c_o}\left[1 + \frac{\beta g(\varphi)}{c_o}\right]^{-1} - \frac{x}{c_o} \quad , \\ &\doteq \varphi - \frac{\beta x g(\varphi)}{c_o^2} \quad . \end{aligned} \tag{3-6}$$

In Eq. (3-6) terms in u/c_o of order greater than one have been ignored. If we define

$$\epsilon \equiv u_o/c_o \quad , \tag{3-7}$$

where

u_o = the peak value of u,

we see that the approximation used to obtain Eq. (3-6) is valid for

$$\epsilon \ll 1 \quad .$$

For ϵ=0.1 in a sinusoidal wave, the sound pressure level is about 175 dB.

Equation (3-6) describes the progressive distortion of the original time base of a signal, where the original time base is represented by the parameter φ and the new time base by t'. The factor $\beta u/c_o^2$ may be thought of as a time shift per unit of propagation distance.

In summary, consider a source particle velocity relation of the form of Eq. (3-2). The Earnshaw solution is

$$u = g(\varphi) \quad , \tag{3-3}$$

where

$$\varphi \doteq t' + \frac{\beta x g(\varphi)}{c_o^2} \quad . \tag{3-6}$$

Equation (3-3) may be used to find the value of u at the field point (x,t) provided Eq. (3-6) can be solved for

$$\varphi = \varphi(x,t') \quad . \tag{3-8}$$

The requirement to find an explicit solution for φ in terms of x and t' is often difficult to meet when the Earnshaw solution is used analytically. In this dissertation, we shall use a computer algorithm based in part on Eq. (3-6). The numerical evaluation of Eq. (3-6) provides a calculation of the distortion of the signal time base and avoids the requirement posed by Eq. (3-8).

b. Shock Propagation Relations

In most instances, use of Eq. (3-6) leads to multivalued waveforms. The onset of multivaluedness indicates the formation of a shock. At the point of shock formation the Earnshaw solution is no longer valid. Pressure, density, particle velocity, enthalpy,* and entropy on either side of the shock and the propagation velocity of the shock are described by use of the Rankine-Hugoniot shock relations [see, for example, Thompson (1972)]. Before stating these relations, we will establish the geometry and variables that will be used in the ensuing discussion. Consider a plane shock wave propagating in a perfect gas. The shock velocity is designated $\bar{V}$; variables downstream (in front of) the shock are identified by the subscript 1 and those upstream (behind) the shock by the subscript 2. The variables that we will use are summarized in Fig. (3-1).

---

*Specific enthalpy is defined as

$$h = e + P\tau$$

where e is the specific internal energy, P the absolute pressure, and τ the specific volume (see, for example, Thompson (1972)).

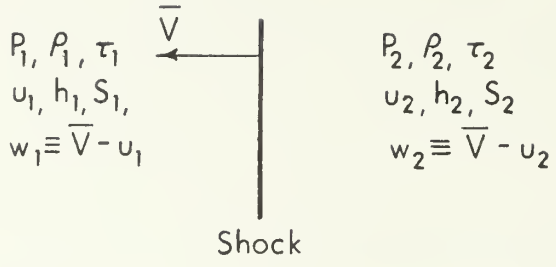

Figure 3-1
A summary of the variables used in the Rankine-Hugoniot relations
w is the relative shock velocity and τ is the specific volume
All other variables are as previously defined

In general, the wave flow fields on either side of a shock are varying fields. Unless stated otherwise, in the applications of the Rankine-Hugoniot relations that we shall consider the wave fields on either side of the shock(s) will be varying. The Rankine-Hugoniot relations may be stated as follows:

the continuity relation $$\rho_2 w_2 - \rho_1 w_1 = 0 \quad , \tag{3-9}$$

the momentum relation $$P_2 - P_1 + \rho_2 w_2^2 - \rho_1 w_1^2 = 0 \quad , \tag{3-10}$$

the energy relation $$h_2 - h_1 + \frac{1}{2}\left(w_2^2 - w_1^2\right) = 0 \quad , \text{ and} \tag{3-11}$$

the entropy relation $$s_2 - s_1 \geq 0 \quad . \tag{3-12}$$

Our first task is to calculate the magnitude of the entropy change at the shock. The first step in this task consists of combining Eqs. (3-9), (3-10), and (3-11) into a single relation that contains only thermodynamic variables. This relation, obtained after some manipulation, is

$$h_2 - h_1 = \tau_1(P_2-P_1) + \frac{1}{2}(\tau_2-\tau_1)(P_2-P_1) \quad . \tag{3-13}$$

The enthalpy and specific volume upstream of the shock may be described in terms of the downstream enthalpy and specific volume by expanding $h(P,s)$ and $\tau(P,s)$ in Taylor series, for example,

$$h_2 = h_1 + \frac{\partial h}{\partial s}(s_2-s_1) + \frac{\partial^2 h}{\partial s^2}\Big)_1 \frac{(s_2-s_1)^2}{2} + \ldots$$

$$\ldots + \frac{\partial h}{\partial P}(P_2-P_1) + \frac{\partial^2 h}{\partial P^2}\Big)_1 \frac{(P_2-P_1)^2}{2} + \ldots \tag{3-14}$$

$$\ldots + \frac{\partial^2 h}{\partial s \partial P}\Big)_1 (s_2-s_1)(P_2-P_1) + \ldots \quad .$$

The series expressions may be evaluated explicitly using the perfect gas relations and the identities

$$T = \frac{\partial h}{\partial s}\Big)_p \tag{3-15}$$

and

$$\tau = \frac{\partial h}{\partial P}\Big)_s \quad . \tag{3-16}$$

Substituting the evaluated series into Eq. (3-13) and solving the resulting expression for (s_2-s_1), one obtains

$$s_2 - s_1 = \frac{\beta R \delta^3}{6\gamma^2} + O(\delta^4) + \ldots \quad , \tag{3-17}$$

where

R = the gas constant.

Hence the change in entropy across the shock is of the order of the shock strength cubed.

Until now, we have assumed simple wave flow. Strictly speaking, the formation of a shock invalidates this assumption. The shock represents a discontinuity in the wave flow field. In general, shocks are subsonic with respect to the flow behind the shock* and, hence, a portion of the wavelets overtaking the shock is reflected from it. The presence of the reflected wave negates the simple wave assumption. However, if the reflected wave is very weak, we may ignore it and thereby preserve the simple wave assumption. A measure of the strength of the reflected wave may be gained by investigating the magnitude of the discontinuity in the Riemann invariant $\hat{s}$ at the shock. Lighthill (1956) has made such an investigation and reports that the change in the quantity $\hat{s}$ is of the order of the change in entropy. We see from Eq. (3-17) that the change in entropy is very small for

*That this is true for weak shocks will be apparent from the subsequent examples contained here. The validity of the comment as applied to stronger shocks is substantiated, for example, by Thompson (1972).

weak shocks and can safely be ignored; similarly, the reflected wave can also be ignored. Therefore, in this work simple wave flow will be taken to exist on either side of the shock.

Having established the magnitude of the entropy change associated with shock propagation, we desire an expression for the shock propagation velocity. Such a relation may be obtained from the Rankine-Hugoniot relations. Equations (3-9), (3-10), and (3-11) may be combined to yield the relation

$$\bar{V}^2 - \beta\bar{V}(u_2-u_1) - c_1^{\,2} = 0 \quad . \tag{3-18}$$

When Eq. (3-18) is solved for the shock speed $\bar{V}$, we obtain

$$\bar{V} = c_1 + u_1 + \frac{\beta}{2}(u_2-u_1) + \frac{\beta^2}{8}\frac{(u_2-u_1)^2}{c_1} + \ldots \quad . \tag{3-19}$$

Substituting Eq. (2-3) evaluated in the downstream region into Eq. (3-19), we obtain the relation

$$\bar{V} = c_o + \frac{\beta}{2}(u_2+u_1) + \frac{\beta^2}{8}\frac{(u_2-u_1)^2}{c_o}\left(1 + \frac{\gamma-1}{2}\frac{u_1}{c_o}\right)^{-1} + \ldots \quad . \tag{3-20}$$

Equation (3-20) gives the propagation velocity of the shock. Recall that in Eq. (3-6) terms of order greater than ϵ^2 were ignored. When we apply this criterion to Eq. (3-20), we obtain

$$\left.\frac{dx}{dt}\right)_{\text{shock}} = \bar{V} = c_o + \frac{\beta}{2}(u_2+u_1) \quad . \tag{3-21}$$

Equation (3-21) is the well-known weak-shock result that the shock velocity is approximately the mean of the propagation velocities immediately upstream and downstream [see, for example, Thompson (1972)].

Equation (3-21) has units of velocity and, in order to be compatible with Eq. (3-6), we need to recast it in units of time shift per unit distance. This recasting is easily accomplished by inverting Eq. (3-21), expanding the right hand side in powers of $(u_1+u_2)/c_o$ and, as before, discarding terms above the first order. In terms of the retarded time t' we then have

$$\left.\frac{dt'}{dx}\right)_{shock} = -\frac{\beta}{2c_o^2}[u_2+u_1] \quad . \tag{3-22}$$

The quantities u_2 and u_1 are obtained from the Earnshaw solution results immediately in front of and behind the shock. The values of u_2 and u_1 used in Eq. (3-22) provide the means of connecting the Earnshaw solution on one side of the shock with the Earnshaw solution on the other side.

c. Application of Weak-Shock Theory

In Subsections (a) and (b) we have derived the basic mathematical tools used in weak-shock theory. These tools are the Earnshaw solution and the shock arrival equation. We must also provide a source relation of the form of Eq. (3-2). Equation (3-17) also is used in weak-shock calculations, but in an indirect way. Equation (3-17) shows that there is dissipation at the shock. The loss mechanism is built into Eq. (3-21), however, and we shall never have to use Eq. (3-17) explicitly.

Rudnick (1952) made explicit use of Eq. (3-17) and for the case of sawtooth wave propagation obtained the weak-shock theory result.

We shall apply weak-shock theory to two problems. In the first problem, only the Earnshaw solution portion of the theory is used. In the second problem the full weak-shock theory is demonstrated.

1) The First Example Problem*

Consider a sound wave whose shape at its source is as shown in Fig. (3-2).

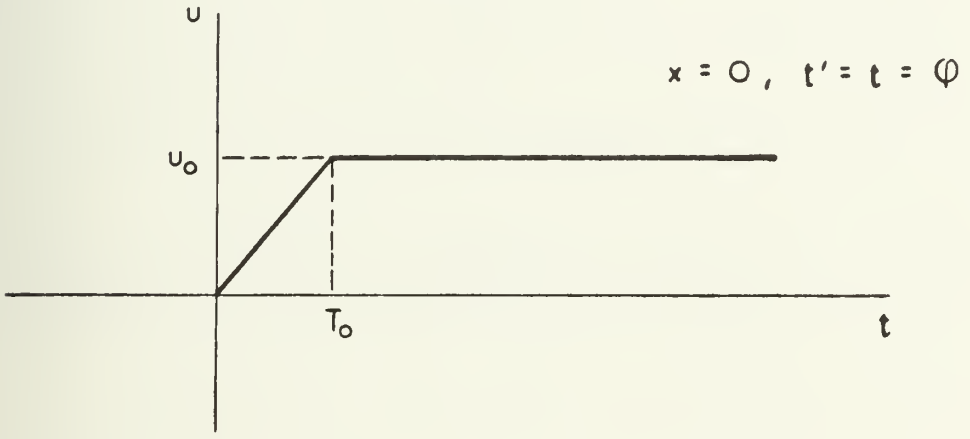

Figure 3-2
The source waveform for the first example.

The source waveform is described analytically by the relations

$$u = \frac{u_o}{T_o} t \qquad 0 \leq t \leq T_o \quad ,$$

$$= u_o \qquad T_o \leq t \quad . \tag{3-23}$$

*Rayleigh (1910) considered an example similar to our first example problem. Rayleigh's example was treated as an initial value problem.

Equation (3-23) is the source relation [see Eq. (3-2)] for this example. Substituting Eq. (3-23) evaluated at $t=\varphi$ into Eq. (3-6), we obtain

$$\varphi = t' \left[1 - \frac{\beta u_o x}{T_o c_o^2}\right]^{-1} \tag{3-24}$$

for

$$0 \leq \varphi \leq T_o \quad ,$$

and

$$\varphi = t' + \frac{\beta u_o x}{c_o^2} \tag{3-25}$$

for

$$\varphi \geq T_o \quad .$$

Equations (3-24) and (3-25) are the explicit solution of φ in terms of x and t' indicated earlier in general terms by use of Eq. (3-8). The solution for u as a function of φ where $\varphi=\varphi(x,t')$ is then

$$u(x,t') = \frac{u_o}{T_o} t' \left[1 - \frac{\beta u_o x}{T_o c_o^2}\right]^{-1} \tag{3-26}$$

for

$$0 \leq t' \leq T_o - \frac{u_o \beta x}{c_o^2} \quad ,$$

and

$$u(x,t') = u_o \tag{3-27}$$

for

$$t' \geq T_o - \frac{u_o \beta x}{c_o^2} \quad .$$

Use of Eqs. (3-26) and (3-27) describes the deformation of the wave shown in Fig. (3-2) for some propagation distance x. Note that at x=0 Eqs. (3-26) and (3-27) reduce to Eq. (3-23).

The distortion evaluated by use of Eqs. (3-26) and (3-27) is shown in Fig. (3-3).

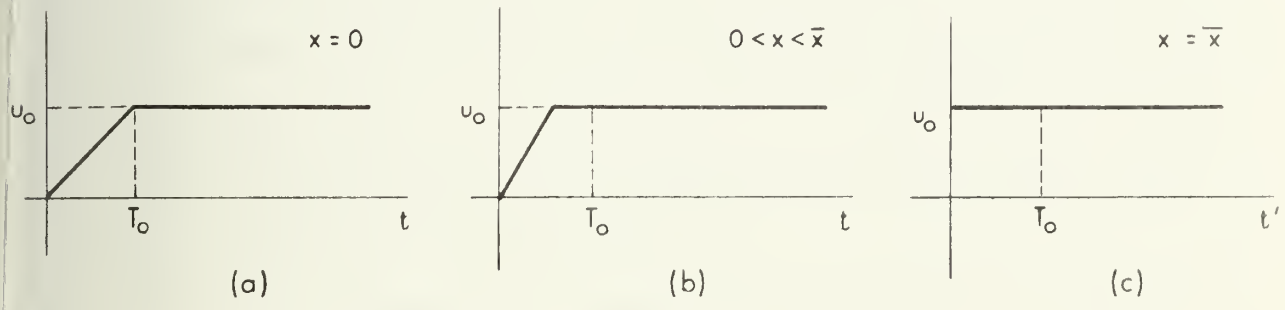

Figure 3-3
The progressive distortion of the Fig. 3-2 waveform
(a) $x = 0$, (b) $0 < x < \bar{x}$, (c) $x = \bar{x}$

Figure (3-3a) repeats the source waveform shown in Fig. (3-2). In Fig. (3-3b) the wave has been distorted. Note from this example that straight line sections remain straight as they are distorted; this is a general result. Figure (3-3c) shows the waveform at the shock formation distance $\bar{x}$. The quantity $\bar{x}$ may be calculated using Eq. (3-26) by noting that u becomes discontinuous at the point

$$\bar{x} = \frac{c_o^2 T_o}{\beta u_o} \quad . \tag{3-28}$$

Equation (3-28) is also a general result applicable to straight line sections not immediately preceded or followed by a shock.

If we continue to apply the Earnshaw solution to the above problem for $x > \bar{x}$ we would obtain multiple valued solutions. Hence, further analysis requires use of the weak-shock relations. In the next example problem the use of the weak-shock relations will be demonstrated for a case containing two shocks.

2) The Second Example Problem

In Fig. (3-4a) we show the source waveform for the second example problem. Note that the slopes of the segments AB and CD are equal. In accordance with results obtained by use of Eq. (3-28) both segments will form shocks at the same value of x. Having equal slopes for the segments AB and CD is merely a convenience to facilitate the subsequent calculations. Had the initial slopes of the segments AB and CD been different, the calculations would have proceeded in a similar, albeit slightly more complex, fashion.

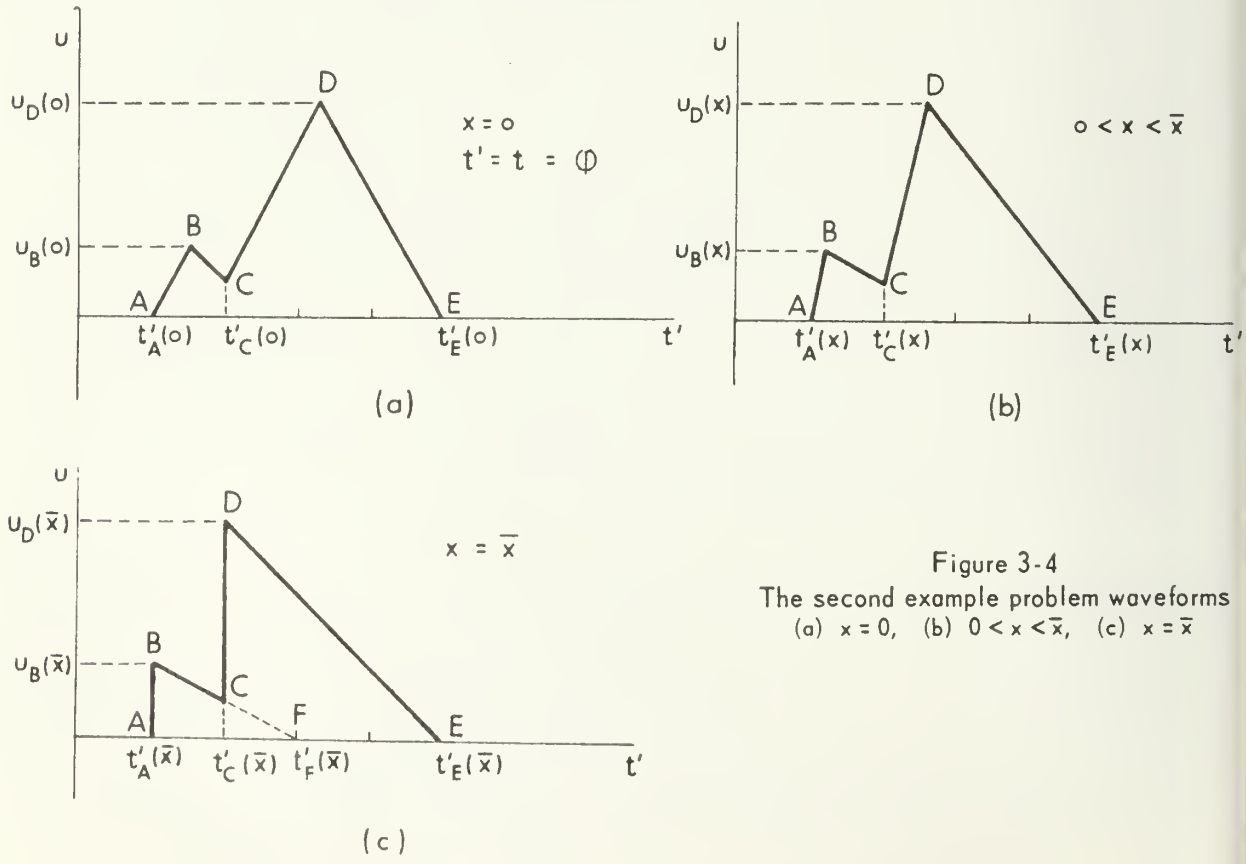

Figure 3-4
The second example problem waveforms
(a) $x = 0$, (b) $0 < x < \bar{x}$, (c) $x = \bar{x}$

In Fig. (3-4b) the wave has been distorted but shocks have not yet formed. Figure (3-4c) shows the waveform at the point of shock formation. Henceforth, we shall refer to the segments AB and CD as the first and second shocks, respectively. The notation that we shall use is as follows:

a) The capital letters A, B, C, D, and E indicate points of slope change of the waveform for some propagation distance x. The point F is the point of intersection of the segment BC and the t' axis.

b) The coordinates of a particular point, such as point A, for some value x are $(u_A(x), t_A'(x))$.

c) Values of u along the segments BC and DE for some value x are indicated by the notation $u_{BC}(x,t')$ and $u_{DE}(x,t')$.

The distortion of the waveform shown in Fig. (3-4a) to the point of shock formation proceeds exactly as indicated for the first example problem. Let us assume that the wave has propagated to the point $\bar{x}$ as shown in Fig. (3-3c) and that we wish to compute the subsequent waveform distortion. For this calculation we shall take the space origin to be the point at which the shocks form. The time of arrival of a particular wavelet at the origin is indicated by the parameter φ. At the origin φ, t, and t' are equal. The source relations for this problem are

$$u_{BC}(0,t') = M_{BC}[t_F'(0) - t'] \qquad (3\text{-}29)$$

for

$$t_A'(0) \leq t' \leq t_C'(0) \quad ,$$

and

$$u_{DE}(0,t') = M_{DE}[t_E'(0) - t'] \tag{3-30}$$

for

$$t_C'(0) \leq t' \leq t_E'(0) \quad ,$$

where

$$M_{BC} = \frac{u_B(0)}{t_F'(0) - t_A'(0)} \quad , \tag{3-31}$$

and

$$M_{DE} = \frac{u_D(0)}{t_E'(0) - t_C'(0)} \quad . \tag{3-32}$$

Substituting in turn Eqs. (3-29) and (3-30) evaluated at $t=\varphi$ into Eq. (3-6), we obtain expressions for φ as a function of (x,t'). The solutions for u as a function of $\varphi(x,t')$ are then

$$u_{BC}(x,t') = \frac{M_{BC}[t_F'(0) - t']}{1 + \frac{\beta M_{BC} x}{c_o^2}} \tag{3-33}$$

for

$$t_A'(x) \leq t' \leq t_C'(x) \quad ,$$

and

$$u_{DE}(x,t') = \frac{M_{DE}[t_E'(0) - t']}{1 + \frac{\beta M_{DE} x}{c_o^2}} \tag{3-34}$$

for

$$t_C'(x) \leq t' \leq t_E'(x) \quad .$$

At this point we do not know the value of $t_A'(x)$ and $t_C'(x)$ because these quantities must be calculated using Eq. (3-22). The quantity $t_E'(x)$ remains a constant equal to $t_E'(0)$ because the particle velocity at point E is zero.

We are now ready to compute the motion of the shock fronts. This computation is performed using Eq. (3-22). In this problem we have identified the times of occurrence of the shocks as $t_A'(x)$ and $t_C'(x)$. Hence, in using Eq. (3-22), we adopt the notation

$$\frac{dt_A'(x)}{dx} = \left.\frac{dt'}{dx}\right)_{\text{shock 1}} \tag{3-35}$$

and

$$\frac{dt_C'(x)}{dx} = \left.\frac{dt'}{dx}\right)_{\text{shock 2}} \tag{3-36}$$

where shock 1,2 denotes the first or second shock, respectively. Evaluating Eq. (3-22) at the first shock, we obtain

$$\frac{dt_A'(x)}{dx} = -\frac{\beta}{2c_o^2} u_{BC}(x, t_A'(x)) \quad . \tag{3-37}$$

At the first shock the velocity downstream of the shock is zero; hence, the quantity u_1 does not appear in Eq. (3-37). Substituting Eq. (3-33) evaluated at $t_A'(x)$ into Eq. (3-37), we obtain

$$\frac{dt_A'(x)}{dx} = -\frac{\beta}{2c_o^2} M_{BC} \frac{[t_F'(0) - t_A'(x)]}{1 + \frac{\beta M_{BC} x}{c_o^2}} \quad . \tag{3-38}$$

The solution of Eq. (3-38) subject to the boundary condition $t_A'(x)=t_A'(0)$ at $x=0$ is

$$t_A'(x) = t_A'(0)\left[1 + \frac{\beta M_{BC} x}{c_o^2}\right]^{1/2} + t_F'(0)\left(1 - \left[1 + \frac{\beta M_{BC} x}{c_o^2}\right]^{1/2}\right) \quad . \tag{3-39}$$

The motion of the second shock is somewhat more complicated because the velocity downstream of this shock is not zero. Substituting Eqs. (3-33) and (3-34) evaluated at $t_C'(x)$ into Eq. (3-22), we obtain

$$\frac{dt_C'}{dx} = -\frac{\beta}{2c_o^2}\left[\frac{M_{BC}(t_F'(0) - t_C'(x))}{1 + \frac{\beta M_{BC} x}{c_o^2}} + \frac{M_{DE}(t_E'(0) - t_C'(x))}{1 + \frac{\beta M_{DE} x}{c_o^2}}\right] \quad . \tag{3-40}$$

The solution of Eq. (3-40) subject to the boundary condition $t_C'(x)=t_C'(0)$ at x=0 is

$$t_C'(x) = t_C'(0)\left[1 + \frac{\beta}{c_o^2} M_{BC}x\right]^{1/2}\left[1 + \frac{\beta M_{DE}x}{c_o^2}\right]^{1/2}$$

$$- \frac{t_F'(0)\beta M_{BC}x\left[1 + \frac{\beta M_{DE}x}{c_o^2}\right]^{1/2}}{c_o^2\left[\left(1 + \frac{\beta M_{BC}x}{c_o^2}\right)^{1/2} + \left(1 + \frac{\beta M_{DE}x}{c_o^2}\right)^{1/2}\right]} \qquad (3\text{-}41)$$

$$- \frac{t_E'(0)\beta M_{DE}x\left[1 + \frac{\beta M_{BC}x}{c_o^2}\right]^{1/2}}{c_o^2\left[\left(1 + \frac{\beta M_{BC}x}{c_o^2}\right)^{1/2} + \left(1 + \frac{\beta M_{DE}x}{c_o^2}\right)^{1/2}\right]} \quad .$$

Equations (3-39) and (3-41) give the retarded times of occurrence of the two shocks for any propagation distance x up to the point of shock merger.

Having solved for $t_A'(x)$ and $t_C'(x)$ we may now calculate the values of particle velocity along the segments BC and DE. Two values of particular interest are

$$u_B(x) = u_{BC}(x, t_A'(x)) \quad , \qquad (3\text{-}42)$$

and

$$u_D(x) = u_{DE}(x, t_C'(x)) \quad . \qquad (3\text{-}43)$$

The expression for $u_B(x)$ turns out to be particularly simple, i.e.,

$$u_B(x) = \frac{u_B(0)}{\left[1 + \frac{\beta M_{BC} x}{c_o^2}\right]^{1/2}} \quad . \tag{3-44}$$

The result for $u_D(x)$ is similar but more complicated and for the sake of brevity we shall not present it here. The amplitude decay function $\left(1+\beta M_{BC} x/c_o^2\right)^{1/2}$ in Eq. (3-44) is of the same form as that for N waves [see, for example, Blackstock (1972)], a not surprising result, since the triangular section ABCF of the original waveform (Fig. 3-4c) is really half of an N wave.

Let us now consider the merger of the two shock waves. In this problem it turns out that for some value of x we obtain the result

$$t_A'(x) = t_C'(x) \quad . \tag{3-45}$$

The value of x satisfying Eq. (3-45) can be found analytically or in a specific case by numerical evaluation. Physically, the equality of the shock arrival times indicates that the two shocks have merged. In this example, the merger results when the second shock overtakes the first. Following the shock merger, the resultant waveform appears as in Fig. (3-5d). The equations describing the retarded time of arrival of the merged shock and the value of particle velocity behind the merged shock are similar to Eqs. (3-39) and (3-44), respectively.

A computer program was written to evaluate the results for this problem. The waveform depicted in Fig. (3-4c) was used as the

source wave. The computations were done in two stages. First Eqs. (3-39), (3-41), (3-44), and the relation for $u_D(x)$ not given here were used up to the point of shock merger. Following shock merger, equations similar to Eqs. (3-39) and (3-44) were used. The results appear in Fig. (3-5). The distances indicated on each drawing are distances in feet with respect to the original shock formation point for this problem. The values of the remaining parameters at the original shock formation point are t_A'=1.0 msec, t_C'=1.25 msec, t_E'=2.0 msec, u_B=5 ft/sec, and u_D=15 ft/sec.

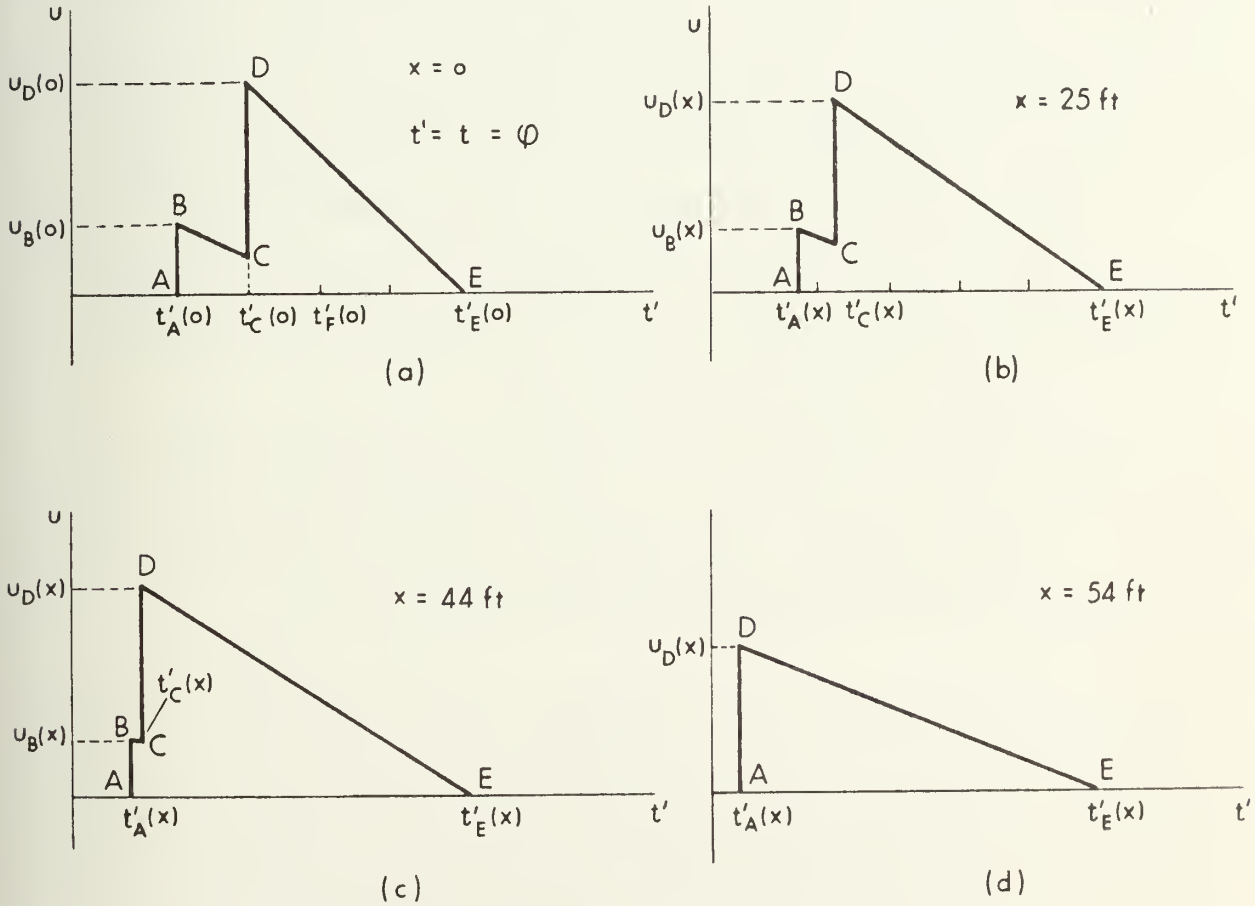

Figure 3-5
The second example problem (cont'd)

(a) The source woveform in the shifted coordinote system.
(b) The source woveform after propogating 25 ft.
(c) Just prior to shock merger.
(d) The simplified waveform ofter shock merger.

The two example problems illustrate several well-known effects that take place in finite-amplitude waves. These effects are as follows:

a) Nonlinear effects cause waves to distort, i.e., positive sloping sections form shocks, and the slopes of negatively sloped sections gradually decrease.

b) Shocks exhibit relative velocity with respect to one another. Hence shocks may merge as the wave propagates.

c) The wave is attenuated even though attenuation is not explicitly included in Eq. (3-21). The reason for this, as discussed earlier, is that attenuation is "built into" Eq. (3-21). Physically, the attenuation is a consequence of the irreversible nature of shock propagation. This point was noted in the discussion following the derivation of Eq. (3-17).

d) The shape of the wave is usually significantly altered as it propagates. Hence, we expect the frequency spectrum to be a function of propagation distance.

e) Straight line segments distort in such a fashion that they remain straight. The slope M is related to the initial slope M_o by an equation of the general form

$$M = \frac{M_o}{1 - \frac{\beta M_o x}{c_o^2}} \quad . \tag{3-46}$$

Positively sloping sections form shocks. The shock formation distance for sections not immediately preceded or followed by a shock in general is

$$\bar{x} = \frac{c_o^2}{\beta M_o} \quad . \tag{3-47}$$

3. A General Technique for Modeling Arbitrary Waveforms by Straight Line Sections

The method used in the preceding example may be generalized for use with any sound wave modeled by straight line sections. In this section, the general solution for a plane shock wave preceded and followed by a straight line velocity field of arbitrary slope is calculated. The waveform at the space origin is shown in Fig. (3-6).

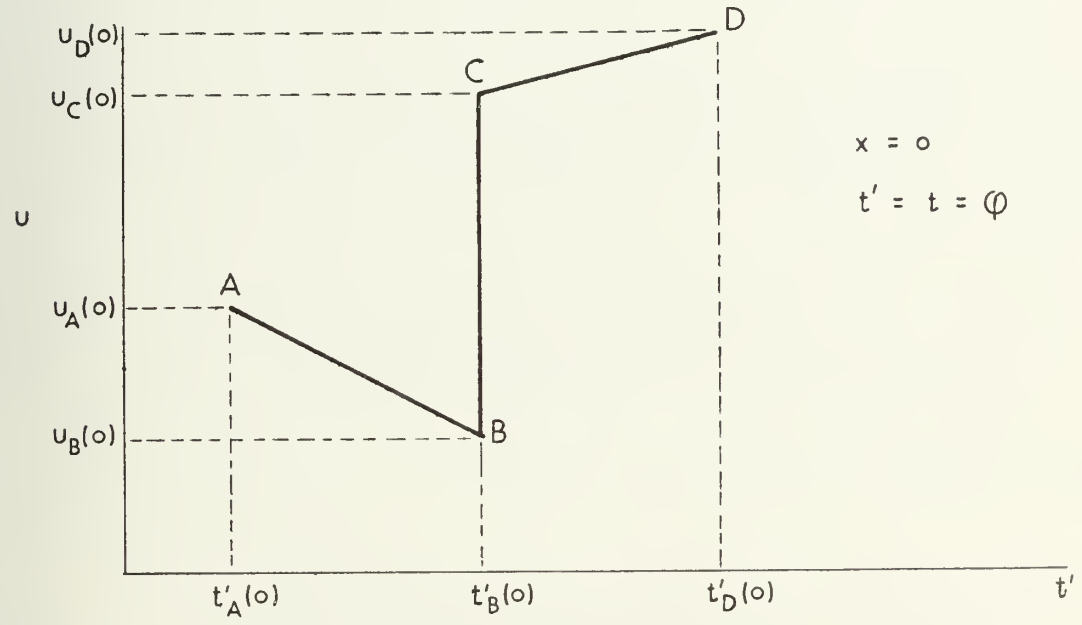

Figure 3-6
A plane shock wave propagating in a disturbed medium.

The notation that we use in this section follows the same rules as the notation used earlier in the second example problem in Section 2 of this chapter. Expressions for the retarded time of shock arrival $t_B'(x)$ and for the particle velocities in front of and behind

the shock are obtained exactly as they were obtained in Section 2. These expressions are

$$t_B'(x) = t_B'(0)\sqrt{1 - A_{AB}x}\sqrt{1 - A_{CD}x}$$

$$+ \frac{A_{AB}t_A'(0) - \beta c_o^{-2}u_A(0)}{A_{CD} - A_{AB}}\left[\sqrt{1 - A_{AB}x}\sqrt{1 - A_{CD}x} - 1 + A_{AB}x\right] \tag{3-48}$$

$$- \frac{A_{CD}t_B'(0) - \beta c_o^{-2}u_D(0)}{A_{CD} - A_{AB}}\left[\sqrt{1 - A_{AB}x}\sqrt{1 - A_{CD}x} - 1 + A_{CD}x\right] \quad ,$$

$$u_B(x) = \frac{c_o^2\beta^{-1}A_{AB}[t_B'(x) - t_A'(0)] + u_A(0)}{1 - A_{AB}x} \quad , \tag{3-49}$$

and

$$u_C(x) = \frac{c_o^2\beta^{-1}A_{CD}[t_B'(x) - t_B'(0)] + u_D(0)}{1 - A_{CD}x} \tag{3-50}$$

where A_{AB} and A_{CD} (closely related to M_{AB} and M_{CD}) are defined by

$$A_{AB} \equiv \frac{\beta}{c_o^2} \cdot \left(\frac{u_A(0) - u_B(0)}{t_A'(0) - t_B'(0)}\right) \quad , \tag{3-51}$$

and

$$A_{CD} \equiv \frac{\beta}{c_o^2} \cdot \left(\frac{u_C(0) - u_D(0)}{t_B'(0) - t_D'(0)}\right) \quad . \tag{3-52}$$

Equations (3-48) through (3-52) are applicable until the propagating shock coincides with one of the end points of the wave section shown in Fig. (3-6). Additionally, these end points could be overtaken by some other shock outside the region defined by Fig. (3-6). Points labeled A and D in Fig. (3-6) will themselves be shifted as described by Eq. (3-6). The earliest time of coincidence of $t_B'(x)$ with either $t_A'(x)$ or $t_D'(x)$ can be calculated. Coincidence with other shocks propagating from outside the region shown in Fig. (3-6) can also be computed. Once the earliest coincidence distance is reached a new set of conditions could be established and the solution continued. While the method appears to be extremely unwieldy, it probably could be made to work, within the limitation that straight line modeling be used. Such an attempt, in a very simple case, has been reported by Hawkings (1970) and was discussed in Chapter 2. Hawkings' computer method produces results that exhibit shock propagation characteristics similar to those shown in Fig. (3-5).

The complexity of solutions of the type typified by Eqs. (3-48) to (3-50) and the great difficulty in adapting them to individual cases convinced us that a numerical approach to the problem would be easier. This approach is described in Chapter 4.

In Chapter 2 we mentioned that use of weak-shock theory produced results equivalent to some of the results of Burgers (1972). We will now demonstrate this fact. In the ensuing discussion let us assume that the propagation distance x is very large. Noise waveforms at very large values of x will have deformed into a series of shock fronts separated by negatively sloped ($\partial u/\partial t' < 0$) straight line sections.

The noise field will then appear as a train of randomly spaced shock waves. The velocity at any point on one of the negatively sloped sections will be described by an equation of the form of Eq. (3-49). That is, the velocity on a negatively sloped section is of the form

$$u(x,t') = \frac{\beta^{-1} c_o^{\,2} A_{AB}(t'-t_A'(0)) + u_A(0)}{1 - A_{AB}x} \quad . \tag{3-53}$$

where the constants in Eq. (3-53) are as defined for Eq. (3-51). The slope of Eq. (3-53) for constant x is

$$\left.\frac{\partial u}{\partial t'}\right)_x = \frac{\beta^{-1} c_o^{\,2} A_{AB}}{1 - A_{AB}x} \quad . \tag{3-54}$$

For very intense waves at long distances from the source $|A_{AB}x| \gg 1$, and we obtain

$$\left.\frac{\partial u}{\partial t'}\right)_x = -\frac{\beta^{-1} c_o^{\,2}}{x} \quad . \tag{3-55}$$

This result which is equivalent to results reported by Burgers (1972) shows that slopes of the continuous portions of a finite-amplitude wave under the aforementioned conditions are all equal and are proportional to x^{-1}. Moreover, the slopes are independent of the original slopes. The asymptotic form of a noise wave is then a series of randomly spaced shocks separated by straight line sections of equal slope. Since the

intershock sections are of equal slope, the shock velocities, though individually varying, remain constant until merger with another shock.

4. Impedance Relations

Both Eqs. (3-6) and (3-21) are in terms of particle velocity. However, we actually measure pressure. In the continuous portion of the wave, pressure can be easily related to particle velocity. Making use of Eq. (2-2) and the isentropic perfect gas relations, we obtain

$$\frac{P_2}{P_1} = \left(\frac{c_2}{c_1}\right)^{\frac{2\gamma}{\gamma-1}} \quad , \tag{3-56}$$

where the subscripts 1 and 2 are used to indicate the beginning and ending values of the variables in an isentropic process. Substituting Eq. (2-3) into Eq. (3-56), we obtain the result for outgoing waves,

$$\frac{P_2}{P_1} = \left[1 + \frac{\gamma-1}{2}\left(\frac{u_2-u_1}{c_1}\right)\right]^{\frac{2\gamma}{\gamma-1}} \quad . \tag{3-57}$$

Expanding Eq. (3-57) in powers of $(u_2-u_1)/c_1$ yields the result

$$P_2 - P_1 = \rho_1 c_1 (u_2-u_1)\left[1 + \frac{\beta}{2}\frac{u_2-u_1}{c_1} + \frac{\beta}{6}\frac{(u_2-u_1)^2}{c_1^2} + \ldots\right] \quad . \tag{3-58}$$

A result similar to Eq. (3-58) may be derived for the pressure change across a shock. Combining Eqs. (3-9), (3-10), and the relative shock velocity definition (see Fig. (3-1)), we obtain

$$u_2-u_1 = \left[(P_2-P_1)(\tau_2-\tau_1)\right]^{1/2} \quad . \tag{3-59}$$

The specific volume $\tau(s,P)$ is expanded in a Taylor series and this series is substituted into Eq. (3-59). The binomial theorem is then used to expand the result, yielding

$$\frac{u_2 - u_1}{c_1} = \frac{\delta}{\gamma} - \frac{\beta}{2}\frac{\delta^2}{\gamma^2} + \frac{3}{8}\frac{\beta^2\delta^3}{\gamma^3} + \ldots \quad . \tag{3-60}$$

By use of the reversion relations [see, for example, Chemical Rubber Company Handbook (1964)] Eq. (3-60) may be written

$$P_2 - P_1 = \rho_1 c_1 (u_2-u_1)\left[1 + \frac{\beta}{2}\frac{(u_2-u_1)}{c_1} + \frac{\beta^2}{8}\frac{(u_2-u_1)^2}{c_1^2} + \ldots\right] . \tag{3-61}$$

Hence, by comparing Eqs. (3-58) and (3-61) we may make the following statement concerning a simple wave transition and a shock wave transition. The series solutions relating the change in pressure to the change in particle velocity in either transition agree in form for terms through the second power in the change in particle velocity. Moreover, if the magnitudes of the transitions in the two cases are equal, the series are equal through the second term. The error involved in discarding terms above the first order in the change in particle velocity may be easily estimated by evaluating the magnitude of the discarded terms. In general, for waves that may be analyzed by weak-shock theory, this error is small and noncumulative. Hence, for the remainder of this dissertation, we shall use the linear impedance relation

$$P - P_o = \rho_o c_o u \quad , \tag{3-62}$$

where we have replaced the 2 variables by a general unsubscripted variable and the 1 variables by their undisturbed values P_o, ρ_o, c_o and $u_o=0$.

5. Tube Wall Effects

In Chapter 2 we mentioned that McKittrick et al. (1967) and Pernet and Payne (1969) had observed asymmetric waves propagating in plane wave tubes. The source waveforms for both experiments were sinusoids. Using weak-shock theory, we would predict sawtooth waves.

Both McKittrick et al. and Pernet et al. concluded that the asymmetry was due to dispersion caused by the tube wall boundary layer. A typical asymmetric waveform reproduced from the paper by McKittrick et al. is shown in Fig. (3-7).

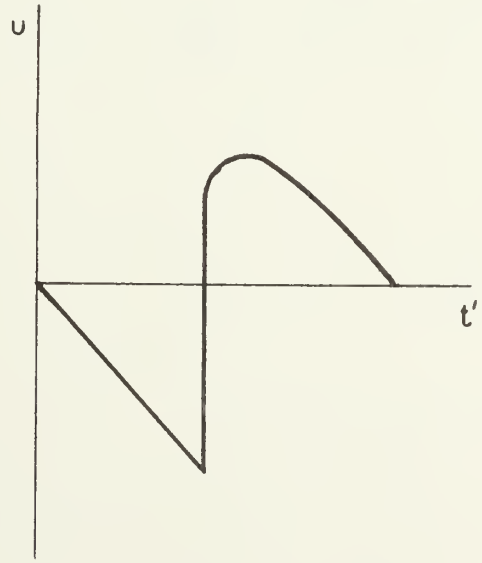

Figure 3-7
A typical shock wave in a plane wave tube.

Coppens (1971) predicted that asymmetry will also be observed before shock formation and based on theoretical considerations concluded that dispersion is the cause.

Since our experimental conditions are very similar to those under which both McKittrick et al. and Pernet et al. worked, it is important to include both tube wall dispersion and attenuation in our analysis. In a wide tube* the approximate expressions for the phase velocity c_ω and attenuation coefficient α obtained from the Kirchhoff theory are

$$c_\omega = c_o\left[1 - \frac{1}{R}\sqrt{\frac{\nu}{2\omega}}\left(1 + \frac{\gamma-1}{\sqrt{Pr}}\right)\right] \quad , \tag{3-63}$$

and

$$\alpha = \frac{1}{R}\sqrt{\frac{\omega\nu}{2c_o^2}}\left[1 + \frac{\gamma-1}{\sqrt{Pr}}\right] \quad . \tag{3-64}$$

*A "wide tube" [the terminology is due to Weston (1953)] is one whose boundary layer thickness Δ is small compared to the tube radius. We shall use Weston's definition of boundary layer thickness, the distance from the tube wall to the point where the principal maximum in particle velocity occurs, i.e., $\Delta = 2.2838(2\nu/\omega)^{1/2}$, where ω is the angular frequency. A further property of a wide tube is that it must not be so wide that losses in the fluid mainstream are comparable to the wall losses. This latter requirement may be stated quantitatively by comparing the expressions for the boundary layer attenuation coefficient and for the unbounded medium attenuation coefficient; one obtains $kR \ll \eta/k\Delta$, where η is a constant determined by the environmental conditions. At 72°F η equals approximately 3.6. Hence, a wide tube is one that meets the combined requirements $\Delta \ll R \ll \eta/k^2\Delta$.

Inspection of Eq. (3-63) shows that the speed of small-signal waves in a tube is less than c_o; the speed approaches c_o only at very high frequencies. Hence, any small-signal nonsinusoidal waveform will be distorted as it propagates in a pipe because the higher frequency components travel faster than the lower frequency components. The differences in phase velocity are small but their effect is cumulative with distance. Use of Eq. (3-63) allows us to calculate the cumulative distortion due to dispersion for small-signal processes. In a nonlinear problem the distortion due to dispersion is less readily calculated because growth of the various harmonics and their intermodulation products is a continuous process.

Equations (3-63) and (3-64) may be used to calculate approximate values of c_ω and α for noncircular ducts if we replace R by D/2 where D is the hydraulic diameter [see, for example, Thompson (1972)]. Therefore, since Eqs. (3-63) and (3-64) are the only portions of modified weak-shock theory that depend upon the pipe shape, the use of the hydraulic diameter concept allows us to also apply the theory to propagation problems in noncircular ducts.

6. Modified Weak-Shock Theory

In this section we shall propose a new theory in which nonlinear effects embodied in weak-shock theory and tube wall effects are combined. The new theory will be called modified weak-shock theory.

For the convenience of the reader, we will restate the Earnshaw solution and the shock arrival equation. The Earnshaw solution is

$$u = g(\varphi) \quad , \tag{3-3}$$

where

$$\varphi \doteq t' + \frac{\beta g(\varphi) x}{c_o^2} \quad . \tag{3-6}$$

The shock arrival equation is

$$\left.\frac{dt'}{dx}\right)_{shock} = -\frac{\beta}{2c_o^2}(u_2+u_1) \quad . \tag{3-22}$$

Given a source waveform, use of the Earnshaw solution and of Eq. (3-22) allows us to calculate the progressive distortion of the continuous portion of the waveform and the movement of the shock front, respectively. As we have indicated previously, our solution technique involves a computer algorithm based upon Eqs. (3-6) and (3-22). The method whereby we account for tube wall attenuation and dispersion is very straightforward. We theorize that the small-signal tube-wall attenuation and dispersion expressions are accurate for short distances. Accordingly, we expect each frequency present to be attenuated and dispersed as described by use of Eqs. (3-63) and (3-64). The attenuation and dispersion relations may be combined in the more compact form given by

$$C_i' = C_i e^{-\alpha_i(1+j)\Delta x} \tag{3-65}$$

where

C_i = the complex amplitude of the ith frequency component of the wave,

C_i' = the complex corrected amplitude,

α_i = the attenuation coefficient evaluated at the angular frequency ω_i, and

Δx = a small distance increment.

In the use of modified weak-shock theory, the transformations between the frequency and time domain are performed by use of an FFT (fast Fourier transform) computer routine. In this routine the various components C_i are assumed to be harmonically related. Therefore, α_i is correctly replaced by $\sqrt{n}\,\alpha_o$, where α_o is the coefficient for the fundamental frequency. Our computer algorithm, which is described in detail in Chapter 4, directly incorporates Eqs. (3-6), (3-22), and (3-65)

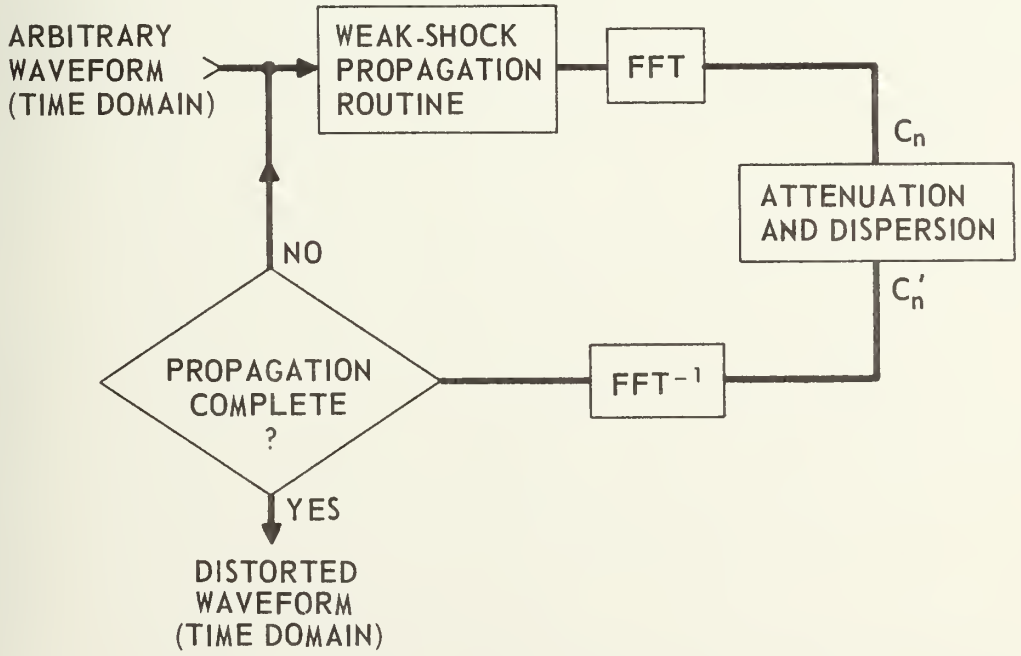

FIGURE 3-8
A SCHEMATIC DIAGRAM OF MODIFIED WEAK-SHOCK THEORY

cast in appropriate forms. The method is summarized in Fig. (3-8).

Implicit in the model that we have called modified weak-shock theory are the following assumptions:

a) Only plane waves are present.

b) The wave amplitude is appropriate, i.e., not too large, for the use of modified weak-shock theory.

c) The pipe is a wide pipe, i.e.,

$$\Delta \ll R \ll \frac{\eta}{k^2 \Delta} \quad .$$

d) The pipe is circular, infinitely long and rigid.

e) The enclosed fluid medium is a homogeneous perfect gas.

CHAPTER 4 THE WAVE PROPAGATION ALGORITHM

1. Introduction

This chapter contains the detailed computer techniques and procedures used to calculate the distortion of a finite-amplitude plane wave of arbitrary form propagating in a pipe. The reader is advised that he need not read Chapter 4 unless he is interested in the actual computational details. For those not so interested, we suggest examination of Figs. (4-4), (4-5), and (4-6) and reading of the paragraph just prior to the figures. This material gives a general idea of the distortion of a high intensity noise waveform and prepares the reader for the results presented in Chapter 6.

In the opening section of the chapter, the weak-shock theory described in Chapter 3 is restated and the pertinent equations are cast into finite difference form; these difference equations are solved, thereby opening the way to the formulation of a computer routine that implements weak-shock theory.

The method used to incorporate attenuation and dispersion into the basic weak-shock algorithm is then considered, and the final form of the modified weak-shock theory is presented. The next portion of the chapter is devoted to outlining the solutions of some minor computational problems and indicating how we selected values for several important program parameters.

The chapter is concluded with a discussion of the programs that were used to calculate power spectral densities.

2. Discretization of the Weak-Shock Theory Equations

The basic equations of weak-shock theory were derived in Chapter 3. For the convenience of the reader we shall repeat the equations here. Consider a plane wave whose time waveform at the source is given by

$$u = g(t) \quad . \tag{3-2}$$

The particle velocity away from the source is then described by

$$u = g(\varphi) \quad , \tag{3-3}$$

where

$$\varphi = t' + \frac{\beta u(\varphi) x}{c_o^2} \quad . \tag{3-6}$$

Equations (3-3) and (3-6) constitute the Earnshaw solution. The Earnshaw solution is used in weak-shock theory to describe the distortion of the continuous portions of the propagating sound wave. Once shocks have formed, the retarded time of occurrence of a particular shock is described by the differential equation

$$\left.\frac{dt'(x)}{dx}\right)_{\text{shock}} = -\frac{\beta}{2c_o^2}\left[u_1(x,t'(x)) + u_2(x,t'(x))\right] \quad . \tag{3-22}$$

The values of u_2 and u_1 used in Eq. (3-22) provide the means of connecting the Earnshaw solution on one side of the shock with the Earnshaw solution on the other side.

It is convenient, at this point, to extend our interpretation of Eq. (3-6) so that use of Eq. (3-6) describes the time shift between t' and any previous retarded time rather than the time shift between t' and the time of generation of the wavelet. The extension is implemented by replacing φ by t'_{old}, t' by t'_{new}, and x by Δx where Δx represents the incremental propagation distance over which t'_{old} is distorted into t'_{new}. Once we have made these substitutions, we obtain

$$t'_{new} = t'_{old} - \frac{\beta u(t'_{old})\Delta x}{c_o^2} \quad . \tag{4-1}$$

Equations (4-1) and (3-22) constitute a system that we shall use to describe the distortion of a source waveform as it propagates. Our goal is to determine the output of this system for an arbitrary input waveform. For simple cases, this determination can be made by analytic methods, but, as Sections 2 and 3 of Chapter 3 suggest, the analytic methods become increasingly cumbersome for complicated waveforms. Hence, we desire a computer method that describes the continuous system represented by Eqs. (3-22) and (4-1). In practice a continuous system can be approximated by replacing the continuous equations by difference equations. This is required if we wish to use a digital computer to calculate the system response to various inputs.

In the system under consideration, the governing relations are very simple and the difference equations can be written by inspection. For higher-order systems, the transition to a difference format is not so simple and a formal mathematical technique is required to ensure the

generation of the proper equations. The state variable techniques used by Ogata (1967) constitute such a method. Proceeding either by the state variables method or simply by inspection, we obtain the difference forms of Eqs. (4-1) and (3-22). These forms are, respectively,

$$t'[(k+1)h] = t'[kh] - \beta c_o^{-2} u[t'(kh)]h \qquad (4\text{-}2)$$

and

$$t_s'[(k+1)h] = t_s'[kh] - \frac{\beta h c_o^{-2}}{2}\left[u_2[kh,t_s'(kh)] + u_1[kh,t_s'(kh)]\right], \qquad (4\text{-}3)$$

where

h = an incremental distance,

$t'[(k+1)h]$ = the value of t' after $k+1$ incremental steps of size h,

t_s' = the value of t' associated with a particular shock,

$t_s'[(k+1)h]$ = the value of t_s' after $k+1$ steps of size h, and

$u_{1,2}[(kh,t_s'(kh)]$ = the value of particle velocity in front of and behind the shock, respectively, after k incremental steps of size h.

A potentially confusing point is raised by the notation $u[t'(kh)]$ used in Eq. (4-2). When we use the Earnshaw solution analytically, we compute the value of u as a function of t' for any point in the (u,t') plane. Note, however, that the value of u associated with a particular wavelet is fixed. In our algorithm we distort the time base using Eq. (3-6), calculating the new time of arrival of some particular wavelet. The values of u in our application of the Earnshaw solution remain constant. Hence, we could conceivably use the source values of u in Eq. (4-2). In our implementation of Eq. (4-2), however, we shift and renumber

the values of u and t' associated with a particular wavelet. The reason for the shifting and renumbering is made clear below. The important consideration here is that, although the value of u associated with a particular wavelet is unchanged from its source value by use of the Earnshaw solution, the location of this point in the sequence of wavelets may be changed. Hence, we specifically keep track of individual values of u as a function of kh.

In Eq. (4-2) note that the value of t'[(k+1)h] is completely determined by the value of t' after kh steps and the corresponding value of u after kh steps. Similarly, the value of t_s' after (k+1)h steps is dependent only upon the value of t_s' after kh steps and the mean particle velocity at the shock after kh steps. Use of Eq. (4-3) requires that the value of $t_s'(kh)$ be retained for use in the calculation of $t_s'[(k+1)h]$. In a complicated wave having many shock fronts, this requirement could become difficult as one shock merged with another. The potential difficulty may be avoided by substituting for u_2 and u_1 in Eq. (4-3) using Eq. (4-2) evaluated at $t_s'(kh)$. Carrying out the above steps, we obtain

$$t_s'[(k+1)h] = t_s'(kh) - \frac{1}{2}\left[t_2'(kh) - t_2'[(k+1)h] + t_1'(kh) - t_1'[(k+1)h]\right] \quad . \tag{4-4}$$

Recognizing that $t_1'(kh) = t_2'(kh) = t_s'(kh)$, we obtain the important result,

$$t_s'[(k+1)h] = \frac{t_2'[(k+1)h] + t_1'[(k+1)h]}{2} \quad . \tag{4-5}$$

Equation (4-5)* is a solution of Eq. (4-3) and provides a very simple method for placing the shock. We stress that Eq. (4-5) is a solution of Eq. (4-3) only for a small step size, that is, it is a solution only of the finite difference form of the shock occurrence equation.

3. The Weak-Shock Theory Wave Propagation Algorithm

A computer algorithm implementing Eqs. (4-2) and (4-5) has been written. The computer language used in this algorithm is FORTRAN IV. We shall explain in detail here the actual steps used in the algorithm. Because the algorithm itself is rather complicated, the reader is encouraged to refer frequently, while reading this section, to the program listing and flowchart that appear in Appendix A. Throughout the ensuing discussion reference to specific variables, arrays, members of arrays, and so on is in FORTRAN notation. Thus, the Ith element of the T array is T(I).

The algorithm is implemented in a subroutine WAVEPROP that is called by a driver program. We shall limit our interest in the present section to this subroutine. A simplified flowchart of WAVEPROP appears in Fig. (4-1).

Before we commence the detailed discussion of WAVEPROP, we shall define and discuss a minor problem that exists in WAVEPROP. We call this problem the "end point" problem. Equation (4-2) distorts values in the T array. Hence, it is possible for the value of time of a

*Equation (4-5) is a finite difference approximation of the "Landau Rule". The "Landau Rule" is fully discussed by Landau and Lifshitz (1959).

point close to either end of the data to be distorted out of the original waveform time base. We refer to a distortion of this nature as an "end point" problem. The reason it is a problem is that in writing WAVEPROP we must make some assumption concerning particle velocity values outside the original time base. In the present version of WAVEPROP we assume that particle velocity values outside the original time base are unknown. Hence, if the time value of a waveform point is distorted outside the original time base we are unable to compute the new waveform at that point. We recognize that other assumptions concerning conditions outside the original time base could have been made and implemented. The present version of WAVEPROP could be modified to accommodate these new assumptions.

Subroutine WAVEPROP contains two self-checking tests that monitor for end point problems and upon detection halt program execution. The tests are identified in WAVEPROP as the variables TLEFT and TRIGHT. When the program is halted a diagnostic message is printed, the form of which is*

EXCEEDED TIME BASE TO [LEFT / RIGHT] DISTANCE = YY KK ITERATIONS

*We omit normal punctuation in lines containing FORTRAN statements where inclusion of the punctuation could give the impression that the punctuation is part of the FORTRAN statement.

The word LEFT or RIGHT indicates that some T array value has been distorted to a value less than the original value of T(1)* or greater than the original value of T (NPOINTS), respectively. The value of distance printed (YY) is the value of the variable DISTANCE in the call to WAVEPROP. The number of iterations printed (KK) is equal to the value of the index being used in loop 1 [see Fig. (4-1)] at the point of program interruption.

End point problems may be easily avoided. We have used two methods, depending upon the type of wave that we are considering. For periodic deterministic waves, we select the phase of the initial waveform in such a fashion that when shocks form, they form in the center of the cycle, and the particle velocities associated with T(1) and T(NPOINTS) are zero. When studying nonperiodic deterministic waveforms or noise waveforms, we place a buffer of points having zero particle velocity at both ends of the original waveform. The subject waveform can then expand its time base during computer propagation into the buffer zones. For the random noise waveforms that we investigate later in this work, buffer zones approximately five percent as long as the total original waveform were successfully used.

The subroutine call is

CALL WAVEPROP(U, T, DISTANCE, DISINC, NPOINTS)

---

*In the form of WAVEPROP presented here, we are required to set T(1)=0.0 However, T(1)=0.0 is merely a convenience and any value of T(1) is acceptable. If a value of T(1) not equal to 0.0 is used, the TLEFT test must be changed to use this new value.

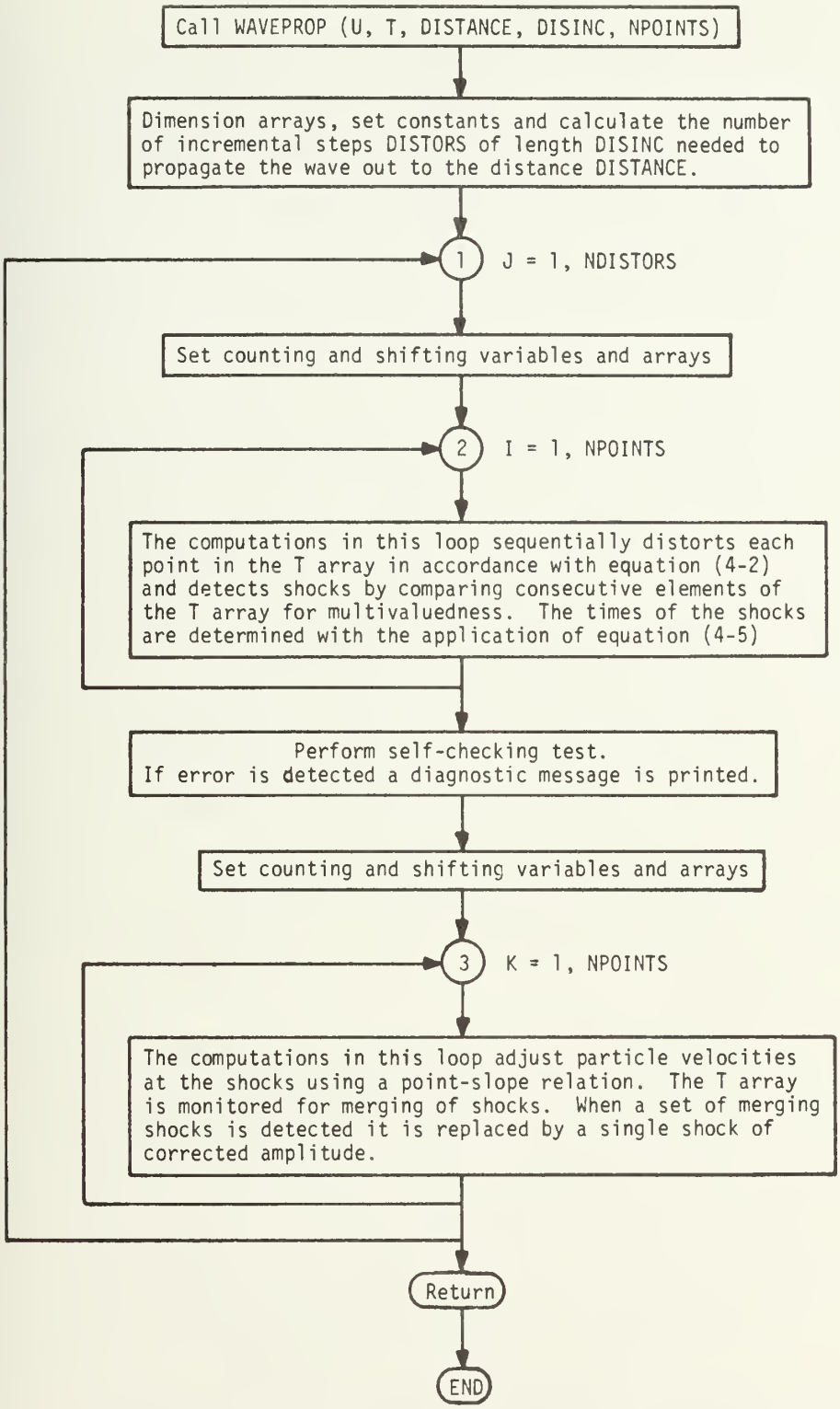

FIGURE 4 - 1

A Simplified Flowchart of Subroutine WAVEPROP

where

U is a real one-dimensional array describing the particle velocity of a point on the subject waveform in either English or metric units. If metric units are used, the small-signal sound speed c_o must be supplied in metric units. If English units are used, c_o at 72°F is already supplied in the program.

T is a real one-dimensional array describing the time coordinate (in seconds) for a particular point on the subject waveform. The doublet (T(I), U(I)) then describes the Ith waveform point.

DISTANCE is a real variable. It is the distance over which we wish to propagate the wave described by U and T.

DISINC is a real variable. It is the incremental step size used to cover the distance DISTANCE.

NPOINTS is an integer variable. It is the number of waveform points.

The wave to be propagated enters the subroutine and is returned through the formal parameters U and T. The quantity NPOINTS must be entered as a variable, not a constant, since WAVEPROP changes NPOINTS and returns a new value. WAVEPROP enables us to calculate the distortion of the wave over the distance given by the real variable DISTANCE. The number of propagation steps NDISTORS is set by the relation

$$\text{NDISTORS} = \text{DISTANCE}/\text{DISINC} + 0.5 \qquad (4\text{-}6)$$

Computer operation causes NDISTORS to round off to the nearest integer. If DISTANCE is not an integral multiple of DISINC, the number of steps

computed may be in error by one. The possibility of such an error is avoided by requiring that DISTANCE be an integral multiple of DISINC.

Referring to Fig. (4-1) we observe that WAVEPROP consists of an outer DO loop (loop 1) that is stepped through the NDISTORS propagation steps and two inner DO loops (loops 2 and 3) that are stepped through the NPOINTS points. For each propagation step the entire waveform must be distorted as prescribed by Eq. (4-2), the shocks (if any are present) placed in accordance with Eq. (4-5), and the velocities at the shocks adjusted to reflect the shock growth or decay. In addition, occurrences of shock merging must be detected and a single shock described at the merger location. In the ensuing discussion of WAVEPROP we have, for clarity, described some operations as occurring serially. In reality several of these operations are performed in a parallel fashion.

The calculations required to perform the tasks outlined in the preceding paragraph are divided between loops 2 and 3 as shown in Fig. (4-1). The function of loop 1 is merely to step the subject wave through the NDISTORS steps thereby propagating the wave the distance DISTANCE. For each NDISTORS step, of course, loops 2 and 3 are used to perform the necessary computations.

Prior to each entry into loop 2, arrays NS and TS and variable NSHIFT are set equal to zero. The quantities TS, NS and NSHIFT are utilized for counting and shifting purposes that will become clear as we proceed.

The first task performed using loop 2 is the sequential distortion of each point in the T array and the detection of any multivaluedness in T following the distortion calculation. The

distortion, computed using Eq. (4-2), is that suffered by a particular wavelet in propagating a distance DISINC. Multivaluedness in T is detected by comparing each T(I) to T(I-1). If for any value of I we find that

$$T(I) \leq T(I-1) \quad , \tag{4-7}$$

multivaluedness is indicated. The variable TLOW is used in the check for multivaluedness. Prior to entry into loop 2, the quantity TLOW is set as follows:

$$TLOW = T(1) - 1.0 \quad . \tag{4-8}$$

The purpose of Eq. (4-8) is to initially set TLOW out of the time span defined in the T array. The quantity T(1) is then distorted and compared to TLOW. Since the typical time shift per propagation step is much less than one second, the initial setting of TLOW should preclude the result

$$T(1) < TLOW \quad . \tag{4-9}$$

Let us assume that result Eq. (4-9) is not realized. TLOW is then changed to T(1) and compared to T(2). The scheme is repeated, that is, TLOW is set equal to T(I-1) and compared to T(I) until we obtain the result (4-7) or loop 2 is completed. Result (4-7) indicates that the sequence of time values stored in the T array is no longer monotonic, which in turn indicates the presence of a shock within the

multivalued region.* If result (4-7) is not obtained, no shocks are present.

The location of the shock, and the number of points within the multivalued region must now be determined. We make the determination by proceeding as before, comparing TLOW to each T(I). When we obtain the result

$$T(I) > TLOW \quad , \tag{4-10}$$

the end of the multivalued region has been identified. In accordance with Eq. (4-5), the shock is then located midway between the vertex** points of the multivalued region. If it is the first shock found, it is labeled NS(1) and its location is stored in TS(1). Shocks detected later are labeled NS(2), NS(3), etc., and their locations stored in TS(2), TS(3), etc. If there are waveform points having indices between the indices of the two vertex points they are counted and their number stored in NSHIFT. The in-between points are now unnecessary since the region is completely described for our purposes by its vertex points. Hence, in order to increase computational efficiency the NSHIFT unnecessary points are shifted out of the U and T arrays and points having indices greater than the index of the right vertex are renumbered.

---

* We use the term multivalued region(s) to indicate those portions of the sequence of times stored in the T array that are not monotonic.

** The right and left vertex points of a particular multivalued region define the time limits of the region, the left vertex point being the low time limit and the right vertex point the high time limit. In Fig. (4-2b) the point (I-1) is the right vertex and the point I is the left vertex of the multivalued region pictured.

An illustration of the occurrence of multivaluedness is shown in Fig. (4-2).

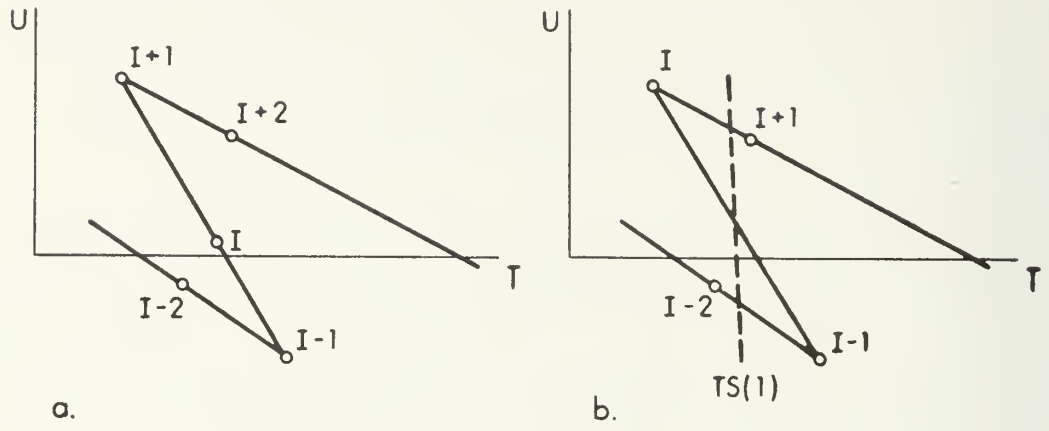

FIGURE 4-2
A SECTION OF A FINITE-AMPLITUDE WAVE ILLUSTRATING THE COMPUTATIONS PERFORMED IN LOOP 2. THE CIRCLES ARE WAVEFORM POINTS.

a. THE WAVEFORM AFTER DISTORTION BY EQ. (4-2).
b. THE WAVEFORM FOLLOWING THE RENUMBERING OF THE POINTS AND THE PLACEMENT OF THE SHOCK (TS(1)).

Figure (4-2a) depicts a section of an arbitrary wave between the points (I-2) and (I+2). The multivalued waveform in Fig. (4-2a) has been generated using Eq. (4-2). Proceeding as described above identifies the (I-1) point and the (I+1) point as the vertex points of the multivalued region. A shock labeled TS(1) (we assume this is the first such region detected) has been placed midway between the vertex points in Fig. (4-2b), the Ith point shown in Fig. (4-2a) has been shifted out, and appropriate points have been renumbered. In Fig. (4-2b) the vertex points are the Ith and (I-1)th points. Figure (4-2b) illustrates the extent of the loop 2 computations. The wave is still multivalued and, while the shock has been located, there has been no adjustment of the

multivalued wave at the shock location. These operations will be performed in loop 3, where the final waveform is computed.

After the completion of loop 2, we test via program steps in WAVEPROP, for end point problems. We then proceed to loop 3 unless an end point problem has been detected, in which case, the program is halted.

The propagation of the wave over the distance DISINC is completed by use of loop 3. The calculations performed in loop 3 complete the waveform corrections at the shocks begun in loop 2, detect shock mergers, and describe the waveform at the point of shock merger. Recall that in loop 2 there was no adjustment of the magnitude of the particle velocity values. All that we did was to implement the Earnshaw solution and calculate the time of occurrence of each shock. The Earnshaw solution does not affect the magnitude of the particle velocity of the waveform points. Hence, all actual adjustment of particle velocity magnitude at the various waveform points is performed in loop 3.

The arrays TS and NS and the variable NSHIFT are again zeroed before we start the loop 3 computations.*

---

*The variable NSHIFT is zeroed because the unnecessary points defined in loop 2 have been shifted out and zeroing NSHIFT is a preparatory step for counting any additional unnecessary points defined during the loop 3 computations. The rationale behind the zeroing of TS and NS is not quite so straightforward. The arrays TS and NS are used in loops 2 and 3 to store shock locations and identifying numbers. We use the information stored in TS and NS within both loops 2 and 3. It turns out to be more efficient, however, to zero TS and NS following the loop 2 computations and recompute the shock locations and identifying numbers during the loop 3 computations.

Let us assume, as we start the loop 3 computations, that the time sequence stored in the T array contains one or more multivalued regions. If it does not, the results of the loop 3 computations merely confirm the monotonicity of the time sequence and control passes back to loop 1. Thus, assuming the presence of multivaluedness in the time sequence, we again scan the T array in order to locate the various multivalued regions and their vertex points. The scan of the T array is done in exactly the same manner as was done in loop 2. Let us assume that we have located the right vertex of a particular multivalued region. We now commence a backward scan through the T array, searching for the first waveform point having a time value less than the time of the shock associated with the region. The purpose of this backward scan is to assist in adjusting the particle velocity in front of the shock. Let us call the T array member of the desired point T(J). The points T(J) and T(J+1) straddle the shock time. The value of particle velocity immediately in front of the shock is computed by using T(J), T(J+1), U(J), U(J+1), and the shock time in a simple interpolation relation. In the actual computation in loop 3 the shock time is called TAVG. The value of particle velocity in front of the shock is given by the relation

$$U(J+1) = U(J) + \frac{U(J+1) - U(J)}{T(J+1) - T(J)} [TAVG - T(J)] \quad . \qquad (4\text{-}11)$$

The T array is then adjusted so that

$$T(J+1) = TAVG \quad . \qquad (4\text{-}12)$$

The net effect of the use of Eqs. (4-11) and (4-12) is to locate a waveform point immediately in front of the shock.

The next computation performed after placement of the waveform point immediately in front of the shock is the removal of unnecessary points. Let us assume that in the aforementioned backward scan one or more waveform points were tested before the desired point in front of the shock was found. These intervening points are now unnecessary because only two points are required to describe a shock. As was done in loop 2, the intervening points are shifted out of the U and T arrays.

We now commence a forward scan of the T array starting at the shock time. The goal of forward scan is to locate the first point having a time greater than the shock time. Once we have located the desired point, the particle velocity and time of the point just behind the shock are calculated using relations similar to Eqs. (4-11) and (4-12). Then any additional unnecessary waveform points are shifted out.

Shock merging, mentioned earlier, is handled as an integral part of the loop 3 calculations previously described. Recall that after we initially locate each shock, the T array is scanned backwards in order to discover the first waveform point in front of the shock. During the backward scan other shocks may be encountered before the desired point is found. In that case, the shock being considered will have overtaken and passed the other shocks that were encountered. The fact that other shocks have been overtaken does not alter at all the loop 3 computations previously described. The only additional computation required is the adjustment of the TS and NS arrays to reflect the adjustment in the location and number of shock.

A particular example of shock merging appears in Fig. (4-3). In considering the waveforms in Fig. (4-3), the reader is cautioned that these drawings exaggerate the distortion that will occur in one propagation step. In using the difference Eqs. (4-2) and (4-5) we assume that the distance step size is very small. Typically,

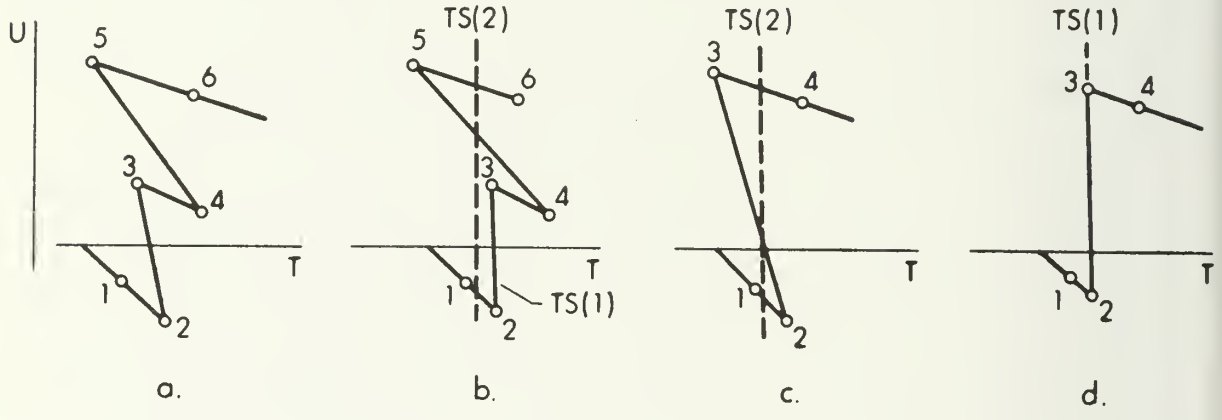

Figure 4-3
A section of a finite-amplitude wave illustrating the computations performed in loop 3. (a) The wave upon entry into loop 3. (b) The wave has been partially corrected by the formation of the shock between points 2 and 3 and the calculation of TS(2). (c) The wave has been further corrected by shifting out data points in the overlap region. (d) The final, fully corrected, waveform.

the change in a time coordinate during one propagation step of size 0.1 ft is less than 10^{-6} sec. In Fig. (4-3) the waveform points have been numbered rather than given the more general labels used elsewhere in this chapter. Figure (4-3a) depicts the subject waveform upon entry into loop 3. Figures (4-3b and 3c) show the waveform as we are processing it during the course of loop 3. In Fig. (4-3b) the first shock TS(1) has been located, points 2 and 3 have been corrected, and the second shock TS(2) has been located to the left of TS(1). The fact that TS(2) is to the left of TS(1) indicates a shock overtaking situation. The first step

in the correction of this situation is indicated in Fig. (4-3c) where waveform points between points 2 and 5 in Fig. (4-3b) have been shifted out and points 5 and 6 renumbered. The final corrected waveform is shown in Fig. (4-3d); note that the shock time has been labeled TS(1).

In the following sequence of figures, the overall effects of nonlinear propagation, as computed using WAVEPROP, are illustrated. For simplicity a source signal consisting of straight line sections has been used. In Fig. (4-4) the source waveform is shown. There are no shocks present initially and the signal contains a number of local extrema. In Fig. (4-5) the signal has been propagated 12 ft using WAVEPROP; several shocks have formed and some of the small shocks have already been overtaken. Figure (4-6) shows the waveform at 24 ft. The waveform is now approaching the asymptotic form described in Chapter 3. The reader should note that the vertical scales in the three figures are different.

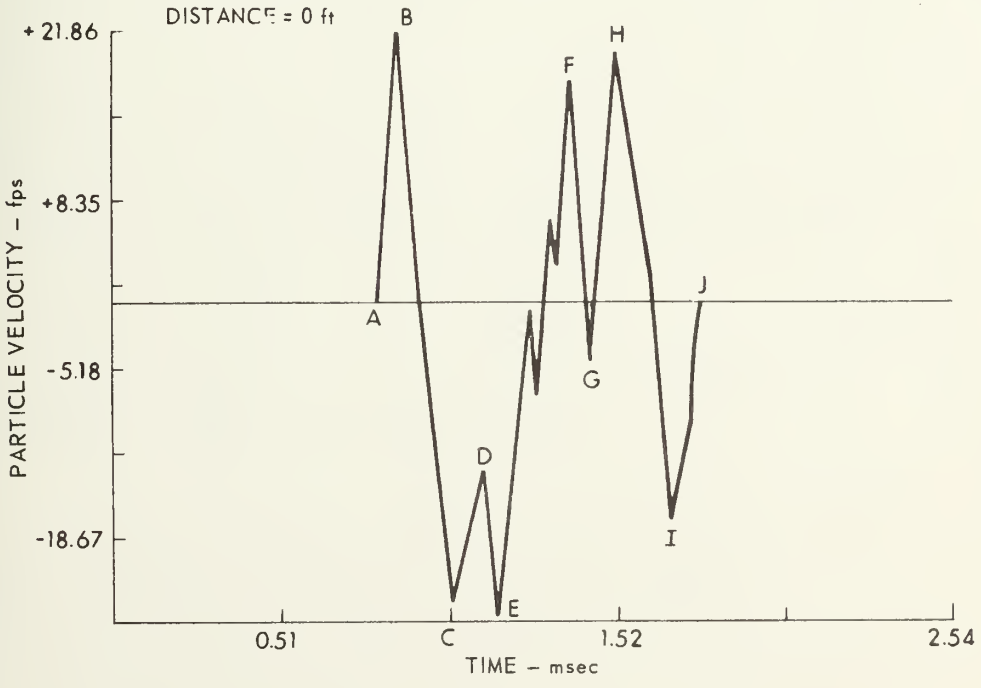

FIGURE 4-4
THE SOURCE WAVEFORM
WAVEFORM EXTREMA HAVE BEEN LABELED TO ASSIST THE READER IN FOLLOWING SPECIFIC WAVEFORM POINTS AS THEY ARE PROPAGATED

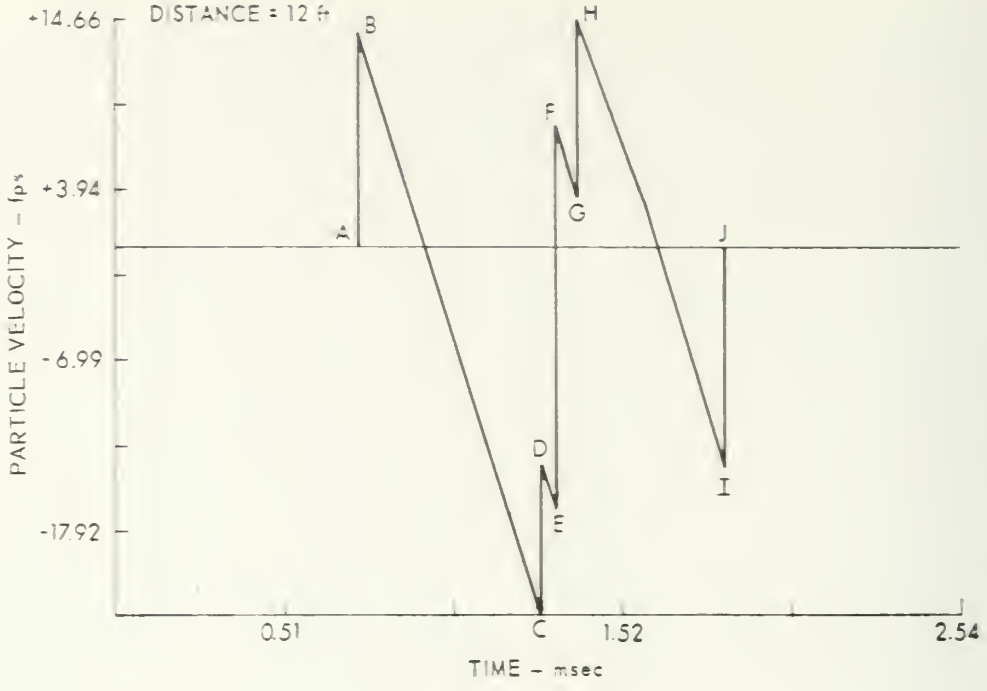

FIGURE 4-5
THE WAVE SHOWN IN Fig. 4-4 PROPAGATED 12 ft

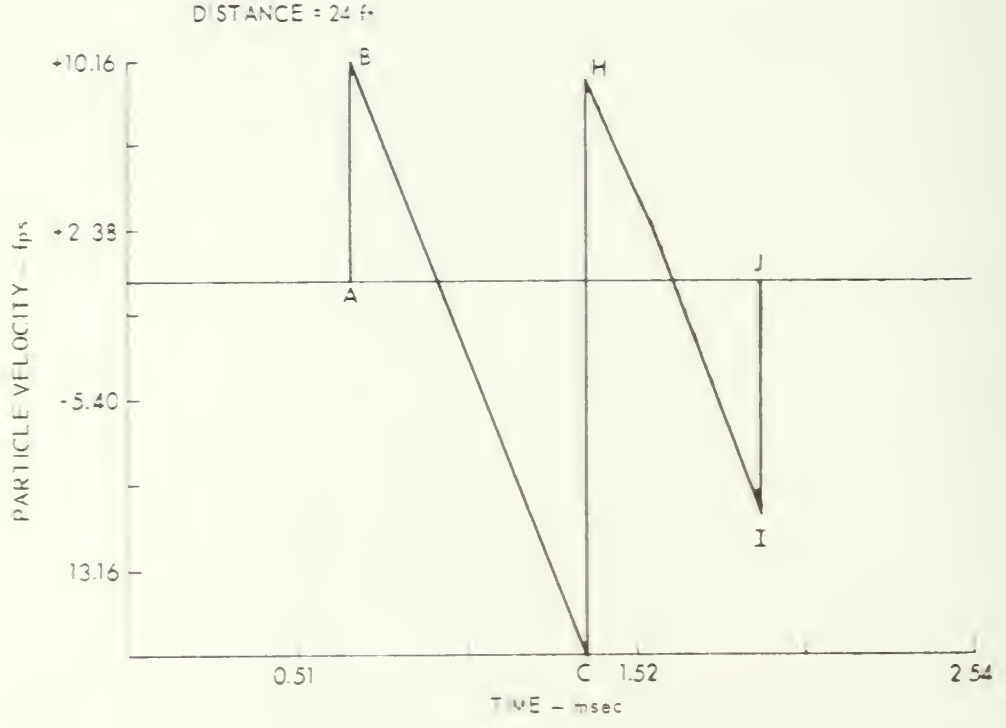

FIGURE 4-6
THE WAVE SHOWN IN Fig. 4-4 PROPAGATED 24 ft
NOTE THAT POINTS D-G HAVE MERGED INTO
THE SHOCK DESCRIBED BY THE SEGMENT CH

4. The Proper Form for Applying the Attenuation and Dispersion Corrections

In Chapter 3 we theorized that attenuation and dispersion can be incorporated into the propagation algorithm by assuming that small-signal tube wall theory may be used even for finite-amplitude waves provided the distance increment of propagation is small.

In this section some mathematical details associated with this incorporation are considered. Nonlinear distortion, as implemented using WAVEPROP, is computed in the time domain. The corrections for attenuation and dispersion are made in the frequency domain. Transformations between the time and frequency domain are performed by use of a fast Fourier transform (FFT) computer subroutine. The FFT is a harmonic analysis. Hence, we must modify Eq. (3-65) as follows:

$$C_n' = C_n e^{-\sqrt{n}\alpha_o(1+j)x} \quad , \qquad (4\text{-}13)$$

where α_o is the value of α at the fundamental frequency. In the study of random waveforms the fundamental frequency is defined as the reciprocal of the time duration of the sample waveform. The actual method of application of Eq. (4-13) is described below.

At any distance x the waveform being propagated F(t') can be approximated by the finite Fourier series,

$$F_N(t') = \sum_{n=1}^{N} U_n \cos n\omega_o t' + UI_n \sin n\omega_o t' \quad , \qquad (4\text{-}14)$$

where

ω_o = the fundamental frequency,

$F_N(t')$ = N term approximation of $F(t')$, and

U_n and UI_n = Fourier coefficients of the nth series term.

We may express the complex amplitude of the nth term of Eq. (4-14) as follows:*

$$C_n = U_n - jUI_n \quad . \tag{4-15}$$

Substituting Eq. (4-15) into Eq. (4-13), we obtain

$$C_n' = U_n' - jUI_n \quad ,$$

where

$$U_n' = e^{-\sqrt{n}\alpha_o x}\left[U_n \cos \sqrt{n}\,\alpha_o x - UI_n \sin \sqrt{n}\,\alpha_o x\right] \quad ,$$

and

$$UI_n' = e^{-\sqrt{n}\alpha_o x}\left[UI_n \cos \sqrt{n}\,\alpha_o x + U_n \sin \sqrt{n}\,\alpha_o x\right] \quad . \tag{4-16}$$

*The FFT used in the actual computations calculates the complex conjugate of the transform. Hence, we shall use the complex conjugate in our frequency domain analysis.

Hence, the proper form of $F_N(t')$ after the attenuation and dispersion corrections is

$$F_N^C(t) = \sum_{n=1}^{N} \left[U_n e^{-\sqrt{n}\alpha_o x} \cos\left(n\omega_o t' - \sqrt{n}\,\alpha_o x\right) + UI_n e^{-\sqrt{n}\alpha_o x} \sin\left(n\omega_o t' - \sqrt{n}\,\alpha_o x\right) \right] , \tag{4-17}$$

where

$F_N^C(t')$ = the corrected form of $F_N(t')$.

The value of x used in Eqs. (4-13), (4-16), and (4-17) is not a distance from the origin; rather it is the distance since the last waveform correction for attenuation and dispersion. In the computer programs that implement modified weak-shock theory (see Section 5 of this chapter), the selection of the proper propagation distance between attenuation and dispersion corrections is a key factor. We have theorized that we can use small-signal Kirchhoff theory when it is applied over a small distance increment. In our programs this small distance increment is designated XL. In the developmental testing of our algorithm, various values of XL were tried. In general, we found that XL must be small but not so small that we encounter the "resampling" problem explained in Section 6 of this chapter. While we cannot offer any formulae or rules for choosing the optimum value of XL, we do give some guidelines in Section 6 of this chapter.

In the computer implementation of weak-shock theory, the corrected coefficients U_n' and UI_n' are computed exactly as shown in Eq. (4-16). We require that the corrected waveform in the time domain be a real function of time. Hence, the correction terms are applied in the frequency domain in such a fashion that sequence $\{U_1', U_2', \ldots, U_n'\}$ is even and the sequence $\{UI_1', UI_2', \ldots, UI_n'\}$ is odd about the (n/2+1)th point.

5. The Modified Weak-Shock Algorithm

In this section we shall show how the various elements of modified weak-shock theory are fit together. Several subroutines are used in our algorithm. Subroutine WAVEPROP has already been described. The other subroutines are described in this section.

a. The "Driver" Programs

In a general sense the implementation of modified weak-shock theory is exactly as indicated in Fig. (3-8). The waveform to be studied is read into the computer and propagated a short distance using WAVEPROP. The resulting distorted waveform is Fourier transformed and the attenuation and dispersion corrections are made. The corrected frequency domain result is then inverse transformed and another propagation step is taken. In this way, the wave is propagated out to the desired distance. In Appendix B typical driver program listings and flowcharts for two cases of interest are presented. The first of the programs, PROGRAM ATENDIS5, was used to generate the theoretical predictions for initially sinusoidal waveforms. The second, PROGRAM NSATDIS, was used for noise waveforms. The fundamental method in both cases is

identical. The programs differ in some minor peripheral aspects. Each program contains provision for propagating the subject wave by both weak-shock theory (i.e., nonlinear effects only) and modified weak-shock theory (i.e., nonlinear effects plus tube wall attenuation and dispersion corrections). Often the program user does not require that both sets of computations be done. In this case, the undesired portion of the program may easily be bypassed by the insertion of appropriate program statements. The variables used in the two programs are defined in the listings which appear in Appendix B. Typical values of some of these variables are discussed in Section 7 of this chapter.

Early in the listings of both NSATDIS and ATENDIS5, the user is cautioned that the dimension of U and T must exceed by two the number of points needed to describe the wave. The reason for the extra points is simple although somewhat obscure. NSATDIS and ATENDIS both call a plotting routine called WAVEPLOT. WAVEPLOT in turn calls a scaling routine (SCALE) that scales numbers to values appropriate for the plot size desired. We utilize the two extra locations in the U and T arrays to store 1) the array minimum value, and 2) the incremental point separation, both of which are calculated by use of subroutine SCALE.

b. The Subprograms

Five subprograms called by programs ATENDIS5 and NSATDIS are described in this subsection. Unless otherwise indicated, flowcharts and listings for these subprograms appear in Appendix C. The functions of three of the subprograms are obvious. The functions of subprograms RESAMPLE and FIXER, however, are not obvious. In Section 6 we include a detailed discussion of the functions of RESAMPLE and FIXER.

1) Function ALPHA. This function is used to calculate the value of the Kirchhoff attenuation and dispersion coefficient α. We implement Eq. (3-64) in function ALPHA. The function call is

A = ALPHA(N,FO)

where

N = the harmonic number, and

FO = the fundamental frequency.

A = a storage location for the number returned by ALPHA.

Since ALPHA is so simple, neither a flowchart nor listing of ALPHA has been included. The radius, R, must be provided by the user in ALPHA.

2) Subroutine FFTC. This subroutine is a fast Fourier transform (FFT) available as a library routine on the CDC 3200 facility at the Applied Research Laboratories, The University of Texas at Austin. It was written in COMPASS by James D. Beard. The subroutine call is

CALL FFTC(X,Y,M)

where

X is a real one-dimensional array containing the real part of the input and output functions,

Y is a real one-dimensional array containing the imaginary part of the input and output functions,

M The number of points in x and y to be transformed is 2^M.

Since subroutine FFTC is a standard library routine, its flowchart and listing are not included here.

3) Subroutine RESAMPLE. This subroutine is used to resample the subject waveform. The subroutine call is

CALL RESAMPLE (U, T, N, NPOINTS, DT)

where

U is a real one-dimensional particle velocity input-output array,

T is a real one-dimensional time input-output array,

N is an integer variable equal to the number of output data points desired,

NPOINTS is an integer variable equal to the number of input data points,

DT is a real variable equal to the sampling interval of the output data points.

The N output data points are computed by an interpolation scheme. A test in the program halts execution if interpolation proceeds beyond the end of the input data. In this case, the diagnostic message

NN EXCEEDED NPOINTS

is printed. The routine will work correctly for N both greater than and less than NPOINTS. Subroutine RESAMPLE requires a scratch space of 1200 floating point words. If the dimension of U and T were to exceed 1200, this scratch space would have to be increased.

4) Subroutine FIXER. The subroutine call is

CALL FIXER (U, T, PHI, N, ISTEP, PER)

where

U is a real one-dimensional particle velocity input-output array,

T is a real one-dimensional time input-output array,

PHI is a real one-dimensional output array, whose Ith element contains the phase shift detected in the Ith call to FIXER,

N is an integer variable, equal to the number of points in the U and T array plus 1,

ISTEP is an integer variable that counts the calls to FIXER,

PER is a real variable equal to the period in seconds of the waveform described by the U and T arrays.

FIXER does not contain any diagnostic tests. Subroutine FIXER calls subroutine RESAMPLE. Hence, FIXER cannot be used without RESAMPLE. FIXER requires 2 scratch arrays of dimension 513 floating point words each. If the dimension of U and T were to exceed 515, these scratch arrays would have to be increased.

5) Subroutine WAVEPLOT. Subroutine WAVEPLOT is used to plot waveforms. The subroutine call is

CALL WAVEPLOT(U, T, DISTANCE, NPOINTS, ISW, TAXIS, UAXIS, VA)

The definitions of the formal parameters are as follows:

U is a real one-dimensional particle velocity array.

T is a real one-dimensional time array.

DISTANCE is a real variable equal to the propagation distance at which the plot is drawn.

NPOINTS is an integer variable equal to the number of data points to be plotted.

ISW is an integer variable switch whose value may be 0 or 1. ISW sets the plot vertical size. If ISW=0 every call to WAVEPLOT produces a plot UAXIS inches high. In subsequent

calls the vertical size of the plotted curve is adjusted to maintain the proper amplitude proportionality between the waveforms at the first call distance and at the later distance.

TAXIS is a real variable equal to the length in inches of the horizontal (time) axis.

UAXIS is a real variable equal to the length in inches of the vertical (particle velocity) axis.

VA is a real variable that adjusts the vertical axis for oscilloscope vertical amplification. When used with ISW=1 it allows direct comparison between oscillograms and computer plots. If ISW=0 set VA=1.

WAVEPLOT calls a number of standard plotting subroutines. The plotter utilized was a CALCOMP model 565. The plotting subroutines are fully explained in the Applied Research Laboratories plot manual (1973). The plotting subroutines used were

a) PLOT,

b) SCALE,

c) LINE,

d) AXIS,

e) PLOTLINE.

One additional plotting subroutine called subroutine PLOTBUFF was used. Use of PLOTBUFF allows us to CALCOMP plot while the computer proceeds with other tasks in the program being processed. Parallel operation of the plotter and computer saves considerable computer time when several plots are constructed. Omission of PLOTBUFF slows program execution but does not otherwise affect it.

6. Computational Details

In the preceding sections, the application of the overall modified weak-shock algorithm was explained. During this explanation we ignored several minor problems and their solutions contained in the overall method. In addition we have not, as yet, indicated how we select several important program parameters. These omissions are rectified in this section.

a. Problem Areas

1) "End Point" Problem. This problem and its solution have already been discussed in detail in Section 3. We list the end point problem here so that the problem area subsection may be complete.

2) Resampling. The sampled data used to represent a particular signal is equally spaced when it is originally inserted into one of the modified weak-shock programs. A characteristic of subroutine WAVEPROP, however, is to distort the time values of sample points by an amount proportional to their particle velocities. There is an additional adjustment of the waveform points at the shock fronts. The end result on the waveform points is twofold. The number of points is reduced as unnecessary points at the shock fronts are shifted out, and the remaining data points are no longer equally spaced. Unequal spacing does not cause any problems so long as frequency domain computations are not required. However, the attenuation and dispersion corrections are performed in the frequency domain, and equally spaced waveform points are required for use in the subroutine FFTC. Thus adjustment of the data points is necessary. In subroutine RESAMPLE a point-slope formula is used to adjust the data points.

A flow chart and listing of this subroutine appears in Appendix C. Subroutine RESAMPLE resamples the waveform and returns the required number of equally spaced samples. Since subroutine RESAMPLE is usually followed by subroutine FFTC, the number of sample points produced by RESAMPLE is normally 2^N+1, where n is a positive nonzero integer.* Application of RESAMPLE cures the unequal spacing problem but at the expense of introducing another problem: RESAMPLE effectively "unshocks" any shocks present in the waveform being resampled. The output of RESAMPLE consists of single valued, equally spaced waveform points. Hence, the minimum shock rise time after resampling is equal to the value of the variable DT used in subroutine RESAMPLE. We call the problem that we have just described the "resampling" problem. Resampling is a problem because the resampled waveform must be propagated using WAVEPROP some short distance before the shocks reform and waveform attenuation at the shock fronts resumes. We can minimize the effects of resampling by minimizing our calls to RESAMPLE. However, calls to RESAMPLE precede, and are a necessary part of the corrections for attenuation and dispersion and we have already required frequent corrections (see Section 4). We have not devised a method of eliminating the resampling problem. The effects of resampling can, however, be minimized subject to the constraint that we make frequent Kirchhoff theory corrections by careful selection of the variable XL. Our guidelines for the selection of XL appear in Subsection 6 of this section.

---

* Subroutine FFTC uses 2^N sample points. The one extra point produced by RESAMPLE is the first point of the next cycle of the wave and, since it is the first point, it has zero particle velocity.

3) Phasing. The problem of "phasing" arises in the correction of deterministic waveforms for thermoviscous attenuation and dispersion. The meaning of the term phasing is best illustrated by a simple example. Consider a deterministic waveform that has been distorted using WAVEPROP and modified further by the application of correction factors in the frequency domain. Before entry into the frequency domain, the sample record consists of one or more complete cycles. The record end points have zero particle velocity. The dispersion correction in the frequency domain changes the overall phase of the reconstituted time waveform. The corrected waveform still consists of one or more complete cycles, but the waveform end points no longer have zero particle velocity. Hence, in the next application of subroutine WAVEPROP, we will encounter an end point problem.

Use of subroutine FIXER enables us to avoid the end point problem. In FIXER we utilize the fact that a full cycle of the wave is present. The end points in the wave are rearranged to form a full cycle starting and stopping on a zero particle velocity point. The phase difference between this waveform and the input waveform is calculated. The phase difference calculation is a measure of the total phase shift due to dispersion. For each entry into FIXER, the phase shift is stored in the appropriate element of the array PHI. A flow chart and listing of subroutine FIXER appears in Appendix C.

FIXER is only used when studying periodic deterministic waves. The same type of phase shift difficulty arises with noise waveforms, but with noise signals another remedy is used. We remarked earlier that noise signals are buffered at either end by a number of waveform

points having zero particle velocity. After each dispersion correction, we merely rezero the first few points in the left buffer and last few points in the right buffer. The rezeroing prevents the occurrence of end point problems.

b. Parameter Selection

Programs NSATDIS and ATENDIS5 contain a number of parameters whose values are user controlled. Values for most of the parameters are not critical. In this subsection we consider four key parameters whose value significantly affects the results obtained using the modified weak-shock algorithm.

1) SF. This parameter is a scale factor that converts the input data to units of particle velocity. Most of our input data was measured directly from oscillograms. The value of SF contains the receiving system sensitivity. In programs NSATDIS and ATENDIS5 the units of SF are ft/sec-in.

2) XINC. This parameter is the incremental step size used in WAVEPROP. The value of XINC used here was determined by comparing results obtained using WAVEPROP to results obtained using an exact expression. Specifically, we calculated the distortion of a sinusoidal wave as a function of distance using WAVEPROP and then computed the fundamental through tenth harmonic amplitudes using FFTC. We compared these results at each distance at which they were computed to the fundamental through tenth harmonics calculated using Blackstock's (1964) exact equation. We found that for values of XINC less than one-tenth of the shock formation distance the differences between the two computations were very small (less than 10% for all harmonics investigated),

and did not grow with distance. For values of XINC greater than one-tenth of the shock formation distance some of the differences became greater than 10%. Using the results of this analysis, we decided that a value of XINC equal to one-tenth of the shock formation distance was appropriate.

For the strongest sinusoidal waves considered here, the shock formation distance is 3.8 ft (see Table V). In the study of noise waves some portions of the waves are so strong that shocks form very close (perhaps as close as 1 ft) to the source measurement location. Therefore we selected 0.1 ft as the value of XINC in all analyses reported here. Cook (1962) selected a step size of one-twentieth of the shock formation distance. Our analysis indicates that one-tenth is adequate.

When considering waves whose shock formation distance is greater than 1 ft larger values of XINC may be used. We have not chosen to make this adjustment in the work reported here.

3) XL. This parameter is the incremental propagation distance between successive attenuation and dispersion corrections. Its selection is a compromise between the necessity for frequent waveform correction and the necessity to minimize the resampling problem (see Subsection 6.a.(2) above). Our guidelines for selecting XL are as follows:

1) Inspect the input record and select the highest peak u_a and the lowest peak u_b that may eventually become part of a shock.
2) Using Eq. (4-2) calculate the net time distortion of points having particle velocities u_a and u_b when propagated a distance XL.

3) Calculate the point spacing of the waveform at the source (i.e., before any distortion).

4) Form ratios between the time values computed in step 2 and the time value computed in step 3.

5) A useful rule of thumb is that XL should be selected in such a way that the ratios formed in step 4 fall between 2 and 7.

The above procedure, while useful, is far from perfect and some experimentation with the value of XL may be required. In the results reported in this work, XL was selected to fall within the limits specified in step 5.

4) NN. The selection of NN, the number of initial waveform points, is a compromise between conflicting demands. We have already discussed the problem associated with resampling. In order to minimize the resampling problem while still using small distance increments a large number of waveform points should be used. A second reason for selecting a large number of data points is to avoid "aliasing".* Yet as the number of points increases, computation time also increases. The major time user in both the ATENDIS5 and NSATDIS programs is the subroutine FFTC. As Welch (1967) points out, the time required to perform a finite Fourier transform on a sequence of length L is approximately $KL \log_2 L$, where K is a constant which depends on the program and the computer used. Therefore from a cost viewpoint we wanted as few data points as possible.

*"Aliasing" is an effect that is present in all spectral computation schemes, both analog and digital. It is the folding of frequency components above the Nyquist frequency back into the true spectrum. Aliasing can be avoided if the sampling frequency exceeds by a factor of 2 the highest frequency in the sampled data. An excellent elementary discussion of the principles of data sampling, including aliasing, appears in a book by Stein and Jones (1967). Stein and Jones refer to aliasing as a spectral ambiguity.

Our solution to this problem was obtained by trial and error. In the developmental testing of our algorithm we utilized waves having fundamental frequencies between 500 Hz and 3500 Hz. We found that by using 512 data points per cycle we obtained excellent results. Increasing the value of NN to 1025 points* gave negligible improvement. Decreasing NN to 257 points resulted in noticeable loss of agreement between our computed and observed waveforms. In the study of noise waveforms the time duration of the signals was longer than in the study of sinusoids. Hence, more waveform points were needed. Again the best method of determining what value of NN to use proved to be trial and error. We usually started with NN=513 points and calculated the noise waveform after propagation. We then repeated the calculation at 1025 points and so on for higher values of 2^N+1 points. When no appreciable change occurred between runs, it was assumed that the number of data points had become adequate. For the noise waveforms reported in this work 1025 points appeared to be enough. The number of data points used

The number of data points used establishes the Nyquist frequency. Since the reviewing system used in our experiments is useful

---

*In Program ATENDIS5 we use $NN=2^N+1$ points. The first 2^N points describe a complete cycle, the last point is the first point of the next cycle. The particle velocity associated with this extra point is zero. The function of the extra point is to prevent the occurrence of an end point problem.

**The frequency characteristic of the microphones used in our experiment is constant up to 70 kHz. Because the microphones are installed in such a way that the signal is observed at a grazing incidence, we must consider the directivity of the microphones. A full discussion of the directivity pattern appears in Chapter 5. It turns out that the microphone directivity limits the bandwidth of the microphones in our experiment to about 27.5 kHz.

sampling rate commensurate with a bandwidth of 27.5 kHz. Hence we desire a 55 kHz sampling rate. The required number of samples then is 55 samples per millisecond. During the investigation of sinusoids, we considered a single cycle. The lowest frequency considered was 500 Hz. For a 500 Hz wave 110 samples/cycle are required to meet the 55 kHz sampling criterion. We need fewer samples/cycle for higher frequency waves. The number of samples used in subroutine FFTC must be an integral power of two. The use of 512 waveform points/cycle easily meets all requirements for the sinusoidal waves investigated here.

In the study of noise waveforms the longest sample record used was 16.27 msec. In this case we used NN=1025. Therefore the sample rate was 63 kHz.

Hence, we conclude that in the cases investigated here the use of 513 sample points for sinusoids and 1025 sample points for noise waves was adequate.

7. Calculation of Power Spectra

The primary purpose of this whole research effort has been to investigate the change in waveform and spectral composition of finite-amplitude noise as it propagates. We decided that the most meaningful spectral calculations would be those showing the change in the source spectrum due to weak-shock effects only. A computation scheme was devised to calculate the power spectrum at various distances from a source of unbounded plane waves. In this program we consider weak-shock effects, but not tube wall attenuation and dispersion. A secondary reason for considering only the weak-shock effects is economic. The application of the tube wall effect corrections represents a major

up to about 27.5 kHz,** we want to provide a time portion of each computer run. Hence in neglecting these corrections we obtain a considerable saving. A schematic diagram of the program, program DOITALL3, appears in Fig. (4-7). A detailed flowchart and listing appears in Appendix D. All arrays and variables used are defined in the listing.

The heart of program DOITALL3 is the calculation of the waveform distortion due to nonlinear propagation and the subsequent calculation of power spectral density. We minimize the effects of resampling by not resampling the wave until it has been propagated the required distance. A measure of economy in the use of core memory is achieved by the multiple purpose use of arrays. The program has a built in capacity for ensemble averaging power estimates. A scratch tape is used to temporarily store computed spectra thereby further decreasing core requirements. The spectral computation scheme is an updated version of the Blackman and Tukey (1959) indirect method. The method is indirect (as opposed to direct) because the autocorrelation function is calculated first, then the power spectral density is computed. The steps in the indirect method are as follows:

1) Let $\{X_1, X_2, \ldots, X_n\}$ be a sequence of data points and Δt the time interval between adjacent points. Compute the autocorrelation function of the sequence $\{X_1, \ldots, X_n\}$. The autocorrelation function is computed by use of an FFT. The autocorrelation function is periodic, values computed using negative lags being stored in the second half of the array.

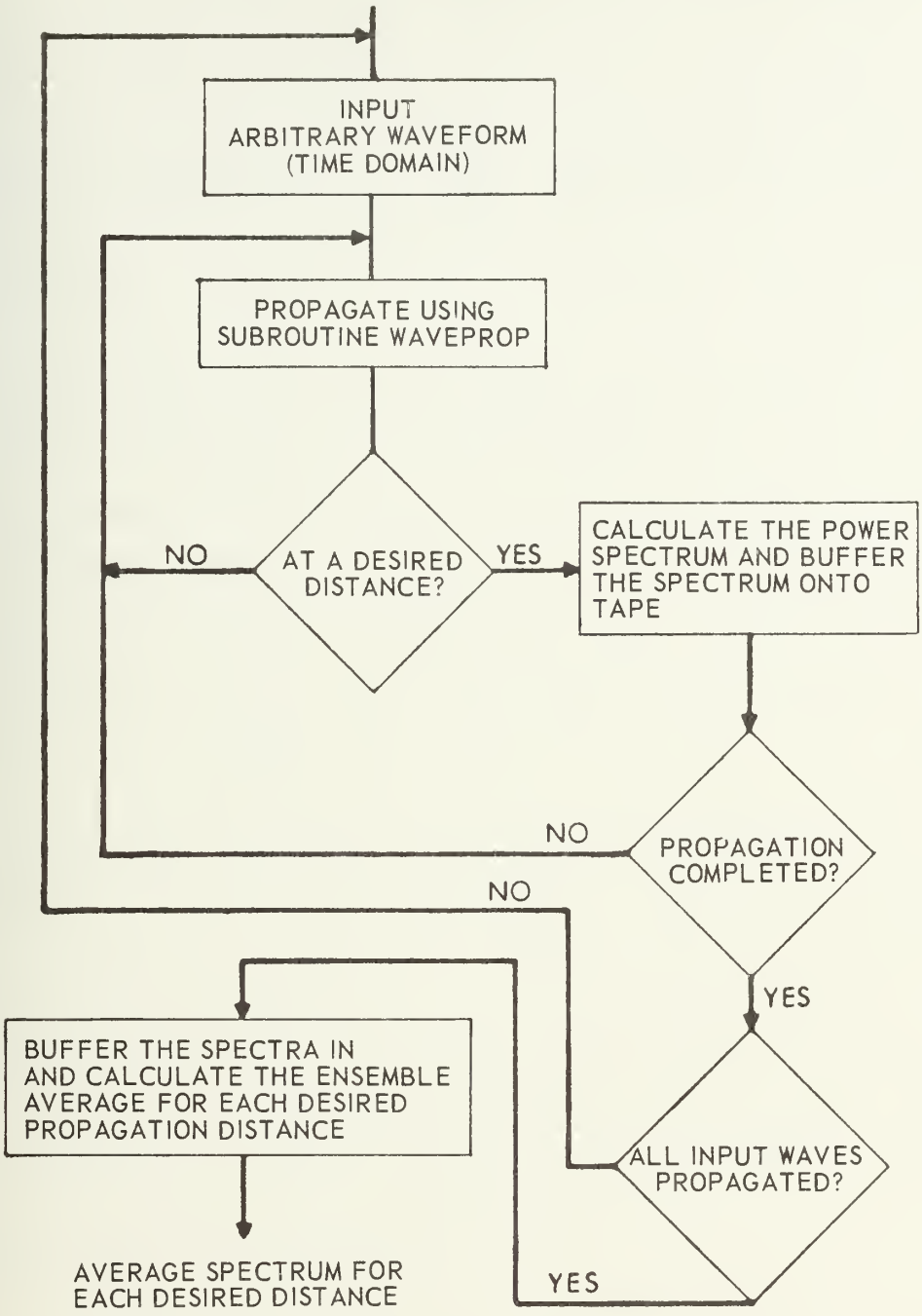

FIGURE 4-7
SCHEMATIC OF PROGRAM DOITALL3

2) Construct a sequence of mean lagged products* $\{C_1, C_2, \ldots, C_m, C_{m+1}, \ldots, C_{2m}\}$ made up of the first m elements and the last m elements of the autocorrelation function. The sequence $C_1, \ldots, C_{2m}$ is an even function about the (m+1)th point. The time interval between elements of the sequence $\{C_1, \ldots, C_{2m}\}$ is $\Delta\tau$, where $\Delta\tau=h\Delta t$, h being a positive nonzero integer.

3) The sequence of mean lagged products is then transformed. Since the mean lagged products form the sample values of an even function, the complex FFT is equivalent to Blackman and Tukey's cosine transform. The sequence of transformed values $\{V_1, V_2, \ldots, V_{2m}\}$ is itself an even function symmetric about every integral multiple of m+1. Blackman and Tukey (1959) call this sequence the sequence of raw spectral density estimates.

4) The refined spectral density estimates are then computed. This computation is made to combat the effects of "spectral leakage" Spectral leakage is caused by energy at frequencies in between the computed harmonics that can be partially added to the energy at a computed harmonic because the true spectrum convolves with the spectrum of the data window. Careful selection of the data window shape can greatly

---

*At the time that the book by Blackman and Tukey (1959) was written, the mean lagged products were computed directly by shifting, multiplying, and adding. Now, of course, as Bingham, Godfrey, and Tukey (1967) have pointed out, the efficient way to perform this calculation is by use of the FFT and the transform pair property of the autocorrelation function and power spectral density.

reduce this leakage. The window used in this work is a hanning window,

$$D(\tau) = \frac{1}{2}\left(1 + \cos\frac{2\pi\tau}{T_m}\right) \qquad |\tau| < T_m$$
$$= 0 \qquad |\tau| > T_m \tag{4-18}$$

where

T_m = the lag time of the mth lag product.

The refined spectral density estimates produced by the indirect method have equivalent degrees of freedom in the CHI-squared sense given by the relation

$$k_r = \left[\frac{n\Delta t}{m\Delta\tau} - \frac{1}{3}\right] \qquad r = 2, 3, \ldots, m$$
$$= \text{half as much} \qquad r = 1, m + 1 \quad , \tag{4-19}$$

where

k_r = degrees of freedom.

Increased statistical stability is, of course, the advantage of the indirect method. In examples presented in Chapter 6 of this work n=1024, h=1, and m=128. Substituting these values into Eq. (4-19), we obtain

$$k_r = 7.77 \qquad r = 2, \ldots, m,$$
$$= 3.88 \qquad r = 1, m + 1 \quad . \tag{4-20}$$

The r=1 and m+1 points are the d.c. value and the value at the Nyquist frequency, respectively. The indirect method in this case gives results as statistically stable as the ensemble average of 3 sets of spectral estimates calculated by the direct method. In the direct method, the sequence $\{X_1, \ldots, X_n\}$ is transformed using the FFT to get the complex coefficients, $A_{k+j}B_k$. These coefficients are then hanned and power terms of the form $A_k^2+B_k^2$ are calculated. The direct method, while computationally simple, has only 2 degrees of freedom. It would appear that the indirect method, because of its greater statistical stability, would be preferable. This is not always the case because frequency resolution is lost when the indirect method is used. For example, in using the sequence of mean lagged products we reduce the number of data points from n to 2 m. Typically, this might be a reduction by a factor of 4. The frequency resolution is degraded by this same factor. Hence, the selection of the parameters used in DOITALL3 dictates the resolution and stability of the resulting power density estimates. The theoretical results obtained using this method and experimentally obtained spectra are presented in Chapter 6.

CHAPTER 5 EXPERIMENTAL EQUIPMENT AND PROCEDURES

1. Introduction

In this chapter we concentrate on the actual pieces of equipment and procedures used to make the experimental measurements that are reported in Chapter 6. The second section contains listings of the various pieces of equipment used in our experiments. Within the listings are detailed discussions of the equipment calibration, characteristics, and, where applicable, accuracy that directly affected our experimental results. In the third section we briefly outline each of our experimental procedures and indicate the particular pieces of equipment from the lists in Section 2 that were used in each procedure. In certain cases where two or more similar devices were available (e.g., two different oscillators) we indicate why the particular device that we used was selected.

The assumptions made in the theoretical development presented in Chapter 3 place physical restrictions upon our experiments. In Section 4 of this chapter these restrictions are analyzed. The final section contains an analysis of the overall accuracy of our measurement equipment.

2. Experimental Apparatus

A generalized schematic of the experimental arrangement appears in Fig. (5-1). All equipment was calibrated, if necessary, before its use. The accuracy of the various calibrations and the precision with which experimental data was gathered contribute directly to the accuracy

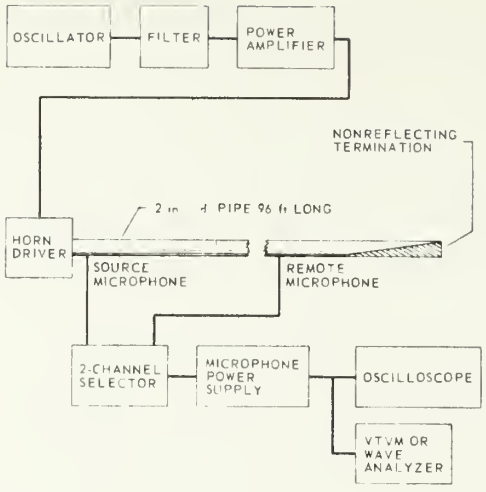

FIGURE 5-1
A GENERALIZED SCHEMATIC OF THE EXPERIMENTAL EQUIPMENT ARRANGEMENT

of the experimental results reported in Chapter 6. Commercially available equipment, calibrated as directed in the applicable technical manual, in all cases met or bettered the manufacturer's nominal specifications. The calibration of locally prepared equipment will be reviewed in this section. The equipment arrangement can be conveniently subdivided into a transmitting system, the pipe, and a receiving system.

a. The Transmitting System

1. General Radio Oscillator Type 1310-A.

2. Bruel and Kjaer Oscillator Type 1022.

3. Beckman Universal Eput and Timer Counter Model 7360 AR.

4. Krohn-Hite Filter Model 315-ACR. The function of this filter was to shape the input spectrum to the sound source in such a fashion that energy outside the sound source passband was not supplied to the sound source.

5. Signal Data Recorder-Reproducer Model AN/UNQ-8(V). The AN/UNQ-8(V) utilized in this experimental work was modified for tape loop operation. An external tape loop transport was added* and the record circuitry was modified in order to disable the normal record push button and to provide for a remote, hand-held record switch. In the work reported herein, the recorder-reproducer was operated in direct record in the loop mode at a tape speed of 30 in/sec. The recorder-reproducer channel utilized was calibrated as directed in the AN/UNQ-8(V) manual prior to its use. The 3 dB down points of the frequency response of the AN/UNQ-8(V) used as indicated above are 50 Hz and 60 kHz.

6. ELGENCO Random Noise Generator Model 603A. We investigated the instantaneous amplitude distribution of the output of the Model 603A. The Model 603A was to be the source of our noise waveforms and we wanted to establish whether the source waveform were truly random.

The output of the Model 603A was analyzed using a standard statistical program called SEQSTAT available on the computer library at the Applied Research Laboratories. The output was alias filtered at 10 kHz using a low pass filter of slope 48 dB/octave. The filter output was then sampled at 25.22 kHz using an analog-to-digital converter. Four sample sequences 50,000 data points in length were formed. In SEQSTAT sequences of 5000 data samples are considered and the mean, variance, skew, and kurtosis of the sample record are computed. In addition a histogram is formed and compared to a gaussianly distributed variable having mean and variance equal to those calculated from the data.

---

*All external and internal modifications to the AN/UNQ-8(V) had been designed and built by R. K. Goodnow of the Applied Research Laboratories staff.

Consider a random variable x having a probability distribution function f(x). The definitions of the first four central moments are [see, for example, Wilks (1963)]

$$\text{Mean} \qquad m = E(x), \tag{5-1}$$

$$\text{Variance} \qquad \sigma^2 = E[(x-m)^2], \tag{5-2}$$

$$\text{Skew} \qquad \gamma_1 = E[(x-m)^3]/\sigma^3, \text{ and} \tag{5-3}$$

$$\text{Kurtosis} \qquad \gamma_2 = E[(x-m)^4]/\sigma^4, \tag{5-4}$$

where the notation E means expected value. For a gaussianly distributed random variable the theoretical value of γ_1 and γ_2 are

$$\begin{aligned} \gamma_1 &= 0 \\ \gamma_2 &= 3.0 \quad . \end{aligned} \tag{5-5}$$

The first four moments of the Model 603A output were calculated for 12 samples records of 5000 samples each and the moments of each sample record were then ensemble averaged. The results were as follows:

$$\begin{aligned} m &= 0.0039 \text{ V}, \\ \sigma &= 1.227 \text{ V}, \\ \gamma_1 &= 0.012, \text{ and} \\ \gamma_2 &= 2.92. \end{aligned} \tag{5-6}$$

The true rms voltage at the output of the alias filter was 1.22 V, agreeing very well with σ. The ensemble averaged histogram of the sampled data agreed closely with the gaussian distribution curve based on (m,σ) in result Eq. (5-6).

We, therefore, conclude that the ELGENCO Model 603A produced nearly gaussianly distributed noise when operated in the 5 Hz to 10,000 Hz range.

7. DuKane Power Amplifier Medallion Model 1A921. This device is power rated by the manufacturer at 200 W true rms and 500 W peak instantaneous power. The Model 1A921 was used to power the ID-75 Horn Driver. The maximum usable output from the Model 1A921 was set by the capacity of the ID-75 (when operated in the pulsed mode). The additional power capability of the Model 1A921 was used to minimize clipping of the amplifier output. If we assume that the amplifier input is gaussianly distributed random noise and the true rms amplifier output is 75 W, then the probability of waveform clipping, obtained from the gaussian distribution function tables [see, for example, Baird (1964)], is approximately 1%. The 3 dB down points of the Model 1A921 frequency response are at 20 Hz and 20 kHz. Hence, the Model 1A921 did not limit the source bandwidth used in the transmit systems in our noise experiments. In fact, as has already been mentioned, the Krohn-Hite filter was used to limit the signal to the amplifier to the bandwidth usable by the horn driver. The rated total harmonic distortion of the Model 1A921 is less than 1 1/2% when operated at output powers less than 200 W rms. Since we operated at powers far less than 200 W, it is unlikely that the Model 1A921 output was significantly distorted. In addition, we monitored the amplifier output using an oscilloscope during our experiments and never observed waveform distortion. Since we are interested in the change in the waveform,the presence of distortion, had any been present, would not have concerned us.

8. University Horn Driver ID-75. The ID-75 has a bandpass filter frequency characteristic. When the ID-75 is operated at 75 W output the 3 dB down points of the passband are approximately 700 Hz

and 2200 Hz. The ID-75 frequency characteristic essentially sets the bandwidth at the source for our noise experiments.

The ID-75 is rated for 75 W rms continuous output. All of our high intensity (approximately 160 dB) results were obtained while pulsing the transmit system. We found that higher overall source SPL's could be reached in the pulse mode. We estimate that the ID-75 in the pulse mode can safely (i.e., nondestructively) accommodate 75 W rms electrical power. At this power level, however, the acoustic output waveforms are somewhat distorted. Examples of the distortion caused by the driver will be presented in Chapter 6. The amount of horn driver induced distortion does not concern us here because, as we mentioned in the discussion of the power amplifier, we are interested in the change in the waveform with propagation. Hence, all we require at the source is that the waveform, whatever it may be, be known.

We investigated the output of the ELGENCO noise generator and established that its output was gaussian. Downstream of the noise generator, however, we have significantly altered the signal by filtering and amplifying it. The filtering and amplifying action are linear transformations and, as is well-known, gaussian processes are invariant under a linear transformation [see, for example, Papoulis (1965)]. Hence in the absence of nonlinear distortion the output of the horn driver is also gaussian. We know, however, that the horn driver at high output levels does nonlinearly distort the signal somewhat. Hence the distribution function of the horn driver output may not be exactly gaussian. The only effect that this possible change in the distribution function has in regard to our computations is its effect on our calculations of spectra. The methods used depend on the noise amplitudes being normally distributed. We acknowledge, therefore, that since the horn driver at high power does

nonlinearly distort our signal somewhat the calculation of spectra may be affected. However, we feel confident that the effect is of a very minor nature.

9. General Radio Pulse Generator Type 1396-A. The Type 1396-A was used in all the finite-amplitude propagation experiments to pulse the transmit system. It was not used in the measurement of the pipe termination reflection coefficient because during the "off" portion of its duty cycle the Type 1396-A has a feedthrough only 40 dB below the output during the "on" portion of the cycle. Since we were interested in reflections more than 40 dB below the incident signal, the Type 1396-A was unsatisfactory for use in reflection measurements.

10. Wavetek Function Generator Model 144. This device was used to pulse the transmit system during the reflection coefficient measurements. The Model 144 exhibits zero feedthrough during the "off" portion of its duty cycle.

11. Daven Attenuator Type T641. This device was used at the Model 1A921 power amplifier input to control the amplifier output level.

12. United Variable Tap Transformer. The transformer was used in a 1:1 configuration to isolate the input of the power amplifier from the laboratory electrical ground.

b. The Pipe

The pipe consists of eight 12 ft sections, seven flanges, one driver mount and a nonreflecting termination. The pipe, less the termination, was originally constructed for the experiments reported by McKittick, Blackstock, and Wright (1967); certain modifications have been made for the present work. The termination is constructed of fiberglass and the pipe sections and fittings of 6061-T6 AL aluminum.

1. The Pipe Sections. The pipe section internal diameter is 2 in. and wall thickness is 1/8 in. The ends of each section were squared and the outside surfaces within 3 in. of the ends were turned round on a lathe to facilitate a close fit with the flanges.

2. The Pipe Flanges. An assembly drawing of one of the pipe flanges appears in Fig. (5-2). The flanges were designed to minimize reflections at the pipe joints. Each flange has a probe hole sized to accept a 1/4 in. microphone. The microphone body is mounted in a teflon holder that seats on the shoulder in the microphone hole [see Fig. (5-2)]. Since the flanges are not of equal diameter, the depth of this shoulder varies in such a fashion that the face of the mounted microphone is always flush with the inside surface of the pipe. The teflon holder also reduces the mechanical pickup of signals propagating in the pipe walls. When not in use, the microphone hole is blocked by an aluminum plug whose end is flush with the inside surface of the pipe. The taper pins ensure exact alignment of the flanges each time the flanges are bolted together.

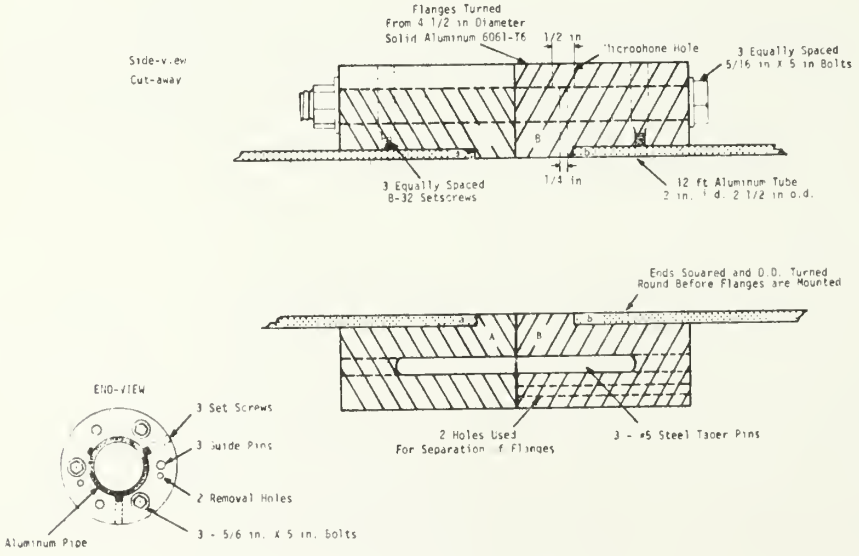

FIGURE 5.2
AN ASSEMBLY DRAWING OF A PIPE FLANGE

3. Horn Driver Mount. The horn driver mount consists of a flange similar to that shown in Fig. (5-2). On the driver side of the flange an 8 in. conical transition piece is used to change the internal diameter from 2 in. to 1 in. to match the throat diameter of the University series horn drivers.

4. The Temination. The pipe termination was built as suggested in the paper by Burns (1971). Of Burns' three termination designs we elected to use the full wave tangent taper. The terminattion consists of two sections which are installed in series in the final length of pipe section. The first section of the termination encountered by the propagating wave consists of a gradually tapered, one meter long wedge. The second section, also one meter long, completely fills the pipe cross section. The density of the fiberglass used is 0.0503 gm/cm^3. The leading edge of the termination is located approximately 5 ft downstream of the seventh (and last) flange. Therefore, the termination did not interfere with readings taken at the seventh flange.

The reflection coefficient of the pipe termination was measured by the pulse method. In Table I we present the reflection coefficient, corrected for the round trip loss due to tube wall attenuation between the measurement point and the termination.

TABLE I

Reflection Coefficients for the Pipe Termination

Frequency (Hz)	Reflection Coefficient (dB)
500	-39.8
750	-35.7
1000	-37.2
1500	-40.8
2000	-42.1
2500	-41.7
3000	-41.8
3500	-42.0
4000	-41.9

Burns (1971) notes that a reflection coefficient appreciably below -40 dB is hard to achieve in practice.

c. The Receiving System

The accuracy of the receiving system calibration established the accuracy of our results. Each system component was calibrated. The accuracy of measurements made with the various devices was determined during the device calibration. In this subsection we report the measurement standard deviations of the various components of the system. Microphone sensitivity H_s was measured. The values of H_s reported here are for the microphone assemblies, i.e., the microphone, preamplifier, and cable, connected as they were used in our experiments.

1. Bruel and Kjaer Preamplifiers Type 2619 and Type 2615. The Type 2615 was used only in the microphone calibration. The Type 2619 preamplifiers were used for all data collection.

2. Bruel and Kjaer Cable Type A00029. This cable is 30 m in length.

3. Laboratory Constructed Microphone Cable. This device was used in conjunction with the source microphone. The cable type is RG-62 B/U. The end fittings are of Bruel and Kjaer manufacture. A careful check was made to ensure that signals detected by the source microphone were not degraded by use of this cable. At frequencies up to 70 kHz no signal distortion or loss of amplitude was observed. The cable is 100 ft in length.

4. Bruel and Kjaer 1/4 in. Microphones Type 4136. The 1/4 in. microphones were calibrated by means of a comparison method. Three Bruel and Kjaer 1/2 in. microphones were calibrated by the chamber reciprocity method [see Bruel and Kjaer (1965)]. The 1/2 in. microphones were used to calibrate a Bruel and Kjaer Type 4220 pistonphone. The pistonphone was then used to calibrate the 1/4 in. microphones. In Table II we present the measured 1/4 in. microphone assembly sensitivities. A microphone assembly consists of a microphone, a preamplifier, and a cable connected in series. The values reported are the sensitivities at 250 Hz, 760 mm Hg, and 200 Vdc polarization voltage.

TABLE II

Microphone Assembly Sensitivities

	H_s(dB re 1 V/μbar)
source assembly	-77.2
remote assembly	-76.8

In the experiments reported in this work 1/4 in. microphone serial 176005, Type 2619 preamplifier serial 327254, and the locally constructed cable were used to monitor the sound at the source. Microphone serial 176007,

Type 2619 preamplifier serial 386559, and Cable A00029 were used at the remote locations. After the completion of the initial calibration, the microphone assembly sensitivities, checked using the calibrated pistonphone, were repeatable within ±0.15 dB. The nominal frequency response characteristic of the 1/4 in. microphones is flat within ±1 dB over the range of 50 Hz to 70 kHz. Series addition of the preamplifier and cable for both the remote and source microphone assembly had no observable effect on the microphone frequency response. The time domain characteristics of the 1/4 in. microphones made them well suited to meet our experimental needs. The nominal rise times are very short (approximately 6 μsec in response to a step input) and the microphones exhibit practically no ringing when installed as they were in our experiments.

Use of a finite size microphone requires that we investigate the integration effect associated with measuring a sound field at a grazing incidence. Mounted as used in the pipe, the microphone is simply a baffled circular piston receiver. The directivity characteristic $D(k,\theta)$ is easily calculated to be [see, for example, Kinsler and Frey (1950)]

$$D(k,\theta) = \frac{2J_1(ka \sin \theta)}{ka \sin \theta} \quad , \tag{5-1}$$

where a = the microphone radius and θ is the angle of incidence with respect to the normal to the microphone face. In the present case $\theta=90°$ and Eq. (5-1) reduce to

$$D(k) = \frac{2J_1(ka)}{ka} \quad . \tag{5-2}$$

For the following reasons we did not correct our reported theoretical waveforms for microphone directivity:

1) The 3 dB down point of D(k) for a 1/4 in. microphone is 27.5 kHz. Only a very small portion of the energy in our measured and computed spectra occurs at frequencies above 27.5 kHz.

2) Test runs, designed to discover the effect of the inclusion of D(k), were made. In these tests the computation algorithm was modified to include D(k) in the calculation of theoretical waveforms. The corrected waveforms (i.e., corrected for microphone directivity) were then compared to uncorrected waveforms computed from similar source data. The comparison showed that the only difference between the two sets of data was a small (5 to 6 μsec) increase in shock rise time in the corrected data. The difference in shock rise time is less than the experimental uncertainty in the recording of our data.

5. Bruel and Kjaer Selector Switch Type 4408. Use of this device allowed us to easily switch back and forth between the two microphones. Use of the 2-channel selector switch had no adverse effect upon signal measurement.

6. Bruel and Kjaer Power Supply Type 2803.

7. Bruel and Kjaer Pistonphone Type 4220. This device was used to check calibrate the microphone assemblies before every data collection.

8. Tektronix Oscilloscope Model 545B with Plug-in Type 1A1. The measurement standard deviation of the model 545B oscilloscope after calibration was ±0.25 dB. The Model 545B was used for several signal monitoring purposes that are outlined briefly in Section 2.

9. General Radio Wave Analyzer Type 1900-A. This device was used in the collection of noise wave spectra. For all spectral measurements reported in this work the 50 Hz crystal was used. The nominal measurement standard deviation of the Type 1900-A used with the Recorder Type 1521B was ±0.2 dB.

10. General Radio Recorder Type 1521B. This pen type recorder was used in conjunction with the wave analyzer to record spectra.

11. Hewlett Packard Oscilloscope Model 181A1AR with 4-Channel Vertical Amplifier Type 1804A and Time Base and Delay Generator Model 1821A. This memory-type oscilloscope was used in the noise experiments. Oscillograms of the noise pulses were made using the memory feature of the Model 181A1AR. At the time that this device was used, it was new and had recently been factory calibrated. The observed measurement standard deviation of the Model 181A1AR was ±0.1 dB.

12. Bruel and Kjaer Filter Type 1610. This 1/3 octave band filter set was used in the measurement of small-signal attenuation coefficients.

13. Bruel and Kjaer Microphone Amplifier Type 2604. This amplifier was used only in the measurement of small-signal attenuation coefficients. We measured the standard deviation of the response of the Type 2604 and obtained ±0.3 dB.

3. Experimental Procedures

We conducted three types of experiments in the research reported here. The experiments were as follows:

a. Measurement of small-signal attenuation coefficients.

b. Measurement of deterministic waveforms.

c. Measurement of noise waveforms.

We shall briefly discuss our procedure and identify the equipment used in each of the experiments. The equipment will be identified by its system number, e.g., the General Radio Oscillator Type 1310-A will be referred to as item a-1. Since the pipe was used in all three experimental procedures it will not be listed in the individual experimental descriptions. Before each experiment the microphone assembly sensitivities were checked using the pistonphone.

a. Measurement of Small-Signal Attenuation Coefficients.

The devices used in this experiment were items a-2, a-3, a-4, a-7, a-8, a-11, a-12, c-1, c-2, c-3, c-4, c-5, c-7, c-8, c-12, c-13. The purpose of this experiment was to provide attenuation coefficients for use in the computation algorithm. The procedure used consisted of generating a low amplitude (typically 105 dB) sinusoid at the source and recording the signal level at the various remote locations. The B and K oscillator and the Beckman timer were used to obtain maximum frequency stability and accurate frequency measurement, respectively. The oscilloscope was used to monitor source electrical and acoustic signals and acoustic signals at the remote locations. The attenuation coefficients were calculated by plotting the observed sound pressure levels as a function of distance and obtaining the best fit line by linear regression.

b. Measurement of Deterministic Waveforms.

The items used were a-1, a-3, a-4, a-7, a-8, a-9, a-11, a-12, c-1, c-2, c-3, c-4, c-5, c-6, c-7, and c-8. The basic procedure used consisted of pulsing the source at a high amplitude and observing the waveform at the various pipe locations. At each location an oscillogram was made using the Model 545B oscilloscope camera. The General Radio Oscillator was used instead of the B and K oscillator because the former

is compatible with the General Radio Pulse Generator. The Model 545B oscilloscope was also used to monitor the electrical signal to the horn driver and the source acoustic signal in order to ensure that the source signal remained stable during a particular data collection period.

c. Measurement of Noise Waveforms. The items used were a-1, a-4, a-5, a-6, a-7, a-8, a-9, a-11, a-12, c-1, c-2, c-3, c-4, c-5, c-6, c-7, c-9, c-10, c-11. This experiment is somewhat more complicated than experiments (a) and (b).

In the noise waveform experiments a pulse of filtered electrical noise was recorded on an endless tape loop. The filter bandpass was 500 to 3500 kHz. The recording was made by gating the output of the ELGENCO noise generator by use of the General Radio Pulse Generator and General Radio Oscillator. The pulse was recorded using the AN/UNQ-8(V) modified, as mentioned earlier, for tape loop operations. The AN/UNQ-8(V) was then used to reproduce the noise pulse. The pulse was amplified and applied to the ID-75 Horn Driver. The acoustic noise pulse was then picked up by the remote microphone and the signal recorded by the Model 181A1AR oscilloscope. This oscilloscope was also used to monitor and record the source signal.

In the noise spectra experiments the ELGENCO Model 603A output was bandpass filtered, amplified, and applied continuously (not pulsed) to the ID-75. Again, the filter bandpass was 500 to 3500 kHz. The maximum sound pressure level that could be safely obtained in the continuous wave (cw) mode was approximately 154 dB. The General Radio Wave Analyzer and General Radio Recorder were used to record spectra at the various pipe measurement stations.

4. Experimental Limitations

Chapter 3 concluded with a listing of several assumptions on which the formulation of modified weak-shock theory is based. For the convenience of the reader, we shall restate these assumptions:

a. Only plane waves are present.

b. The wave amplitude is appropriate for the use of modified weak-shock theory.

c. The pipe is a wide pipe, i.e.,

$$\Delta \ll R \ll \frac{\eta}{k^2 \Delta}$$

d. The pipe is circular, infinitely long, and absolutely rigid.

e. The enclosed fluid medium is a homogeneous perfect gas.

In this section we shall explain the physical limitations placed on our experiments by the assumptions stated above.

The plane wave assumption establishes an important operating restriction. The cutoff frequencies of nonplanar modes in a circular pipe are inversely proportional to the pipe radius. Hence, the selection of the pipe i.d. establishes for practical purposes the upper limit on the source frequency. The cutoff frequencies are given by the relation

$$f_{mn} = \frac{P_{mn} c_o}{2\pi R} \quad . \tag{5-3}$$

In Eq. (5-3) P_{mn} is the nth root of the equation

$$J_n'(P_{mn}) = 0 \tag{5-4}$$

where J_n' = the derivative of the nth order Bessel function. The first several cutoff frequencies are given in Table III. The row and column indices in Table III identify the root of Eq. (5-4) used in Eq. (5-3) to calculate the given frequency.

TABLE III

Cutoff Frequencies (Hz) in a 2 in. i.d. Circular Pipe

	m = 0	m = 1	m = 2
n = 0	0	8280	15170
n = 1	3940	11510	18410
n = 2	6590	14500	21550

The (0,0) mode is planar. The (0,1) and (0,2) modes are spinning modes and the (1,0) mode is radial. In order to avoid the generation of nonplanar modes at the source, source frequencies in the experiments reported here were maintained below 3940 Hz.

The waveform steepening caused by nonlinear propagation shifts energy to frequencies well above the 3940 Hz limit. Does this energy transferred to high frequencies generate nonplanar modes? We are unable to conclusively answer this question, but we feel that it does not. Our experimental data and that of other researchers [see, for example, Pernet and Payne (1969)] indicates that high frequency components generated by nonlinear steepening of plane waves remain planar. The planar shock seems to represent a very stable mode of propagation in a tube.

We have assumed a plane particle velocity wave whereas in reality the particle velocity must vanish at the pipe wall. Hence, the particle velocity phase front is plane only outside the boundary layer. We measure pressure, however, and the pressure is planar across the pipe

cross section through the boundary layer. Therefore, measurements made with microphones flush with the tube wall are completely acceptable.

Modified weak-shock theory is applicable if the waves being considered are not too strong. Blackstock (1964) maintains that waves having sound pressure levels less than 174 dB may be treated by weak-shock theory. Temkin (1969), in a more detailed analysis, limits weak-shock theory to 165 dB. In our work the maximum sound pressure level reached was 162 dB. In Appendix E we present our analysis of the maximum amplitude that may be considered using weak-shock theory. Our results indicate that 165 dB is a realistic and practical figure.

The wide pipe assumption does not impose any restrictions on our experiments over and above those restrictions already imposed by the limitations of our equipment. The low frequency limit, set by the ID-75 response, is approximately 700 Hz. The high frequency limit, set by the microphone frequency response, is 27.5 kHz. Within the frequency range of 700 Hz to well above 27.5 kHz our pipe is a wide pipe.

The upper limit of the wide pipe assumption, i.e., $R \ll \eta/(k^2\Delta)$, was derived by comparing Kirchhoff theory to thermoviscous losses in the pipe mainstream. We ignored other loss mechanisms. If we include relaxation in the mainstream attenuation and compare the boundary layer attenuation coefficient and the mainstream attenuation coefficient, we find that the frequency at which the two coefficients approach each other is significantly lower than in the case where relaxation effects are ignored. Using the results of Bass, Evans, and Sutherland (1970), we have made the above comparison and found that for frequencies less than 100 kHz the boundary layer attenuation coefficient exceeds the mainstream term.

Hence, we conclude that we incur negligible error in our results by ignoring relaxation effects.

The final assumption is a consequence of our use of Kirchhoff theory and also of the simple wave flow assumption. The pipe termination is meant to make the pipe free of reflection and, in this sense, simulate an infinitely long pipe. The figures in Table I make clear that the pipe is indeed a progressive wave tube.

5. Analysis of the Expected Measurement Accuracy

The accuracy of the absolute sound pressure level measurements reported in this work may be easily estimated. If we assume that the various errors are independent and that each is normally distributed, the standard deviation of the measurement is

$$S = [a^2 + b^2 + c^2 + \ldots.]^{1/2} \quad , \qquad (5\text{-}5)$$

where a, b, c, etc., are the standard deviations of responses of the vario components used to make a particular measurement and S is the standard deviation of the overall system response. The measurement standard deviations for the equipment used in each experiment are listed below. Values marked by the symbol* are worst case values obtained from the various equipment technical manuals. All other values, not so marked, were measured. The measurement standard deviations are

a) Microphone assembly calibration: 0.15 dB.

b) Pistonphone output: 0.2 dB*

c) Voltage calibration of the microphone amplifier: 0.2 dB.

d) Reading uncertainty: 0.1 dB.

e) Polarization voltage deviation from 200 V: 0.2 dB*.

f) Uncertainty in the frequency response of the measuring

equipment: 0.3 dB*.

g) Voltage calibration of the Tektronix Oscilloscope 545B: 0.25 dB.

h) Voltage calibration of the HP 181A1AR oscilloscope: 0.1 dB.

i) Voltage calibration of the General Radio Wave Analyzer and Recorder: 0.2 dB*.

In Section 2 we listed the equipment used in each experiment. Using Eq. (5-5) and the standard deviations listed above, we may calculate the measurement standard deviation for the three experiments as follows:

a. Measurement of Attenuation Coefficients. The measurement standard deviation S_a is

$$S_a = [a^2 + b^2 + c^2 + d^2 + e^2 + f^2]^{1/2} = \pm 0.54 \text{ dB} \quad . \tag{5-6}$$

b. Measurement of Deterministic Waveforms. The measurement standard deviation S_b is

$$S_b = [a^2 + B^2 + d^2 + e^2 + f^2 + g^2]^{1/2} = \pm 0.55 \text{ dB} \quad . \tag{5-7}$$

c. Measurement of Noise Waveforms. The measurement standard deviation S_c is

$$S_c = [a^2 + b^2 + d^2 + e^2 + f^2 + h^2]^{1/2} = \pm 0.5 \text{ dB} \quad . \tag{5-8}$$

Noise spectra were also measured. The standard deviation for the spectral measurements is obtained by replacing item h in Eq. (5-8)

by item j from the list of standard deviations. The resulting value of S_c is ±0.53 dB.

Since the three accuracy numbers are all about the same, we can safely say that the standard deviation of the measurements is ±0.5 dB. If we refer to the cumulative distribution function for a gaussian random variable [see, for example, Baird (1964)], we see that the value of S may be interpreted as measuring that there is a 68% chance of obtaining errors less than S, a 90% chance of obtaining errors less than 1.65 S, and a 99% chance of obtaining errors less than 2.58 S. Thus, with a standard error of ±0.5 dB the probability of obtaining errors larger than ±0.8 dB is about 10%.

CHAPTER 6 EXPERIMENTAL AND THEORETICAL RESULTS

1. Introduction

In Chapter 6 we present and discuss the theoretical and experimental results that we have obtained. The chapter is divided into several subsections, each devoted to a particular group of results. The subsections are as follows.

1. Introduction.

2. Measurement of tube wall attenuation coefficients.

3. Results concerned with waves that are sinusoidal at the source.

4. A comparison of results obtained using waves that are sinusoidal at the source with those of other researchers.

5. Noise waveform results.

6. Predictions and measurement of noise spectra.

7. The relation of our noise waveform results to results obtained using the "Burgers turbulence" model.

Prior to each experimental measurement, the environmental conditions in the laboratory were carefully measured. The laboratory building is maintained at 72° ±2°F. The realtive humidity, although not specifically controlled, also tends to be quite constant. The range of relative humidities observed during the course of our experiments was from 40% to 60%. Building pressure varies with outside pressure. Nearly constant temperature means that the small-signal sound speed c_o is nearly constant.

The experimental results described here were obtained by making measurements at the eight pipe probe holes. We refer to the distances from the source to these locations using the nearest integer number of feet. The exact distance from the horn driver diaphragm to the various measurement locations is given in Table IV.

TABLE IV

Measurement Locations

Measurement Location	Exact Distance from Source (ft)
1	0.855
2	13.015
3	25.065
4	37.175
5	49.255
6	61.355
7	73.435
8	85.495

In the theoretical results the distances indicated are the exact distances used in the computations. The very small differences between the propagation distances used in the theoretical calculations and the actual distances shown in Table IV are insignificant. The waveform at the point x=1 ft is referred to as the source waveform in the results discussed below. Although the true source is the horn driver diaphragm, we are not concerned here with the actual waveform at the diaphragm. Rather we are concerned with the change in the waveform as it propagates. Hence, for our purposes we may regard the 1 ft measurement location as the source point. The use of a stationary source location is consistent with assumptions made in the derivation of Eq. (3-6).

In several of the figures in the chapter comparisons are made between theoretical and experimental waveforms. The source waveform used in the theoretical computations was the observed source waveform. Hence, the theoretical and experimental waveforms at the point x=1 ft are identical.

2. Measurement of Thermoviscous Attenuation Coefficients

Figure (6-1) shows the measured attenuation in the 2 in. i.d. tube as a function of frequency. Each measurement, except the 500 Hz measurement, was repeated several times. The data is represented in the figure by a point at the measurement mean value and a bracketed line representing the standard deviation of the measurement. The 500 Hz measurement was only performed once. Hence, we do not have a standard deviation for it.

The solid line in Fig. (6-1) is a theoretical curve obtained by use of Eq. (3-64). Our measured values are approximately 10% greater than the corresponding theoretical values. The deviation between our experimental results and the Kirchhoff theory is similar to other reported deviations, e.g., 8% by Pernet and Payne (1969) and 13% by Mariens (1957). The values used to evaluate Eq. (3-64) were those for 72°F, 50% relative humidity, and 760 mm Hg. Handbook values for these environmental conditions are c_o = 34631 cm/sec, ρ_o = 1.191 (10^{-3}) g/cm^3, α = 1.85 (10^{-4}) g/sec-cm, and P_r = 0.71.

3. Results Concerned with Waves That are Sinusoidal at the Source

The basic purpose of our theoretical and experimental investigation of the propagation of an originally sinusoidal signal was

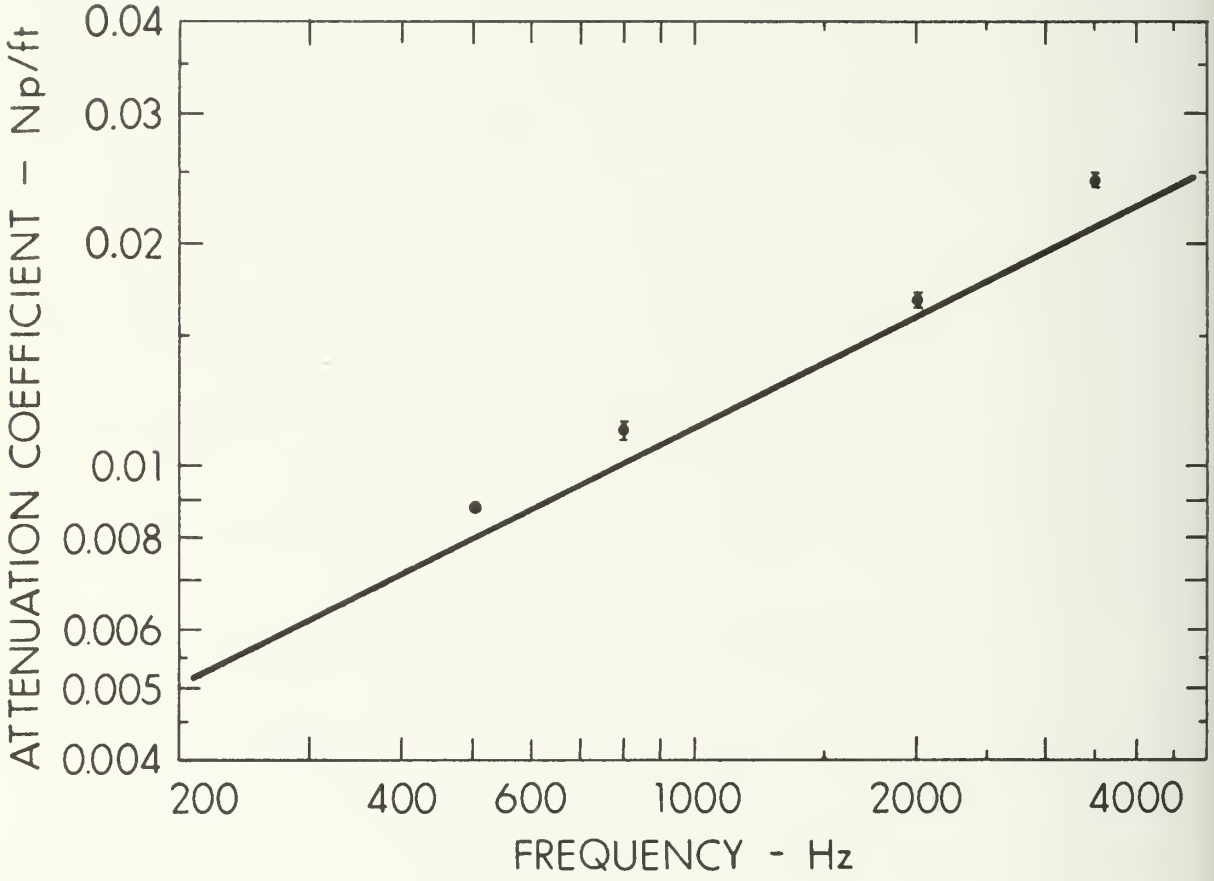

FIGURE 6-1
A COMPARISON OF KIRCHHOFF ATTENUATION THEORY (SOLID LINE) WITH OBSERVED DATA

to evaluate the performance of our computer algorithm and our equipment. This section then is devoted to the results of our developmental testing. The experimental results presented here are similar to those of McKittrick et al. (1967) and some of those of Pernet and Payne (1969). Thus we cannot claim any novelty as to the measurements. We can, however, claim originality for our theoretical results. Modified weak-shock theory is more general than previous theories dealing with the propagation of periodic signals in pipes.

In Figs. (6-2), (6-3), (6-4), and (6-5) experimentally observed waveforms are compared to waveforms computed using modified weak-shock theory. The fundamental frequency attenuation coefficient used in the computation algorithm was obtained from the experimental data shown in Fig. (6-1). Basic information pertaining to the waveforms shown in Figs. (6-2) through (6-5) is summarized in Table V.

TABLE V

INFORMATION PERTINENT TO THE WAVEFORMS SHOWN IN FIGS. (6-2) THROUGH (6-5)

Figure	Fundamental Frequency (Hz)	Source SPL (dB)	Shock Formation Distance* (ft)
6-2	800	159.2	10.42
6-3	2000	160.0	3.80
6-4	3500	148.8	8.26
6-5	2000	160.0	3.80

* The shock formation distance $\bar{x}$ shown in Table V was calculated using the relation

$$\bar{x} = (\beta \epsilon k)^{-1} \quad . \tag{6-1}$$

Equation (6-1) is derived using dissipationless nonlinear theory. Since we include dissipation in our modified weak-shock theory, the actual shock formation distances in our experiments were somewhat greater than the distances shown in Table V.

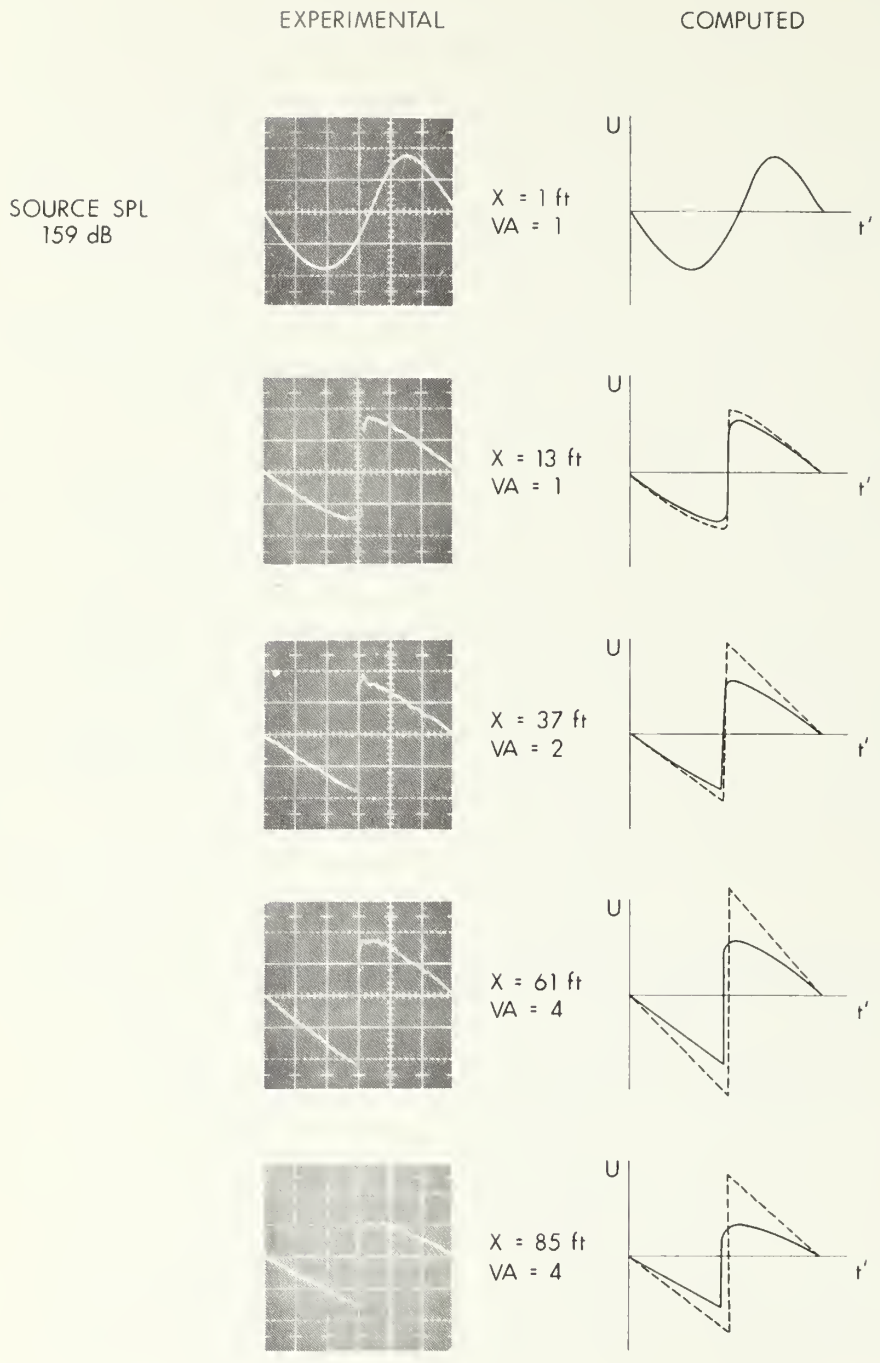

FIGURE 6-2
A COMPARISON OF EXPERIMENTAL AND COMPUTED WAVEFORMS
VA STANDS FOR VERTICAL AMPLIFICATION
FREQUENCY IS 800 Hz

EXPERIMENTAL COMPUTED

Source SPL
160 dB

X = 1 ft
VA = 1

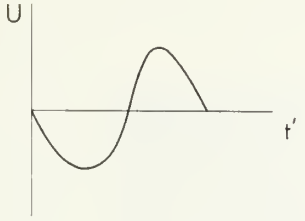

X = 13 ft
VA = 2

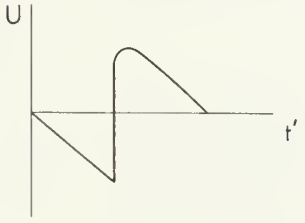

X = 37 ft
VA = 4

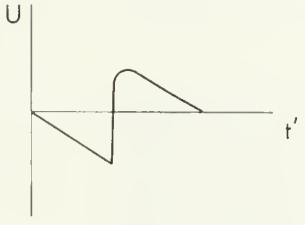

X = 61 ft
VA = 10

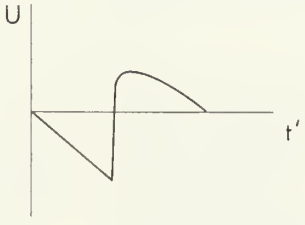

X = 85 ft
VA = 10

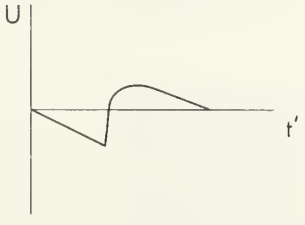

FIGURE 6-3
A COMPARISON OF EXPERIMENTAL AND COMPUTED WAVEFORMS
VA STANDS FOR VERTICAL AMPLIFICATION
FREQUENCY IS 2000 Hz

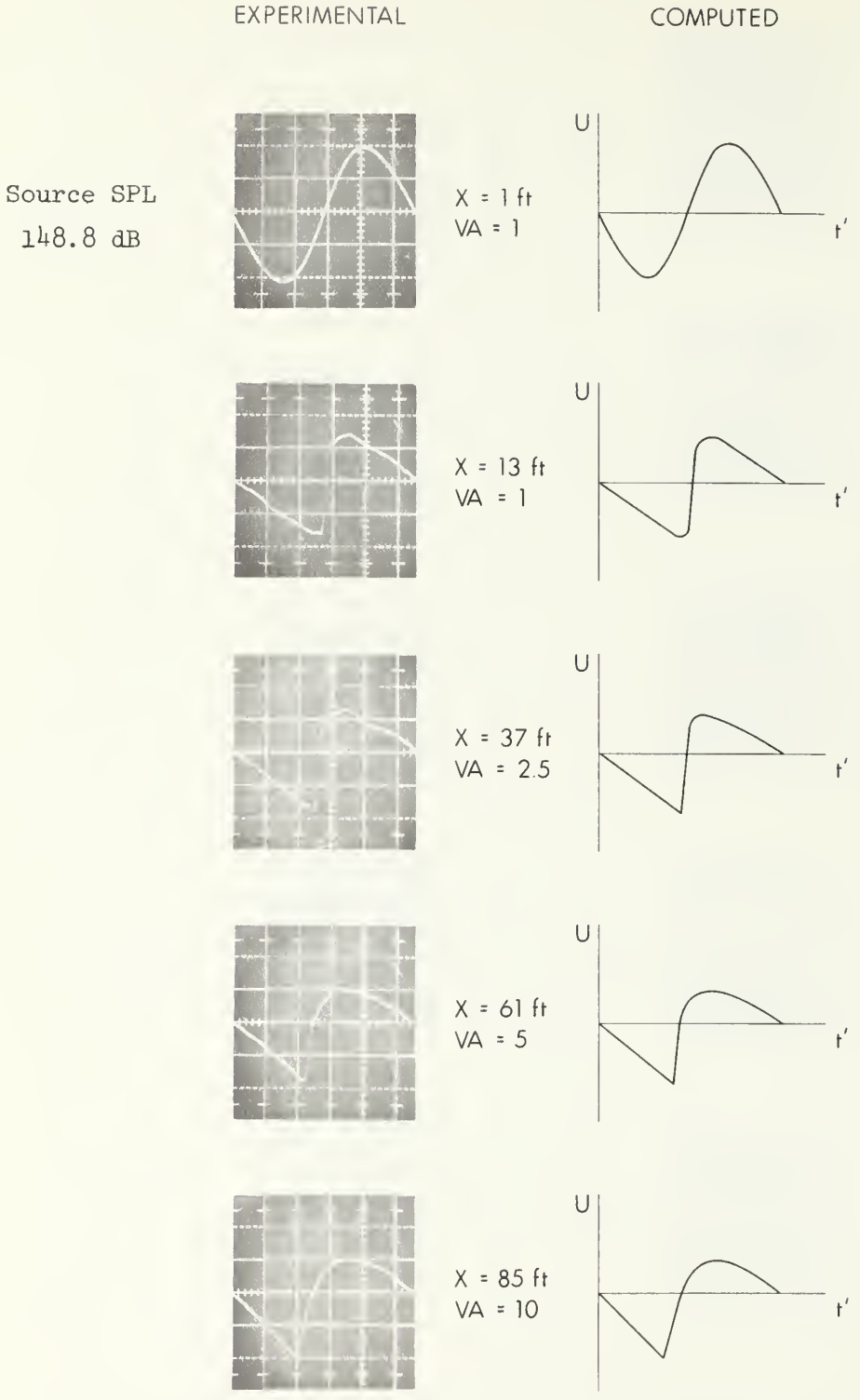

FIGURE 6-4
A COMPARISON OF EXPERIMENTAL AND COMPUTED WAVEFORMS
VA STANDS FOR VERTICAL AMPLIFICATION
FREQUENCY IS 3500 Hz

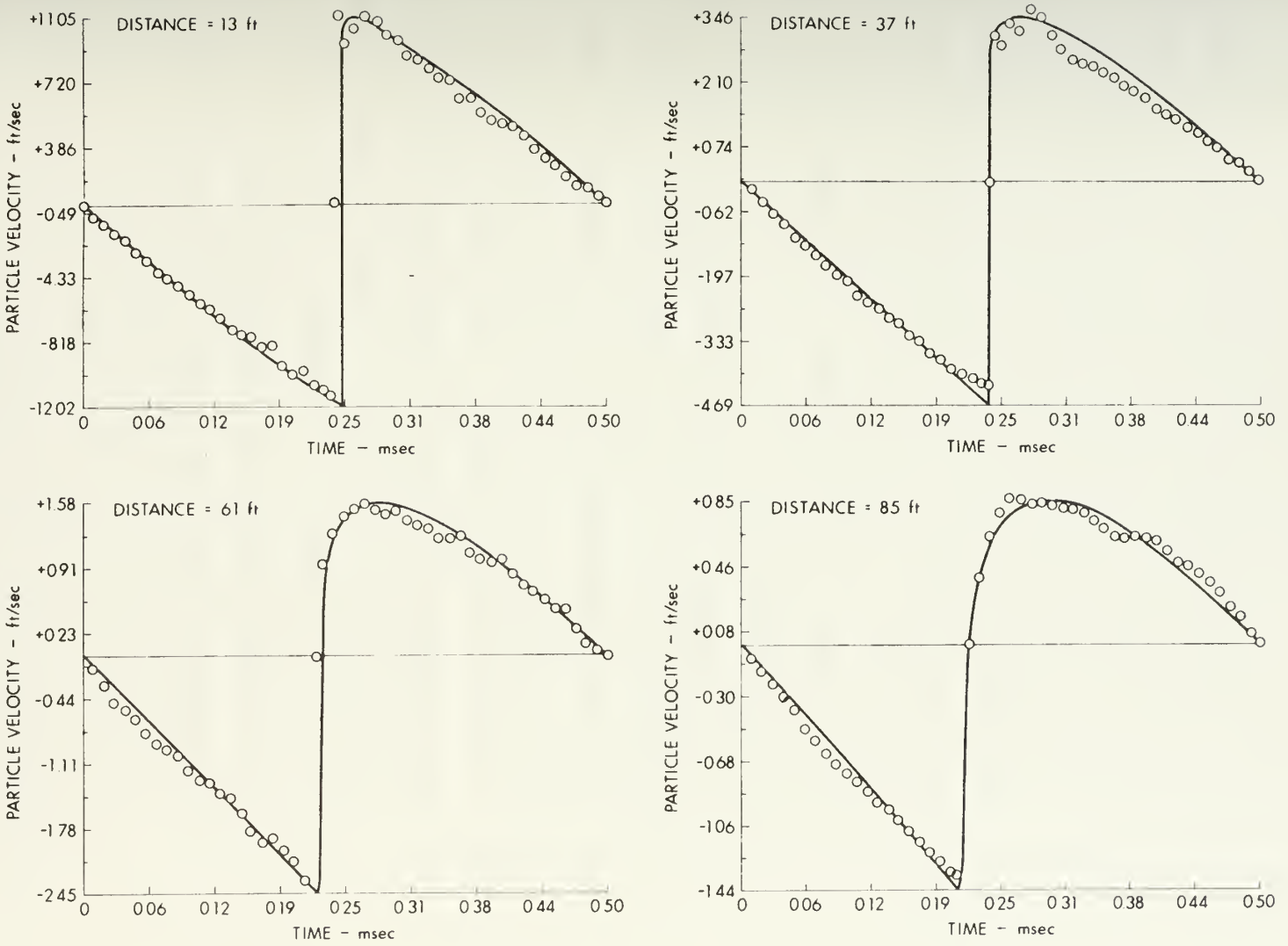

FIGURE 6-5
A COMPARISON OF EXPERIMENTAL AND COMPUTED WAVEFORMS FOR A 2000 Hz SINUSOID

In Fig. (6-2) we present a comparison of theoretical and experimental waveforms at five different locations. The fundamental frequency is 800 Hz. The dashed waveforms were calculated by omitting the wall effects portion of the algorithm. Thus the dashed waveforms are the waveforms that one would expect for plane waves in an open medium and, of course, are the same waveforms one could compute analytically from ordinary weak-shock theory, if the source waveform can be described analytically. The source waveform is already somewhat distorted, primarily because of nonlinearities in our sound source. The source distortion does not concern us, however, because our interest is in the change in the waveform given some initial state.

The observed waveforms agree closely with those predicted using modified weak-shock theory for all measurement distances reported. At the point x=13 ft the observed wave is still fairly symmetric. The only apparent effect of the tube wall on the observed signal is a small decrease in the amplitude over that predicted using ordinary weak-shock theory. The effects of dispersion are not evident at this point because dispersion is a cumulative effect and the wave has not propagated a great enough distance for it to be evident. At the point x=37 ft and beyond the observed waveforms exhibit the asymmetry previously described. Notice that the wave peak is rounded, the trough is sharply angled, and the shock is to the left of the zero crossing at the source. The minor "raggedness" evident on the experimental oscillograms will be considered in our discussion of Fig. (6-5).

What is the cause of the observed waveform asymmetry? In order to answer this question let us assume for the moment that there is no

dispersive or attenuative effect due to the pipe wall. In that case the small-signal sound speed for a sinusoid of any frequency propagating in the pipe is the free field sound speed c_0. Now let us assume further that a finite-amplitude wave is propagating in the pipe. Nonlinear effects cause the generation of harmonic frequencies. In the absence of dispersion each harmonic* propagates at the speed c_0. Hence the various harmonics remain in step. Eventually the distortion of the waveform by nonlinear effects leads to a sawtooth wave. Analysis of the symmetric shape and well known Fourier series for the sawtooth amply demonstrates that the various harmonics are indeed in step. Next let us introduce attenuation due to the pipe wall. In this case each harmonic is attenuated in accordance with Eq. (3-64). The sawtooth shape will be altered somewhat, but the resulting waveform will still be symmetric because the harmonics will have remained in step. Let us finally admit the presence of dispersion. Now each harmonic travels at a speed given by Eq. (3-63). Since higher frequency harmonics travel faster than lower frequency harmonics the harmonics cannot stay in phase. The loss of phase coherence of the various harmonics leads us to conclude that dispersion is the cause of the waveform asymmetry.

Now let us consider the particular shape of the asymmetric waveforms. The fact that higher frequency harmonics travel faster than the lower frequency ones means that the troughs of the various

---

*We draw an important distinction here between the propagation velocity of a wavelet and the propagation velocity of some harmonic. The wavelet travels at a speed given by use of Eq. (2-4). The harmonics are being continuously generated by nonlinear effects but the propagation velocity of the harmonic itself is given in the absence of dispersion by the small-signal sound speed.

harmonics will become lined up whereas the peaks will spread apart. Therefore the trough of the overall waveform will be sharply angled whereas the peak will be broad and rounded; at the same time the zero crossing will shift to the left of its original position. The reader may quickly convince himself that our analysis is plausible by sketching the first several harmonics of a sawtooth and then displacing the various harmonics for the case in which speed increases with frequency. The resulting overall waveform will exhibit the asymmetry described here.

Figure (6-3)* shows a comparison of 2000 Hz fundamental frequency experimental and theoretical waves. The dashed weak-shock waveforms included in Fig. (6-2) have been omitted in Fig. (6-3). At the point x=13 ft the wave has traveled about 3 shock formation lengths so that on the basis of ordinary weak-shock theory we would expect a sawtooth wave. Because of wall effects, however, there is some rounding of the peak of the wave.

In Fig. (6-4) the fundamental frequency of the waves is 3500 Hz. The purpose of Fig. (6-4) is to demonstrate that our method is applicable to waves having fundamentals at least as high as 3500 Hz. We have not quantitatively defined the point at which a finite-amplitude wave no longer contains shocks.** Qualitatively, however, we can observe that the shocks in the waveforms at the point x=85 ft are badly degraded.

---

*Figure (6-3) has previously been reported by Pestorius and Blackstock (1972).

**Blackstock (1966) calculates the inception of "old age" as occurring at the point

$$x = \alpha_o^{-1} \qquad (6\text{-}2)$$

In the case shown in Fig. (6-4) evaluation of Eq. (6-2) yields $\alpha_o^{-1}=40$ ft.

In Fig. (6-5) the sets of waveforms at the points x=13 ft, x=37 ft, x=61 ft, and x=85 ft shown in Fig. (6-3) have been enlarged and overlaid. The agreement between theory and experiment in each comparison is excellent. In particular note that the waveforms agree at the point x=85 ft as well as they agree at the shorter distances, thereby indicating that there are no apparent cumulative errors in our method. Similar comparisons of the waveforms shown in Figs. (6-3) and (6-4) have been made. In general the experimental and theoretical waveforms shown in Figs. (6-2) and (6-3) agree with one another in a manner similar to the agreement shown in Fig. (6-5).

The minor "raggedness" in the experimental data appears to be due to scattering from minor irregularities in the pipe and pipe flanges near the microphone. The raggedness appears to be shock excited since it is not apparent until shocks are present. The pattern of these waveform irregularities is very repeatable cycle to cycle, but the pattern can be varied at any particular measurement location by disassembling and reassembling the pipe flange at that location. We have not conducted any further analysis of the waveform irregularities since, no matter what their origin is, they are minor compared to the effects that we are studying.

4. A Comparison of Results Obtained Using Waves That are Sinusoidal at the Source with Those of Other Researchers

In Figs. (6-6) and (6-7) we compare some of our results obtained using waves that are originally sinusoidal with those of Pernet and Payne (1971a) and Coppens (1971), respectively. In Fig. (6-8) we compare results obtained using weak-shock theory, modified weak-shock

theory, and the theory derived by Rudnick (1952). Each of these comparisons will be discussed in turn.

Pernet and Payne (1971) were concerned with wave propagation problems in which finite-amplitude distortion is significant but shocks do not form. In the developmental testing of their analytic model, high intensity (e.g., 160 dB) sinusoids were generated and the levels of the fundamental and the first nine harmonics recorded as a function of distance. Although the intensity of these sinusoids was too great for analysis using their method, they did given the experimental data for a 500 Hz sinusoid and its first nine harmonics. We have modified program ATENDIS5* in such a way that we may calculate the amplitude of the fundamental and the 2nd through 5th harmonics of a 500 Hz sinusoid as a function of distance. In Fig. (6-6) we have compared the Pernet and Payne data (solid curves) for these signals with our theoretical predictions (symbols). In the calculation of the theoretical data, our measured value of the fundamental frequency attenuation coefficient was used [see Fig. (6-1)]. The agreement between the experimental data and theory is quite good although our theory points lie slightly above the data. Of course, since we do not know the accuracy of their measurements an absolutely quantitative comparison is difficult to make. The important fact is that the Pernet and Payne data provide an independent check of modified weak-shock theory as implemented by our algorithm. The Pernet

*For those readers who did not read Chapter 4, program ATENDIS5 is a computer program wherein we combine weak-shock theory and tube wall attenuation and dispersion. Program ATENDIS5 was used to compute the theoretical results presented in Sections 3 and 4. A similar program, Program NSATDIS, was used to compute the results in Sections 5, 6, and 7. Programs ATENDIS5 and NSATDIS are very similar in content. The reason for using two separate programs was primarily for convenience.

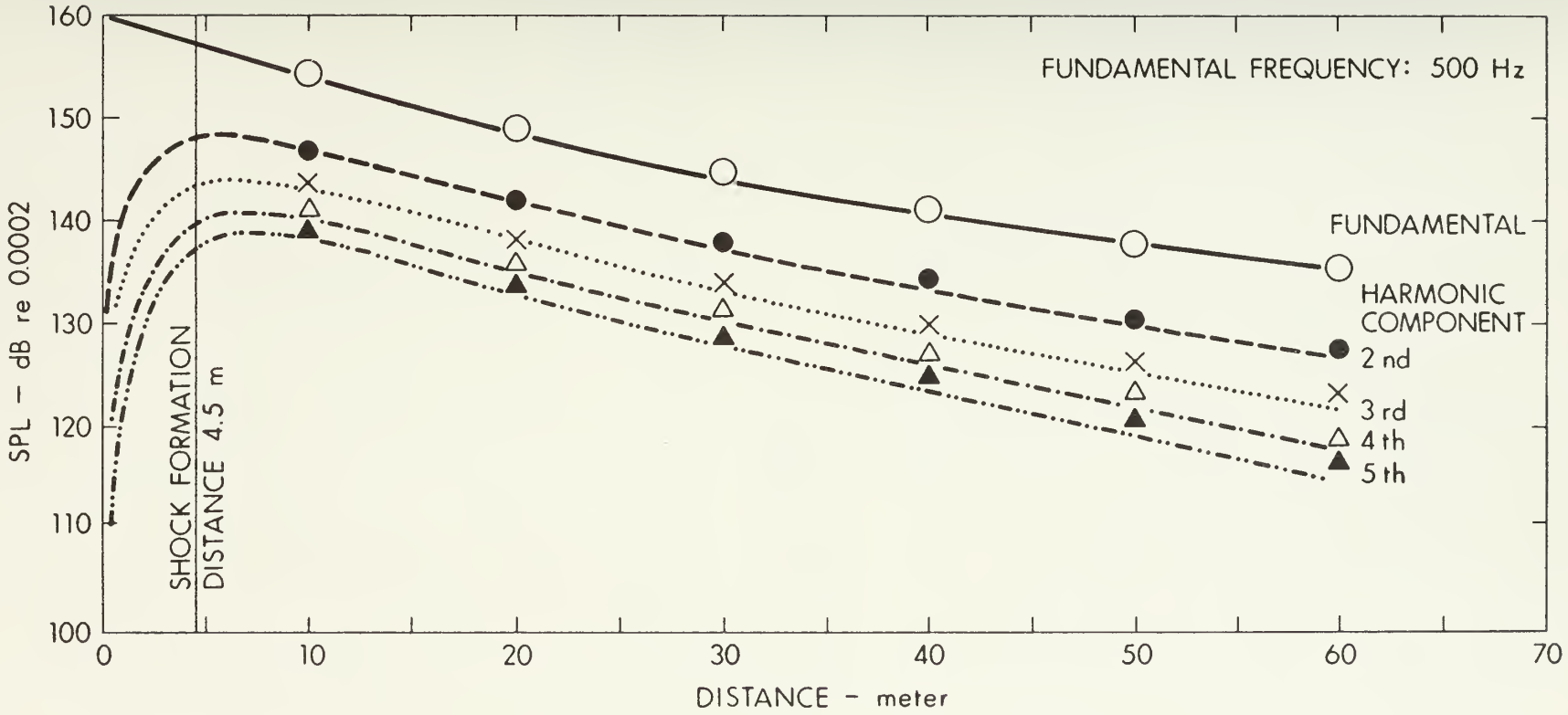

FIGURE 6-6
A COMPARISON OF DATA TAKEN FROM PERNET AND PAYNE (SOLID LINES) VERSUS MODIFIED WEAK SHOCK THEORY

and Payne paper contains several other sets of data that could be checked against our theory. These checks have not been performed for want of time.

Coppens' (1971) results are purely theoretical and are valid only for propagation distances that preclude shock formation. Several plots are given that depict the waveform distortion that occurs as an originally sinusoidal wave propagates in a pipe. These plots are similar in content to the theoretical curves shown in Figs. (6-2) through (6-5). Coppens defined two dimensionless parameters as follows:

$$\ell = \alpha_o x \quad , \tag{6-3}$$

and

$$\frac{M\beta}{\delta_1} = \frac{\beta\epsilon k}{2\alpha_o} \quad . \tag{6-4}$$

Evaluation of Eqs. (6-3) and (6-4) at the point x=61 ft using a source sinusoid having a sound pressure level value of 142 dB and a frequency of 2000 Hz yields the values ℓ=0.99 and $M\beta/\delta_1$=1.0 . These two values closely match the parameter values for one of Coppens' published waveforms. Hence, we may directly compare our theory and experimental data with Coppens' theory. In Fig. (6-7) we have compared modified weak-shock theory (solid line), our experimental data points (circles), and Coppens' theory (dotted line). The agreement between our theory and data is excellent. Coppens' theory also agrees closely with ours. The differences between the two theoretical curves are probably due to the difference in the value of the fundamental frequency attenuation coefficient used in each analysis.

PARAMETER	COPPENS (DOTTED LINE)	MODIFIED WEAK SHOCK (SOLID LINE)	DATA (CIRCLES)
$\frac{\beta \epsilon k}{2a_0}$	1.0	1.0	1.00 ± 0.02
DISTANCE - ft	62.2	61.4	61.4

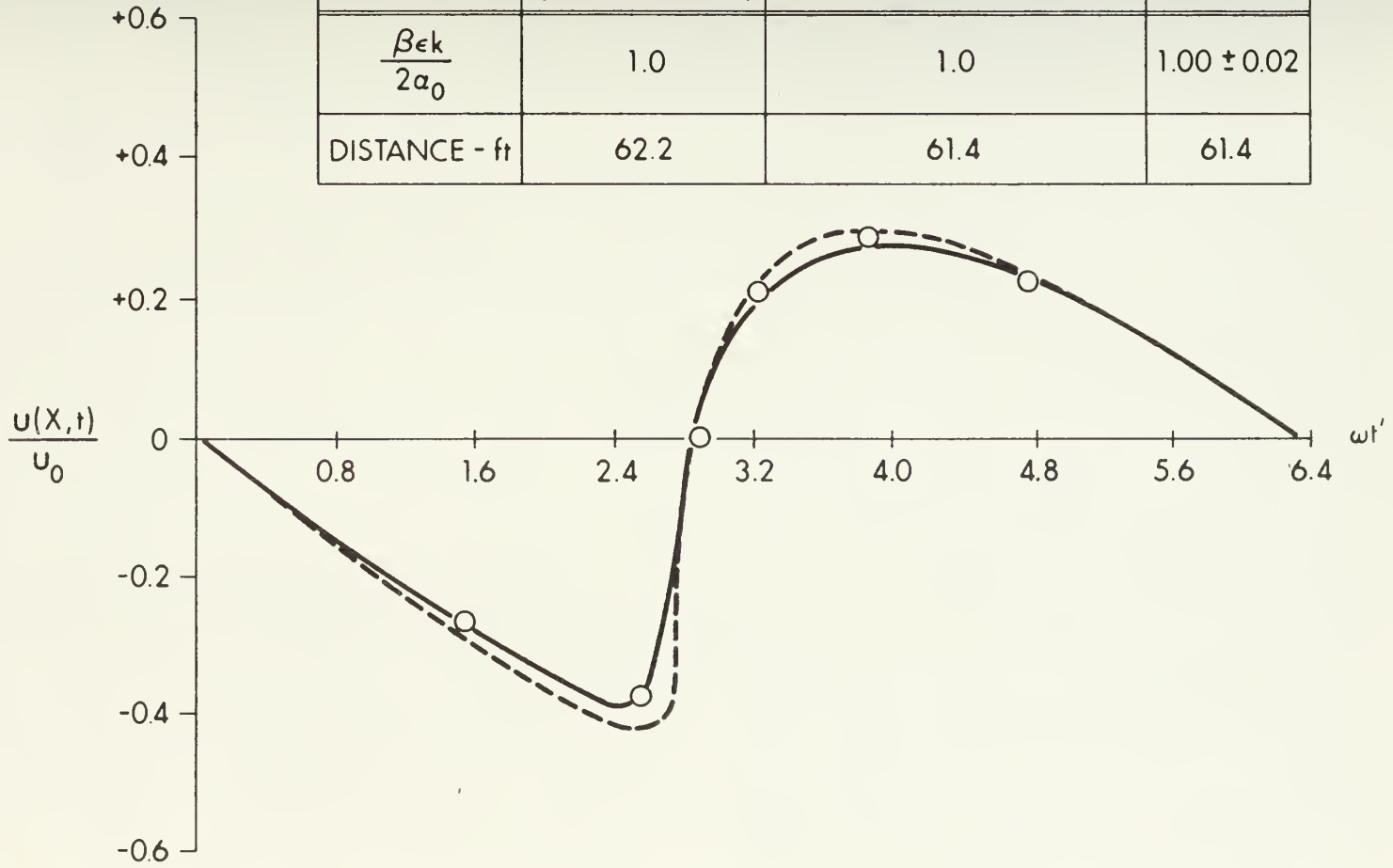

FIGURE 6-7
A COMPARISON OF MODIFIED WEAK-SHOCK THEORY (SOLID LINE), EXPERIMENTAL DATA (CIRCLES) AND COPPEN'S THEORY (DOTTED LINE)

Coppens used the Kirchhoff theory value while we used a value that we had measured. The measured value exceeded the theoretical value by 10% and the difference is probably the cause of the greater signal attenuation evident in our results.

In modified weak-shock theory we combine shock effects and pipe wall effects in an iterative fashion. A possible alternate computational scheme consists of combining the nonlinear and pipe wall attenuation (but not dispersion) in a nonlinear differential equation. Rudnick (1952) derived such an equation for the propagation of sawtooth waves. Recasting Rudnick's equation in terms of the variables used here, we obtain

$$\frac{dP_{max}}{dx} = -\alpha P_{max} - \frac{\beta k}{\pi \rho_o c_o^2} P_{max}^2 \quad , \qquad (6\text{-}5)$$

where

P_{max} = peak acoustic pressure, and

α = the attenuation coefficient calculated using Rudnick's "zero-order correction" method.

The first term on the right hand side of Eq. (6-5) accounts for thermoviscous attenuation and the last term accounts for attenuation due to the effects of nonlinear propagation. The solution of Eq. (6-5) subjects the boundary condition that $P_{max} = P_{max}(0)$ at x=0 is

$$P_{max} = \frac{P_{max}(0)\, e^{-\alpha x}}{1 + \frac{\beta k P_{max}(0)}{\alpha \rho_o c_o^2 \pi} (1 - e^{-\alpha x})} \quad . \qquad (6\text{-}6)$$

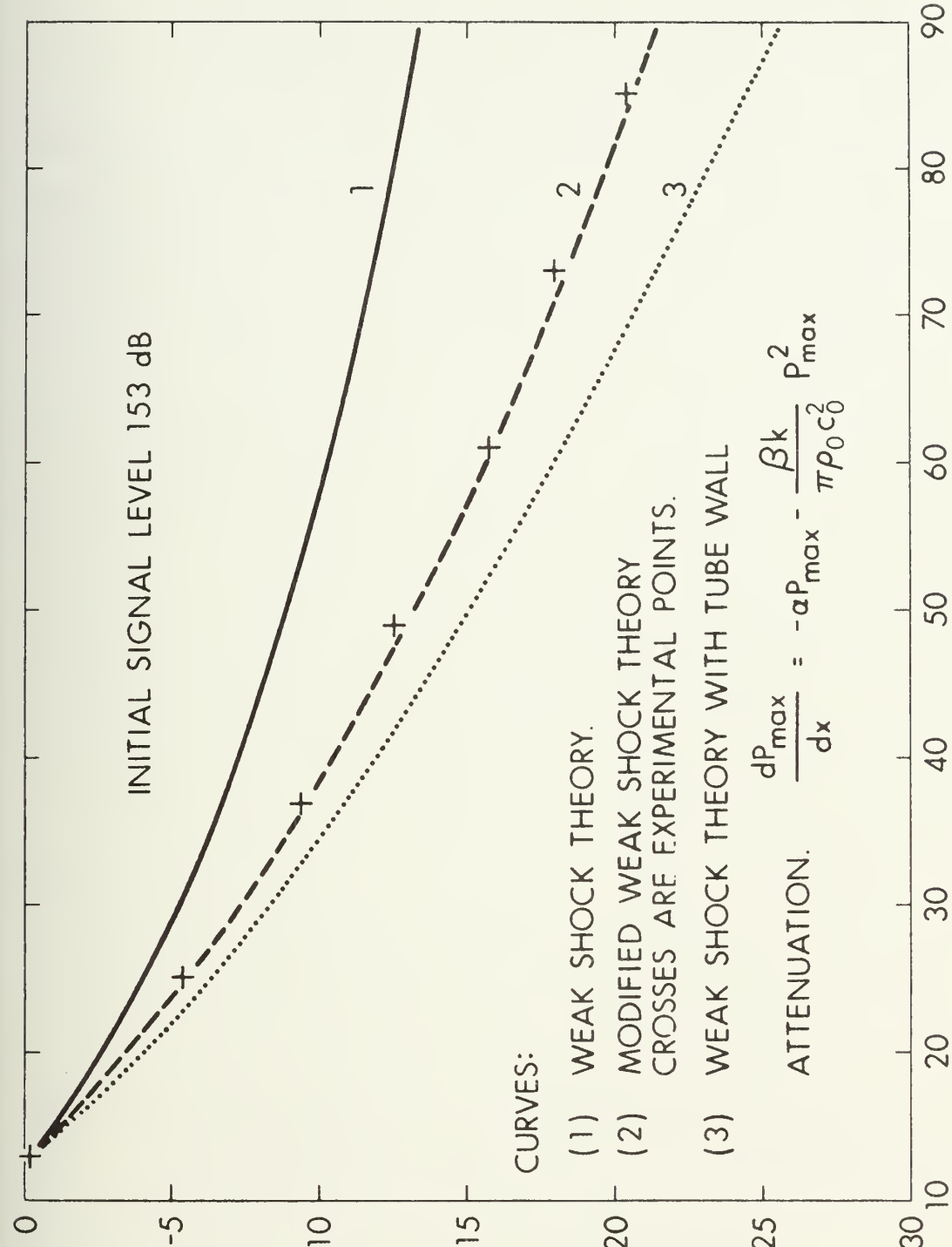

FIGURE 6-8
20 $\log_{10}$ ΔP vs DISTANCE

In Fig. (6-8)* we compare our theory and experimental results with predictions obtained using Eq. (6-6). Referring to the waveforms presented in Fig. (6-3), we selected the experimental waveform at the point x=13 ft as a starting point for our calculations. This waveform is appropriate because it is almost sawtoothed in shape (use of Eq. (6-6) requires that the wave be a sawtooth to begin with). The data presented in Fig. (6-8) shows the change in peak-to-peak amplitude of the wave as it propagates. Curve 1 is the result obtained using weak-shock theory, curve 2 is the result obtained using modified weak-shock theory and curve 3 is the result of calculations based on Eq.(6-6). The experimental points confirm the middle curve. Use of weak-shock theory predicts too little attenuation because absorption due to the tube wall boundary layer is neglected. Yet when we linearly add the wall absorption we predict too much attenuation. The key to the agreement between our theory and experimental data is our inclusion of dispersion in modified weak-shock theory. The severe rounding of the peaks of the shocks caused by dispersion in effect reduces the shock amplitude. Referring to Eq. (3-17), we see that attenuation at the shock depends upon the shock amplitude. Hence, dispersion inhibits the attenuation associated with the shock. The combined effects of the reduced shock attenuation and the tube wall attenuation then yield the results shown in the middle curve.

*Figure (6-8) has previously been reported by Pestorius and Blackstock (1972).

5. Noise Waveform Results

As we noted in the introductory chapter, we are especially interested in the finite-amplitude distortion of noise waveforms. In Figs. (6-9)* and (6-11) comparisons are made between measured and computed noise waveforms. In Fig. (6-10)* comparison is made between weak-shock theory and modified weak-shock theory using some of the waveforms in Fig. (6-9). The theoretical results in Figs. (6-9), (6-10), and (6-11) were computed using program NSATDIS. As was done in the examples in Section 3, the source waveform for use in the noise waveform computations was obtained by sampling the observed wave at the point x=1 ft. In these computations the theoretical value of α_o was used rather than the measured value because a direct measurement could not be made at the fundamental frequency [61.4 Hz for the waves shown in Fig. (6-9) and 78.2 Hz for the waves shown in Fig. (6-11)].

Computed and measured waveforms are shown in Fig. (6-9). The SPL at the source was 160 dB. The agreement between theory and experiment is quite good. Note, however, that unlike the results given in Section 3, the apparent agreement between the theoretical results shown and the measurements deteriorates slightly as the propagation distance gets large. We believe that adjustment of the incremental distance steps in our program could minimize this small disagreement. However, the necessary adjustment was not deemed worthwhile in terms of the cost of the additional computer time required and, hence, was not performed.

---

*Figures (6-9) and (6-10) have previously been reported by Pestorius and Blackstock (1973a).

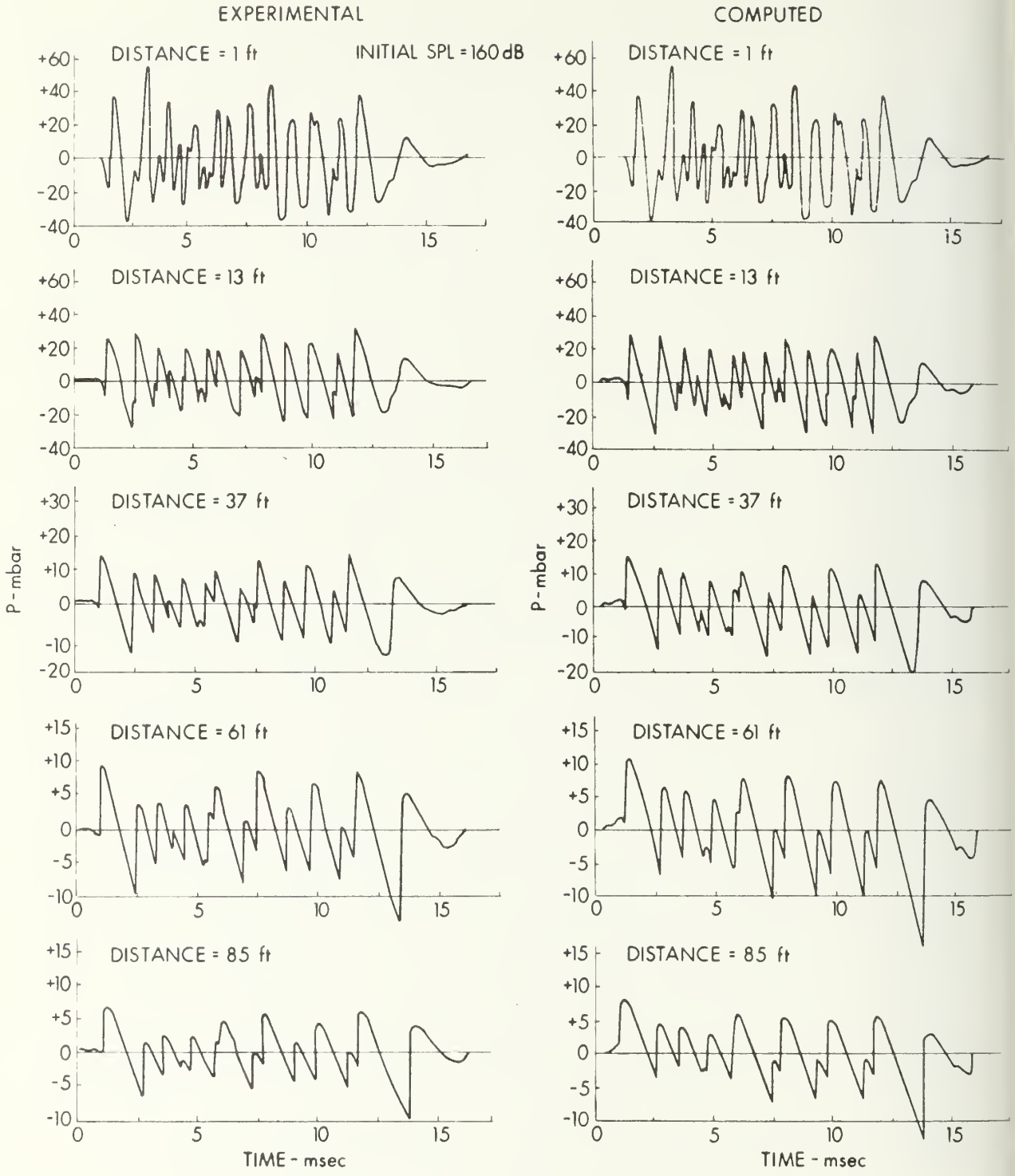

FIGURE 6-9
NOISE PULSE I AT VARIOUS DISTANCES

In Fig. (6-10) the computed waveforms at 13 ft and 85 ft, shown in Fig. (6-9), are repeated and compared to waveforms computed by using the algorithm based on weak-shock theory alone. It is clear that the wall effects have a very significant influence on the waveform, particularly at the greater distance. This increased influence is caused by the fact that the effects of attenuation and dispersion are cumulative with distance and the fact that the nonlinear effects grow weaker with distance.

Figure (6-11) is similar to Fig. (6-9) except that a different sample pulse is shown. Figure (6-11) is included to demonstrate that the results shown in Fig. (6-9) are not atypical. The sound pressure level for the pulse shown in Fig. (6-11) was 155 dB.

The waveforms shown in Figs. (6-9) and (6-11) undergo marked change as they propagate. The source waveforms in both examples are free of shocks. At the point x=13 ft, however, the waveforms in both examples have numerous shocks. Since individual positive sloping sections are very steep, the first shocks form within a few feet of the source point.

Let us now restrict our attention to the results shown in Fig. (6-9). At the points x=13 ft and x=37 ft the waves are still very intense and the rounding effect at the wave peaks due to dispersion is not very evident. The lack of noticeable rounding indicates that the dispersive effects are being obscured by the much stronger nonlinear effects. At the points x=61 ft and x=85 ft the rounding of the wave peaks is very evident. Note also that the propagating wave simplifies considerably as the shocks merge with one another. These waveform

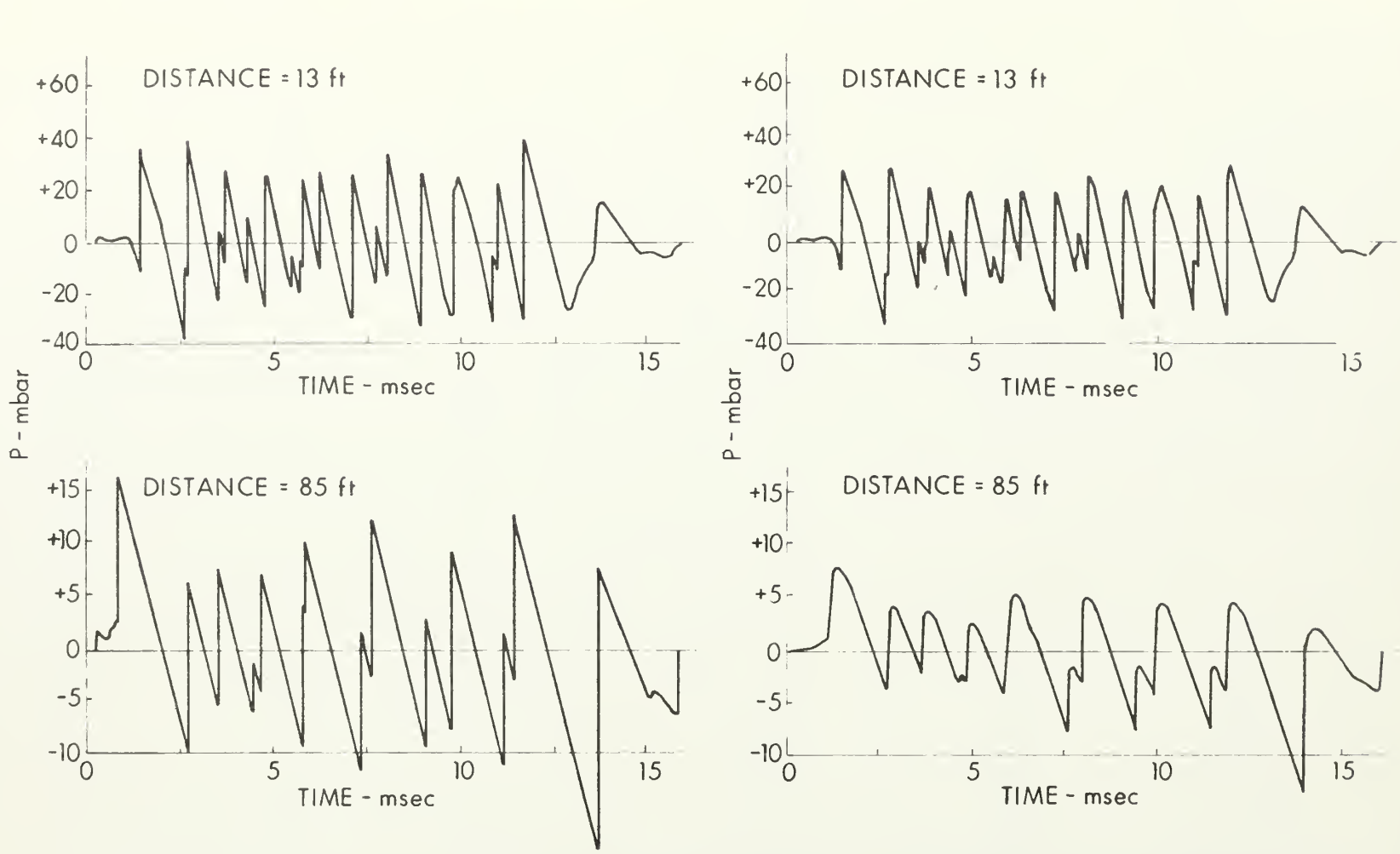

FIGURE 6-10

A COMPARISON OF WEAK SHOCK THEORY AND WEAK SHOCK THEORY MODIFIED BY TUBE WALL EFFECTS

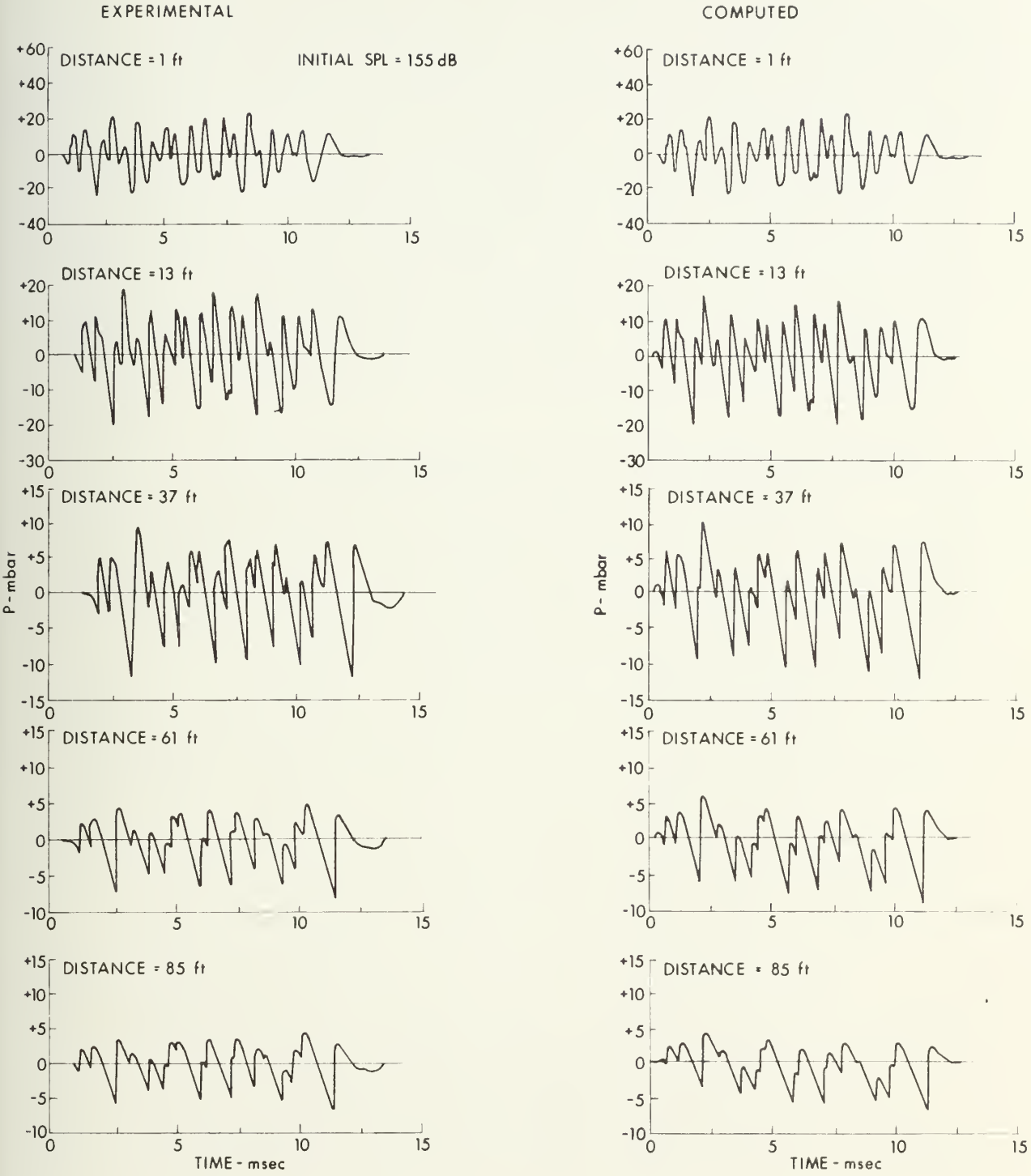

FIGURE 6-11
NOISE PULSE II AT VARIOUS DISTANCES

changes can, of course, be used to predict changes in the wave spectrum as a function of distance. We shall, however, defer the discussion of spectra until Section 6.

In the preceding paragraph we restricted our attention to the results shown in Fig. (6-9), but, in general, the above remarks apply also to the results shown in Fig. (6-11). The source SPL for this latter example was lower (155 dB). Therefore the effects of dispersion become evident sooner than in the example shown in Fig. (6-9).

6. Predictions and Measurements of Noise Spectra

In this section we present three sets of spectral results. The first two sets are computer generated and include the effects of nonlinear propagation, but do not include the effects of the tube wall. The last group of spectra were obtained experimentally.

We used the waveforms at the point x=1 ft in Figs. (6-9) and (6-11) as the input data for program DOITALL3* in order to compute the first set of results. Spectra were computed at the point x=1 ft, and, following "computer propagation", at the points x=49 ft and x=73 ft. These results appear in Figs. (6-12)** and (6-13), respectively.

In the second group of results the spectra are entirely computer generated. The source waveforms were obtained using the digitally filtered output of a computer random number generator. The results of these computations appear in Fig. (6-14). As in the previous group of results

---

*For those who did not read Chapter 4, DOITALL3 is a computer program used to calculate spectra. The computation method used is the Blackman and Tukey (1959) indirect method.

**Figures (6-12), (6-14), and (6-15) have been previously reported by Pestorius and Blackstock (1973b).

spectra at the points x=1 ft, x=49 ft, and x=73 ft are presented.

The third set of results are shown in Fig. (6-15). These results were obtained using the General Radio Wave Analyzer and Recorder. A 50 Hz crystal was used in the wave analyzer. The frequency range was scanned very slowly to give a long integration time. Stable statistical estimates were obtained in this manner. The noise signal was produced by bandpass filtering the output of the ELGENCO Model 603A noise generator, power amplifying this output, and applying it to a horn driver attached to the plane wave pipe.

We will now consider in turn each of these sets of results. In Figs. (6-12) and (6-13) three spectra are presented. The equivalent bandwidth of the spectral estimates is 50 Hz. The spectra shown in both figures were normalized by dividing each spectrum data point by the maximum value in the respective source spectrum. Had the propagation been in accordance with linear acoustic theory, the three spectra in each figure would have been identical. The flattening and spreading of the spectra shown in Figs. (6-12) and (6-13) are the result of nonlinear effects. In particular, the spectra at the points x=49 ft and x=73 ft actually cross over the source spectrum indicating a net increase in energy at frequencies above the crossover frequency. In order to investigate the effects of aliasing inherent in spectral computations, the frequency at which the source waveforms were sampled was increased to 196 kHz and the spectral computations were repeated. The analysis showed that aliasing was minimal and, in particular, that no large line components were present above the frequencies shown in Figs. (6-12) and (6-13).

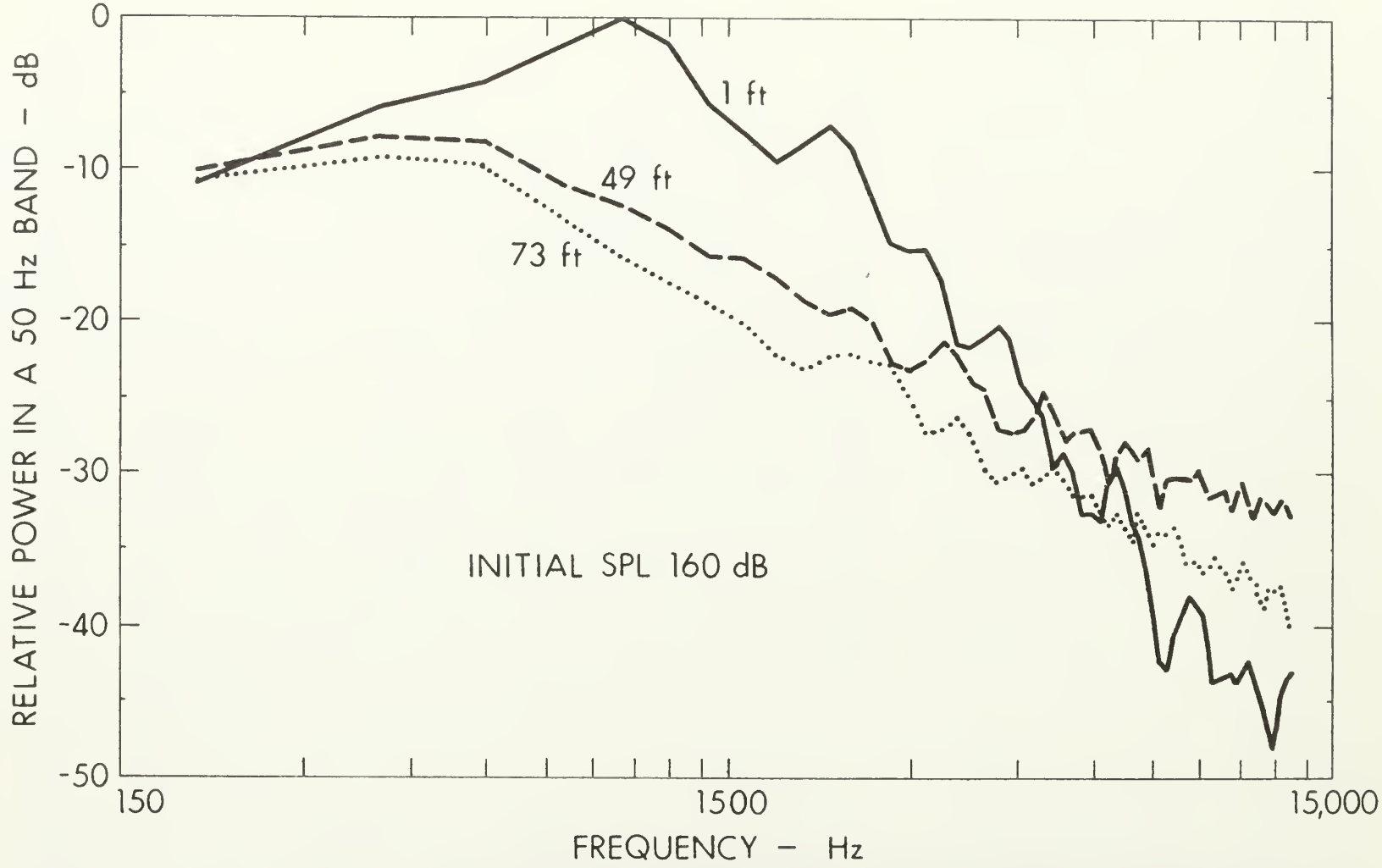

FIGURE 6-12
SPECTRUM OF NOISE PULSE I
AT VARIOUS DISTANCES

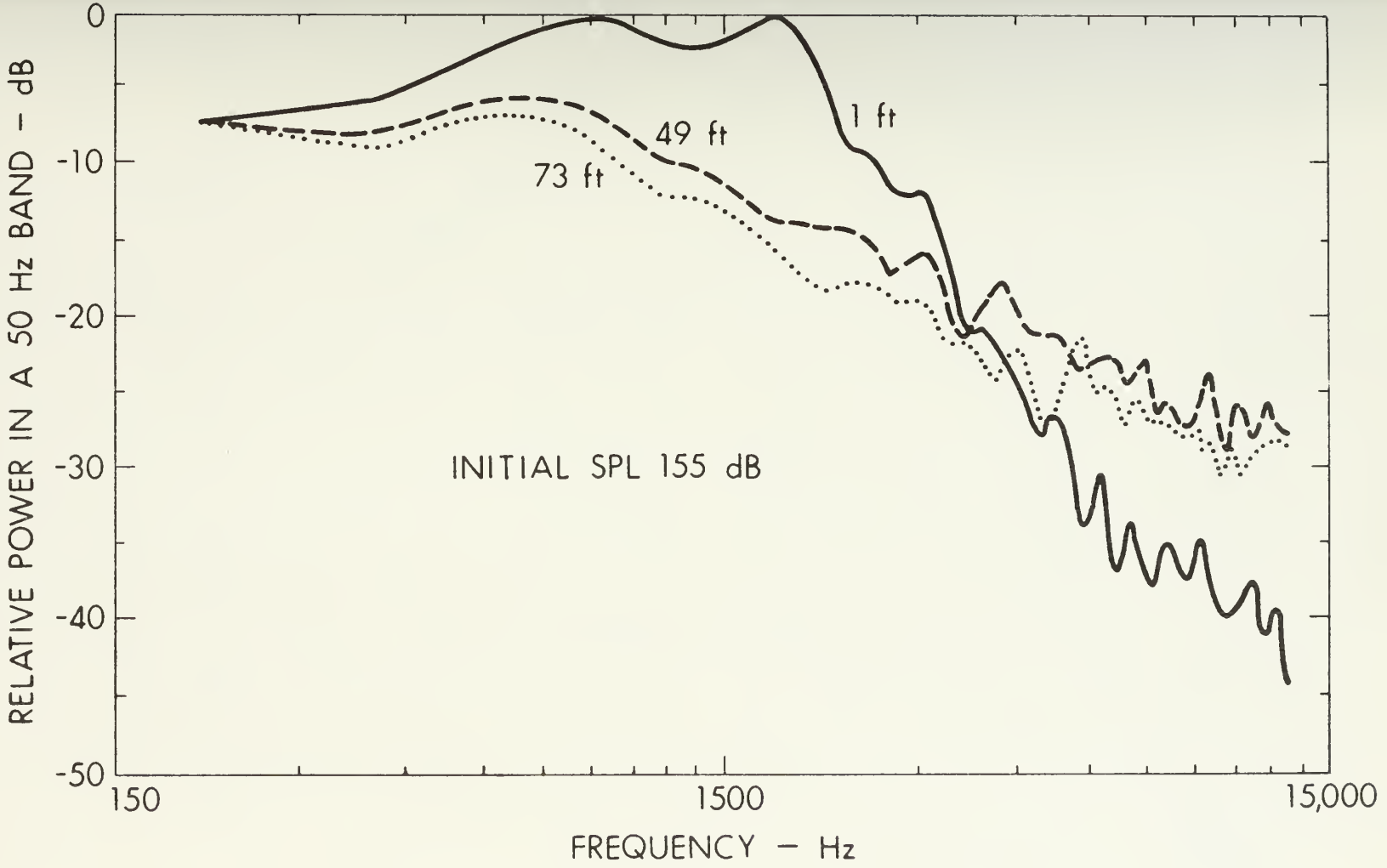

FIGURE 6-13
SPECTRUM OF NOISE PULSE II
AT VARIOUS DISTANCES

The purpose of this group of results then was to 1) predict the spectral changes due to nonlinear effects for particular noise waveforms, and 2) to investigate the effects of aliasing present in our spectral computations.

The purpose of the spectral measurements shown in Fig. (6-14) was to predict as closely as possible the actual average spectral shape of noise waves propagated in our pipe. The 3 dB down points used in the digital filter program were 700 Hz and 2200 Hz and the slopes of the skirts of the source spectrum closely match those observed at the horn driver output during our initial system calibration. The spectra in Fig. (6-14) are smoother than those in Figs. (6-12) and (6-13) because of increased averaging.

In Fig. (6-15) actual experimental spectra are shown. The results are very similar to the results shown in Figs. (6-12), (6-13), and (6-14). In particular, the high frequency crossover shown in all three of the former figures appears in Fig. (6-15). The low frequency crossover predicted in the results shown in Fig. (6-14) was observed and appears in Fig. (6-15). Since the source spectrum shown in Fig. (6-14) was tailored to match our average source conditions as closely as possible, the verification of the low frequency crossover prediction is especially significant. The total dissipation suffered by spectral components shown in Fig. (6-15) is greater than that suffered by the same components shown in the computed results because the spectra shown in Fig. (6-15) have suffered tube wall losses as well as nonlinear attenuation. The local spectral peaks at about 8 kHz shown in Fig. (6-15) are apparently due to a resonance in the horn driver.

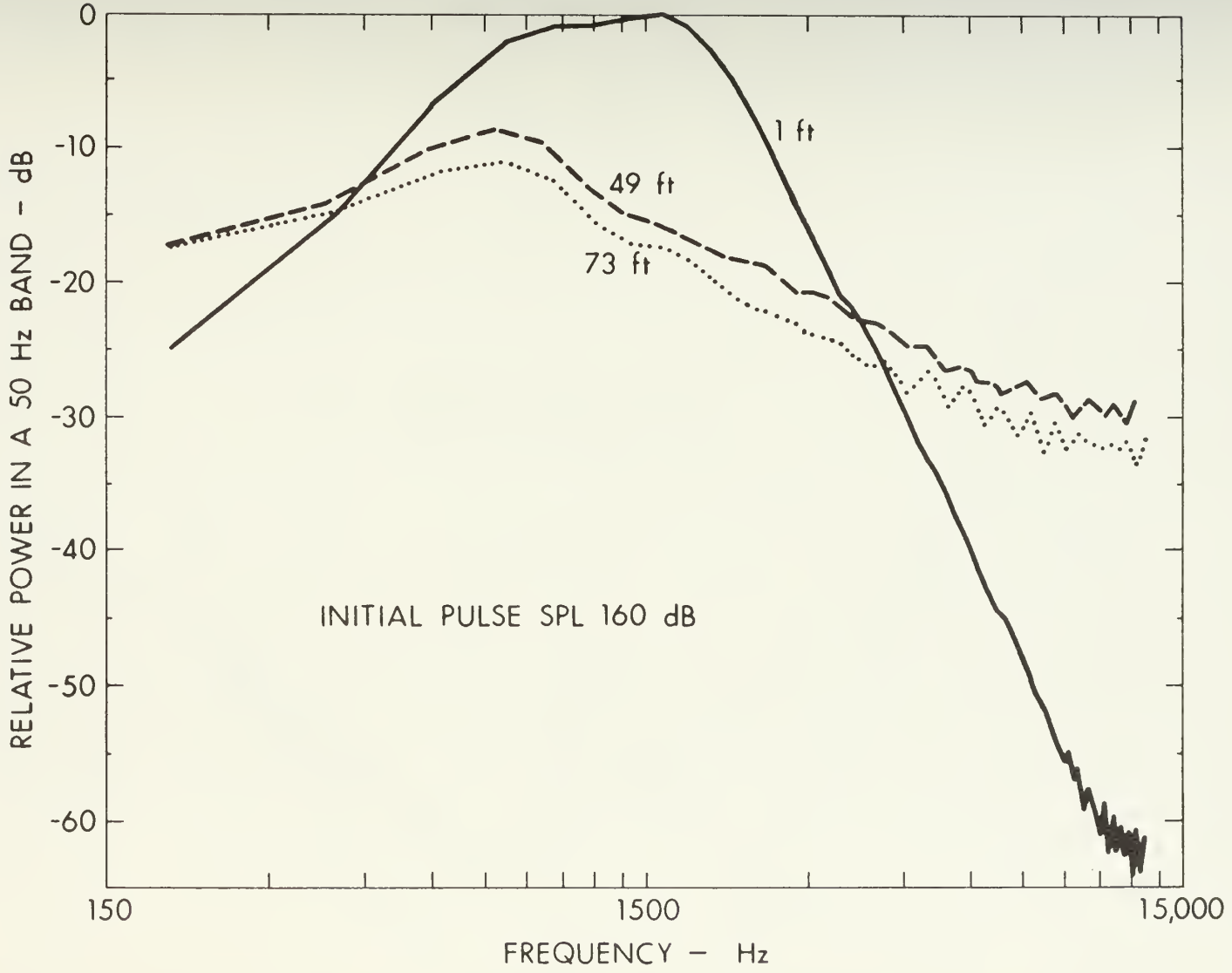

FIGURE 6-14
COMPUTER GENERATED NOISE SPECTRA

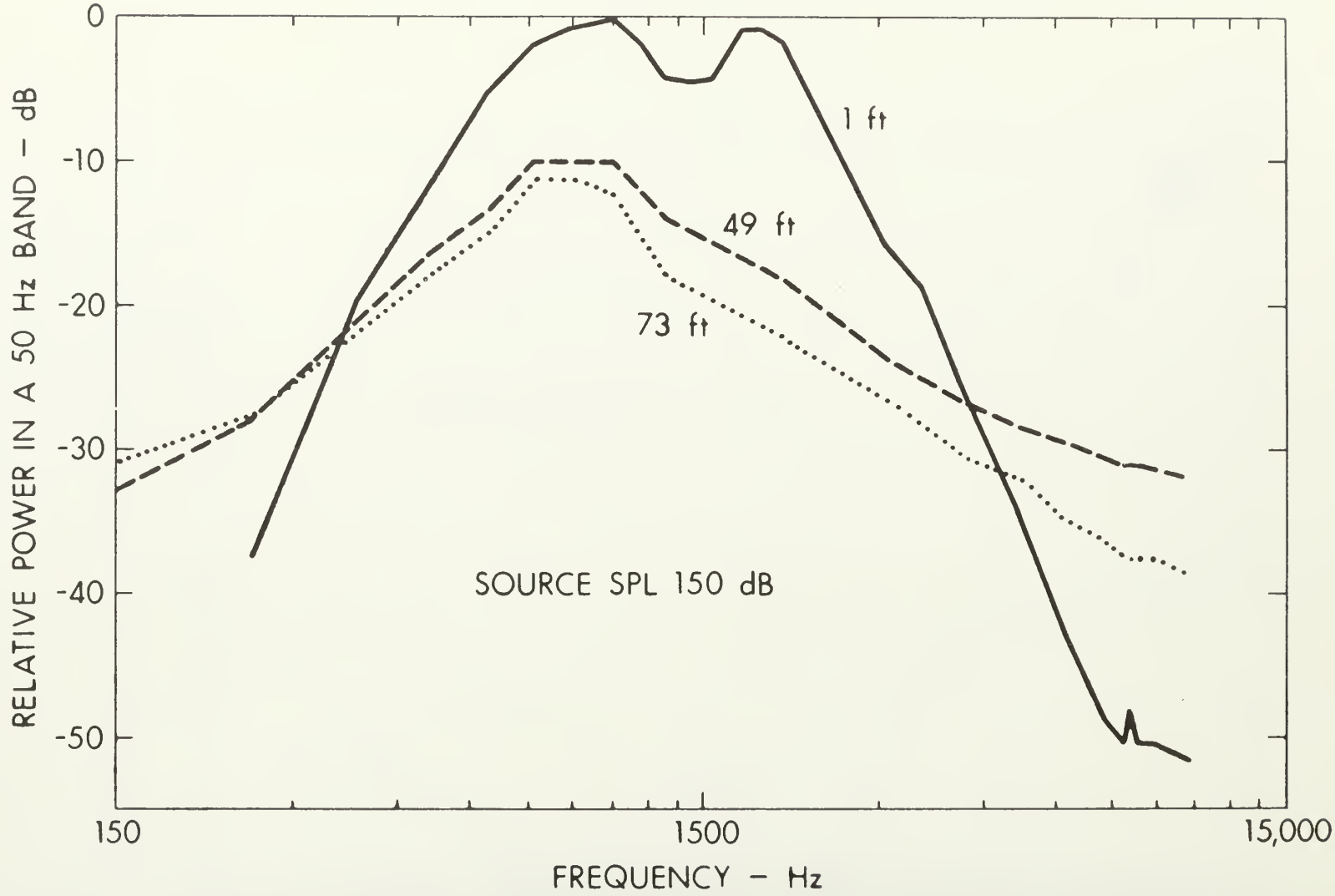

FIGURE 6-15
EXPERIMENTAL SPECTRUM AT VARIOUS DISTANCES

Let us now consider the change in the wave spectra interpreted in terms of the waveform changes noted in the previous section. We observed that the waves simplified significantly as a function of distance. In particular the number of zero crossings diminishes. The waveform simplification represents a transfer of energy to the lower end of the spectrum. Conversely, the presence of nonlinear steepening means that the high frequency end of the spectrum is also enhanced. In fact, the high frequency build-up commences as soon as the wave is formed whereas the low frequency effect requires the presence of shock fronts. Once the shocks in a particular noise sample have all formed, the flow of energy will proceed only toward the low end of the spectrum. Thus the overall effect of nonlinear propagation is to flatten out the wave spectrum.

Alternatively, these same effects can be understood as the result of the intermodulation of various source spectral components. If we think of the source spectrum as a band of closely spaced line components, each component will interact with each other component to produce difference frequencies (low frequency build-up) and sum and harmonic frequencies (high frequency build-up). These two explanations, one in terms of time domain behavior and the other in terms of the frequency domain, are, of course, equivalent.

The noise results presented here and in Section 5 represent the heart of the results presented in this work. In the next few paragraphs we will note the most significant aspects of these results.

Let us consider the waveform results first. Nonlinear effects cause a systematic simplification of noise waveforms as a function of

distance. In the two examples shown in Section 5 the waves approach a shape consisting of shock fronts separated by negatively sloping sections. Because of dispersion these sections are somewhat curved. If we draw straight line tangents to these sections we find that all the tangent slopes are very similar. Hence (ignoring the effects of dispersion) we observe experimentally the asymptotic waveform predicted by Burgers.

Let us now turn to the spectral results. It is quite clear that the effects of nonlinear propagation cause marked changes in noise spectra. In particular the high and low frequency spectral components may exhibit a net increase in energy as a function of distance. The high frequency build-up commences as soon as the finite-amplitude wave is formed. The low frequency effect requires the formation of shocks. The cascading of energy to lower frequencies observed here verifies Kraichnan's (1968) predictions concerning spectral shifting to lower wavenumbers.

Since the low frequency energy cascade requires the presence of shocks, we expect to observe it at a higher SPL than that required to observe the high frequency cascade. We have begun a preliminary study of the threshold SPL necessary to cause the high frequency crossover to occur. In our plane wave tube the crossover occurs for source SPLs of 132 to 135 dB and above. We have not, to date, investigated the threshold of the low frequency crossover except to note that it is not evident at 135 dB.

7. The Relation of Our Results Obtained Using Noise Waveforms to Results Obtained Using the "Burgers Turbulence" Model

In Chapter 3 we derived, via weak-shock theory, the result that for large value of x the shape of finite-amplitude noise waves is equivalent to the random "sawtooth profile" obtained using the Burgers turbulence model. In particular we found that the slopes of the continuous sections of the wave became independent of their initial slope and proportional to x^{-1}. In Fig. (6-10) the waveform at the point x=85 ft computed using weak-shock theory clearly exhibits the characteristics of a random sawtooth. In addition, if we ignore the effects of dispersion in the experimental and theoretical results shown in Figs. (6-9) and (6-11), we observe that the waveforms for the larger values of x look like random sawtooth waves. Hence, we have theoretically, via weak-shock theory, and experimentally confirmed the random sawtooth profile predicted by Burgers (1972).

In the spectral results presented in the previous section we observed both experimentally and theoretically the waveform simplification and downward energy cascade predicted by Kraichnan (1968).

We shall report here on our attempt to computationally verify the value of ξ predicted by Tatsumi and Kida (1972). They derived the result that the number of shocks in a "random sawtooth" varies as

$$N(t) = N_o\left(\frac{t_o}{t}\right)^{\xi} \quad . \tag{2-8}$$

Converting Eq. (2-8) to our boundary value problem notation, we obtain

$$N(x) = N_o\left(\frac{x_o}{x}\right)^{\xi} \quad . \tag{6-7}$$

Tatsumi and Kida predicted for very large Reynolds number (very large amplitude waves) and for very large values of propagation distance that the value of ξ should approach 1/2. Using our program NSATDIS, we have made a check of the validity of this prediction. Inspection of Figs. (6-9) and (6-11) show that at 13. ft the waveforms are approaching the asymptotic random sawtooth form. Hence, we selected the computed waveforms at the point x=13 ft as our source waveforms and 13 ft as the value of x_o. We then calculated, using the weak-shock theory portion of program NSATDIS, the waveforms for values of x greater than x_o. In Burgers' equation the effects of nonlinear steepening, including attenuation at the shocks, are combined with the effects of thermoviscous attenuation in the continuous portion of the wave. Tatsumi and Kida's use of the large Reynolds number assumption, however, removes the effects of attenuation in the continuous portion of the wave leaving only the attenuation at the shocks. Therefore, our use of only the weak-shock theory portion of program NSATDIS is consistent with Tatsumi and Kida's analysis. Calculations of ξ were made using the waveforms described above. The source levels in these cases, however, proved to be too low to adequately approximate the assumption of very high Reynolds number. Therefore, using the computer we scaled the waveform shown in Fig. (6-9) to a source level of 175 dB. The value of ξ was calculated by plotting the waveform at various propagation distances, counting the number of shocks and using Eq. (6-7). The results of these computations are presented in Table VI.

TABLE VI

Calculation of ξ for x_o=13 ft

Source SPL (dB)	ξ
155	0.097
160	0.1999
175	0.281

The values of ξ given in Table VI are far lower than the value 1/2 predicted by Tatsumi and Kida. Note that ξ appears to be increasing as the source level is increased and for a strong enough source might approach the value 1/2. However, the source level required to obtain the value 1/2 would certainly exceed the levels shown in Table VI and would, therefore, be too high for the use of weak-shock theory. Hence, we conclude that Tatsumi and Kida's asymptotic value of ξ cannot be computationally verified by the use of weak-shock theory because weak-shock theory is not valid at the amplitudes required for ξ to approach 1/2.

CHAPTER 7 CONCLUDING REMARKS

1. Introduction

In Chapter 7 we present a brief summary of the major results of our research and draw conclusions based upon these results. We then consider the general question of the importance of dispersion in the study of propagation in pipes. We conclude by indicating some possible avenues of further experimental and theoretical research.

2. Summary of Results

The major results presented in this work can be divided into three categories: the development of a computational method for handling the propagation in a tube of finite-amplitude waves of arbitrary source waveform, results obtained using originally sinusoidal waves, and results obtained using noise waves. We will summarize in turn the results in each of these categories.

In Chapters 3 and 4 we developed our computational algorithm. Our method is based upon weak-shock theory, with the added provision that we account for absorption and dispersion due to the tube wall boundary layer. This provision is very important because it enables us to accurately predict the shape of sound waves propagating in a pipe. In addition, it extends the validity of weak-shock theory downward into the region of waves too weak to be treated by ordinary weak shock theory or even pertubation analysis but still too strong for linear theory to be adequate. As Blackstock (1972) notes, ordinary weak-shock theory does not, in general, work for very weak waves because it does not contain any attenuation effects other than that due to the shocks. The fact that the modified weak-shock algorithm includes tube wall attenuation as well as

shock attenuation means that our method should not have a lower strength limit.

Although we developed the algorithm for the specific case of propagation in tubes, the extension of the method to describe the propagation of waves in an unbounded medium is straightforward.

The studies of waves generated by a sinusoidally driven source were carried out to test our theoretical-computational algorithm. In Figs. (6-2) through (6-5) we see excellent agreement between our theoretical predictions and observed data. Comparison with the measurements made by Pernet and Payne (1971a) provides an independent verification of our method. The comparison with Coppens' (1971) theoretical results gives assurance that our method is valid for waves too weak to form shocks as well as for stronger ones. We cannot claim novelty for the experimental results obtained using sinusoidal waves because the waveform distortion, including the asymmetry, has been reported previously by McKittrick et al. (1967) and Pernet and Payne (1969).

As we stated in Chapter 1, our major interest has been in the propagation of finite-amplitude noise. In Chapter 6 two types of noise results are presented: waveforms and spectra. The former show very clearly the changes that take place in the waveform because of nonlinearity, for example, waveform steepening, reduction in the number of zero crossings, and general waveform simplification. Two examples of noise pulses are presented in Chapter 6 in Figs. (6-9) and (6-11). In both cases agreement between theory and experiment is, in general, excellent. Analysis of the results shown in Fig. (6-10) indicate the importance of the inclusion of

the tube wall attenuation and dispersion in our theory. The results shown in Figs. (6-9), (6-10), and (6-11) amply illustrate the effects of nonlinear propagation.

The changes in the noise waveforms with distance are reflected in the waveform spectra shown in Chapter 6. Examples are presented in Figs. (6-12), (6-13), (6-14), and (6-15). In Figs. (6-12) and (6-13) computed spectra, calculated using the source waveforms in Figs. (6-9) and (6-11), respectively, are shown. The spectra in Fig. (6-14) are entirely computer generated. In Fig. (6-15) experimental spectra obtained using a wave analyzer are depicted. Comparison of Figs. (6-14) and (6-15) demonstrates general agreement between theory and experiment. The spectra in Figs. (6-12) through (6-15) are perhaps our most important results. Analysis of these figures shows that the spectra associated with both experimental and computed waves undergo marked change as the wave propagates. These changes have not been observed by previous researchers although Kraichnan (1968) and Ffowcs Williams (1965) did predict the low frequency energy cascade. The high and low frequency cascades and actual spectral crossovers mean that nonlinear effects may cause a net increase in energy at some frequencies as the waves propagate.

In Chapter 6, Section 7, we reviewed results that showed similarities between results obtained using weak-shock theory and those obtained using Burgers' equation. In addition we attempted to verify Tatsumi and Kida's (1972) asymptotic value of the quantity ξ. The value of ξ is a measure of the randomness of a turbulent field, or, as in our case, a noise wave. We were unable to verify the predicted value.

3. Conclusions

We will consider first our theoretical-computational method. We conclude that our modified weak-shock algorithm is novel in that it is more general than previously proposed schemes that deal with the propagation of plane finite-amplitude waves in pipes. It is original in that results produced using it are valid both before and after shock formation, the results include both nonlinear and pipe wall effects, and the method works for arbitrarily shaped input waves. Previous methods, while containing some of the above features, do not contain them all.

We will consider next results obtained using a sinusoidally driven source. Our theoretical-computational model has been experimentally verified when using waves that are sinusoidal at the source over the frequency range of 500 to 3500 Hz and the source sound pressure level range of 142 to 160 dB. Although the actual experimental verification of the theory is at present limited to the frequency and source level ranges reported here, we believe strongly that modified weak-shock theory is applicable over a much wider range of experimental conditions. In particular, the theory should be useful for source sound pressure levels up to 165 dB and should not have a lower strength limit.

We will now consider our noise results. Our model adequately describes the propagation distortion of broadband noise waves both before and after the formation of shocks. The frequency band limits at the source in our experiments were 700 Hz and 2200 Hz and the source strength limits were 155 dB and 160 dB. As in the previous case we believe that our

theory is applicable over a wider range of experimental conditions than those used in our experiments.

The spectral content of noise waveforms has been investigated theoretically and experimentally for various propagation distances. Significant spectral shaping, attributable to nonlinear effects, has been predicted and these theoretical predictions have been experimentally confirmed. We conclude,that nonlinear steepening causes a shift of energy to higher frequencies whereas the merging of shocks and the attendant waveform simplification causes a shift of energy to lower frequencies. The high frequency build-up commences as soon as the nonlinear wave is formed at the source. The low frequency build-up, however, is associated with a more mature stage of the distortion, after the shocks have formed. Therefore, we expect to see the high frequency enhancement at considerably lower SPL's than the low frequency effect.

Let us now turn to the body of material included here that relates to Burgers model of turbulence. We have demonstrated that use of weak-shock theory produces several results that are in agreement with results obtained by use of the Burgers turbulence model. However, we were unable to verify the asymptotic value of ξ predicted by Tatsumi and Kida (1972). The general agreement between the sets of results indicates that the two theories while quite different in outward appearance and originally intended application are actually very similar. The failure to verify the predicted value of ξ merely indicates that the value $\xi = 1/2$ cannot be verified using weak-shock theory. We conclude that if ξ approaches $1/2$ it does so at wave amplitudes for which weak-shock theory is invalid.

4. The Question of Dispersion

In Chapter 2 we announced our intention of including dispersion in our analysis. Later in Chapter 3 we indicated in a more complete manner why dispersion was important in our particular problem. In this section we shall indicate why dispersion is important in some instances and may be ignored in others. The reader is cautioned that our views on this subject are to an extent speculative and are not as yet fully verified by laboratory observations.

Let us first consider finite-amplitude waves propagating in a pipe that are too weak to form shocks. A wealth of experimental results has been obtained for this case. The experimental work includes that of Thuras, Jenkins, and O'Neil (1935), Blackstock (1962b), Burns (1966a), Pernet and Payne (1969), and Cruikshank (1966). Each of the above researchers either ignored dispersion entirely or reported that its effects were slight. In work where source levels are restricted to levels insufficient to form shocks only the first few harmonics of the fundamental wave frequency reach appreciable levels. Let us concentrate our attention now on the second harmonic. The observations that we shall make about the second harmonic can, in general, be extended to higher harmonics. One may think of the second harmonic as being generated all along the propagation path by interaction of the fundamental with itself. This concept is often referred to as the "virtual source" concept. As long as both fundamental and second harmonic have the same propagation speed, the second harmonic signal produced at a distance x, say, is in phase with all the second harmonic signals produced at distances less than x and traveling

the remaining way to point x as a second harmonic. However, if there is dispersion, the various second harmonic signals arriving at point x will not be perfectly phased. Now in the case of dispersion due to tube wall effects, the dispersion is quite small, and a sizeable distance is required for the imperfect phasing to have an appreciable effect. In the experiments mentioned earlier the distances used were not sufficient for dispersion to be very noticeable. For weak waves, the primary signal components are the fundamental and the second harmonic (and perhaps the third harmonic as well). Since the dispersion over a frequency range of only a few octaves is very small, the effects of dispersion are not noticeable until the distance becomes great.

Let us now consider waves whose source levels are sufficient to cause the formation of shocks. In this case the fact that many harmonics are present means there is an appreciable spread in the propagation speeds of the wave components. Hence we expect to see evidence of dispersion at short propagation distances. For instance, in both the work reported here and in the work of McKittrick et al. (1967) the effects of dispersion are readily apparent in the form of waveform asymmetry. As source levels are increased beyond approximately 155 dB, however, the signs of dispersion close to the source disappear. In our Fig. (6-9), for example, the waveforms at distances less than 61 ft do not exhibit the rounded peaks characteristic of the effects of dispersion. The reason is that the nonlinear steepening effect is very strong and it keeps the peaks sharp in spite of dispersion. In other words, for very strong waves dispersion is not absent; its effects are merely obscured by the more powerful nonlinear effects.

Summarizing the above discussion, we conclude that for weak waves and relatively short distances dispersion may be ignored. For waves of moderate source level the effects of dispersion are readily apparent and dispersion must be included in the analysis. Finally, for very strong waves, the effects of dispersion are small compared to the nonlinear effects and, at short distances, can probably be ignored.

In discussions contained in this section we have been purposely vague about the sound pressure levels and distances for which dispersion should or should not be considered. The discussion presented here is intended as a general set of guidelines useful in the analysis of propagation of finite-amplitude waves in pipes. A more definitive study leading to a classification of the importance of dispersion in terms of source level, frequency, and propagation effects needs to be carried out.

5. Avenues of Further Experimental and Theoretical Research

As is usually the case with long analyses, we came to the end with as many new questions as we have found answers to old ones. In this section we shall indicate some possible avenues of continued research that may build upon the present work.

The results presented here are limited to plane waves. In most practical propagation problems, however, the wave motion is cylindrical or spherical. Therefore, a need exists to modify our programs so that cylindrically and spherically spreading waves may be considered. Since weak-shock theory expressions have been derived for both cylindrically and spherically spreading waves, the modification should not be difficult to implement. A significant simplification will accrue in that dispersion is negligible for waves in an open medium.

We have not applied our theory to deterministic waveforms other than sinusoids. A research project devoted to the investigation of multiple frequency source waveforms should certainly be worthwhile. The application of weak-shock theory to waves having multiple frequency components at the source is very difficult to handle analytically. The use of our weak-shock algorithm will greatly reduce the time required to obtain problem solutions.

In Chapter 2 we mentioned Blackstock's integro-differential equation. Thus far there are no known solutions of this equation. In addition it is not known whether the equation could be used alone or whether it would have to be supplemented when shocks form by use of the Rankine-Hugoniot relations. A research effort aimed at obtaining anlaytic or numerical solutions to Blackstock's equation might be fruitful.

In the previous section we discussed in very general terms the importance of dispersion in various pipe-borne wave propagation problems. A fuller, more detailed experimental and theoretical analysis of this topic is needed.

Another very important need is an analysis and classification of the effects reported in our study of noise waves. This analysis should investigate the effect of varying the noise bandwidth. The information obtained should be reduced so that engineering estimates of spectral changes can be made. The analyses should be directed also at answering whether or not phase information is important. We have essentially thrown phase information away. Finally, consider a case where

we have a noise spectrum but not the noise waveform. How good a prediction of subsequent spectra may be made based upon the information given? We do not know the answer to this question as yet.

Lastly, we feel that the work begun in Appendix E needs attention. We have indicated that for very strong waves ordinary weak-shock theory is inadequate. However, the three-term solution and integral solution given in Appendix E cannot as yet be regarded as full theories because the assumption of simple flow implicit in their derivation needs to be investigated.

APPENDIX A

LISTING AND FLOW CHART OF SUBROUTINE WAVEPROP

```
      SUBROUTINE WAVEPROP (U,T,DISTANCE,DISINC,NPOINTS)                    C   1
      DIMENSION TS(200), LOCS(200), T(1), U(1)                             C   2
C                                                                          C   3
C  ************************************************************************C   4
C                                                                          C   5
C     WAVEPROP IS THE WEAK-SHOCK WAVE PROPAGATION ALGORITHUM.              C   6
C                                                                          C   7
C  ************************************************************************C   8
C                                                                          C   9
C     CALL PARAMETERS ---                                                  C  10
C                                                                          C  11
C     U         -- U IS A REAL ONE DIMENSIONAL ARRAY DESCRIBING THE PARTILEC  12
C                  VELOCITY OF A POINT ON THE WAVE FORM IN EITHER ENGLISH  C  13
C                  OR METRIC UNITS.  IF METRIC UNITS ARE USED CO, THE SMALL C  14
C                  SIGNAL SPEED OF SOUND, MUST BE SUPPLIED IN METRIC UNITS.C  15
C                                                                          C  16
C     T         -- T IS A REAL ONE DIMENSIONAL ARRAY DESCRIBING THE TIME   C  17
C                  SECONDS) COORDINATE FOR A PATICULAR POINT ON THE WAVEFORMC  18
C                  THE DOUBLET (U(I),T(I)) THEN DESCRIBES A WAVEFORM POINT C  19
C                  IN THE PARTICAL VELOCITY-TIME PLANE.                    C  20
C                                                                          C  21
C     DISTANCE --                                                          C  22
C     DISTANCE -- A REAL VARIABLE.  IT IS THE DISTANCE OVER WHICH THE WAVEC  23
C                  IS TO BE PROPAGATED.                                    C  24
C                                                                          C  25
C     DISINC    -- A REAL VARIABLE.  IT IS THE INCREMENTAL STEP SIZE USED  C  26
C                  COVER THE DISTANCE, DISTANCE.                           C  27
C                                                                          C  28
C     NPOINTS   -- AN INTEGER VARIABLE.  IT IS THE NUMBER OF POINTS USED   C  29
C                  DESCRIBE THE WAVE FORM TO BE PROPAGATED.                C  30
C                                                                          C  31
C  ************************************************************************C  32
C                                                                          C  33
      PERIOD = T(NPOINTS)                                                  C  34
      B = 1.205                                                            C  35
      CO = 1136.                                                           C  36
      ETA = B/CO**2                                                        C  37
      DISFACTR = ETA*DISINC                                                C  38
      NDISTORS = DISTANCE/DISINC+0.5                                       C  39
      DO 140 NDISTOR=1,NDISTORS                                            C  40
         NS = NSHIFT = 0                                                   C  41
```

```
      TLOW = T(1)-1.0                                                    C  42
C     CCCCCCCCCCCCCCCCCCCCCCCCCCCCCCCCCCCCCCCCCCCCCCCCCCCCCCCCCCCCCCC  C  43
C                                                                        C  44
C     THIS LOOP TESTS FOR SHOCKS AND SHIFTS OUT POINTS                   C  45
C     IN THE DOUBLED VALUED REGION                                       C  46
C                                                                        C  47
C     CCCCCCCCCCCCCCCCCCCCCCCCCCCCCCCCCCCCCCCCCCCCCCCCCCCCCCCCCCCCCCC  C  48
      DO 30 INDEX=1,NPOINTS                                              C  49
         NPOINT = INDEX-NSHIFT                                           C  50
         T(NPOINT) = T(INDEX)-U(INDEX)*DISFACTR                          C  51
         U(NPOINT) = U(INDEX)                                            C  52
         IF (T(NPOINT).GT.TLOW) GO TO 30                                 C  53
         TAVG = (T(NPOINT)+T(NPOINT-1))/2.0                              C  54
         DO 10 I=1,NS                                                    C  55
            IF (TAVG.LE.TS(I)) GO TO 20                                  C  56
10       CONTINUE                                                        C  57
         NS = NS+1                                                       C  58
         TS(NS) = TAVG                                                   C  59
         LOCS(NS) = NPOINT                                               C  60
         GO TO 30                                                        C  61
20       NSHIFT = NSHIFT+NPOINT-LOCS(I)                                  C  62
         LOC = LOCS(I)-1                                                 C  63
         T(LOC+1) = T(NPOINT)                                            C  64
         U(LOC+1) = U(NPOINT)                                            C  65
         TS(I) = (T(NPOINT)+T(LOC))/2.0                                  C  66
         NS = I                                                          C  67
30    TLOW = T(NPOINT)                                                   C  68
      NPOINTS = NPOINTS-NSHIFT                                           C  69
      TLEFT = AMNIF(T(1),T(NPOINTS))                                     C  70
      IF (TLEFT.LT.0.0) 40,50                                            C  71
40    PRINT 150, DISTANCE,NDISTOR                                        C  72
      STOP                                                               C  73
50    TBIG = AMXIF(T(1),T(NPOINTS))                                      C  74
      IF (TBIG.GT.PERIOD) 60,70                                          C  75
60    PRINT 160, DISTANCE,NDISTOR                                        C  76
      STOP                                                               C  77
70    CONTINUE                                                           C  78
      IFLAG = NSHIFT = 0                                                 C  79
      TLOW = T(1)-1.0                                                    C  80
C     CCCCCCCCCCCCCCCCCCCCCCCCCCCCCCCCCCCCCCCCCCCCCCCCCCCCCCCCCCCCCCC  C  81
C                                                                        C  82
C     THIS LOOP ADJUSTS VELOCITIES AT THE SHOCKS AND SHIFTS OUT POINTS   C  83
C     IN THE OVERLAP REGION THAT OCCURS WHEN SHOCKS OVERTAKE             C  84
```

```
C                                                                       C  85
C     CCCCCCCCCCCCCCCCCCCCCCCCCCCCCCCCCCCCCCCCCCCCCCCCCCCCCCCCCCCCCCC  C  86
         DO 130 INDEX=1,NPOINTS                                         C  87
            NPOINT = INDEX-NSHIFT                                       C  88
            T(NPOINT) = T(INDEX)                                        C  89
            U(NPOINT) = U(INDEX)                                        C  90
            IF (IFLAG.EQ.1) GO TO 100                                   C  91
            IF (T(NPOINT).GT.TLOW) GO TO 120                            C  92
            TAVG = (T(NPOINT)+T(NPOINT-1))/2.0                          C  93
            IFLAG = 1                                                   C  94
            I = NPOINT-2                                                C  95
            GO TO 90                                                    C  96
 80         I = I-1                                                     C  97
            NSHIFT = NSHIFT+1                                           C  98
            T(I+2) = T(NPOINT)                                          C  99
            U(I+2) = U(NPOINT)                                          C 100
 90         IF (TAVG.LT.T(I)) GO TO 80                                  C 101
            U(I+1) = U(I)+(U(I+1)-U(I))*(TAVG-T(I))/(T(I+1)-T(I))       C 102
            T(I+1) = TAVG                                               C 103
            GO TO 130                                                   C 104
 100        IF (T(NPOINT).LT.TAVG) GO TO 110                            C 105
            U(NPOINT-1) = U(NPOINT-1)+(U(NPOINT)-U(NPOINT-1))*(TAVG-T   C 106
     $      (NPOINT-1))/(T(NPOINT)-T(NPOINT-1))                         C 107
            T(NPOINT-1) = TAVG                                          C 108
            IFLAG = 0                                                   C 109
            GO TO 120                                                   C 110
 110        NSHIFT = NSHIFT+1                                           C 111
            GO TO 130                                                   C 112
 120        TLOW = T(NPOINT)                                            C 113
 130     CONTINUE                                                       C 114
 140  NPOINTS = NPOINTS-NSHIFT                                          C 115
      RETURN                                                            C 116
C                                                                       C 117
C                                                                       C 118
 150  FORMAT (1H1,*EXCEEDED TIME BASE TO THE LEFT*,//,10X,*DISTANCE=*,   C 119
     $E15.5,10X,I5,3X,*ITERATIONS*)                                     C 120
 160  FORMAT (1H1,*EXCEEDED TIME BASE TO THE RIGHT*,//,10X,*DISTANCE=*,  C 121
     $E15.5,10X,I5,3X,*ITERATIONS*)                                     C 122
      END                                                               C 123-

WAVEPROP    P   02226   C   00000   D   00000
```

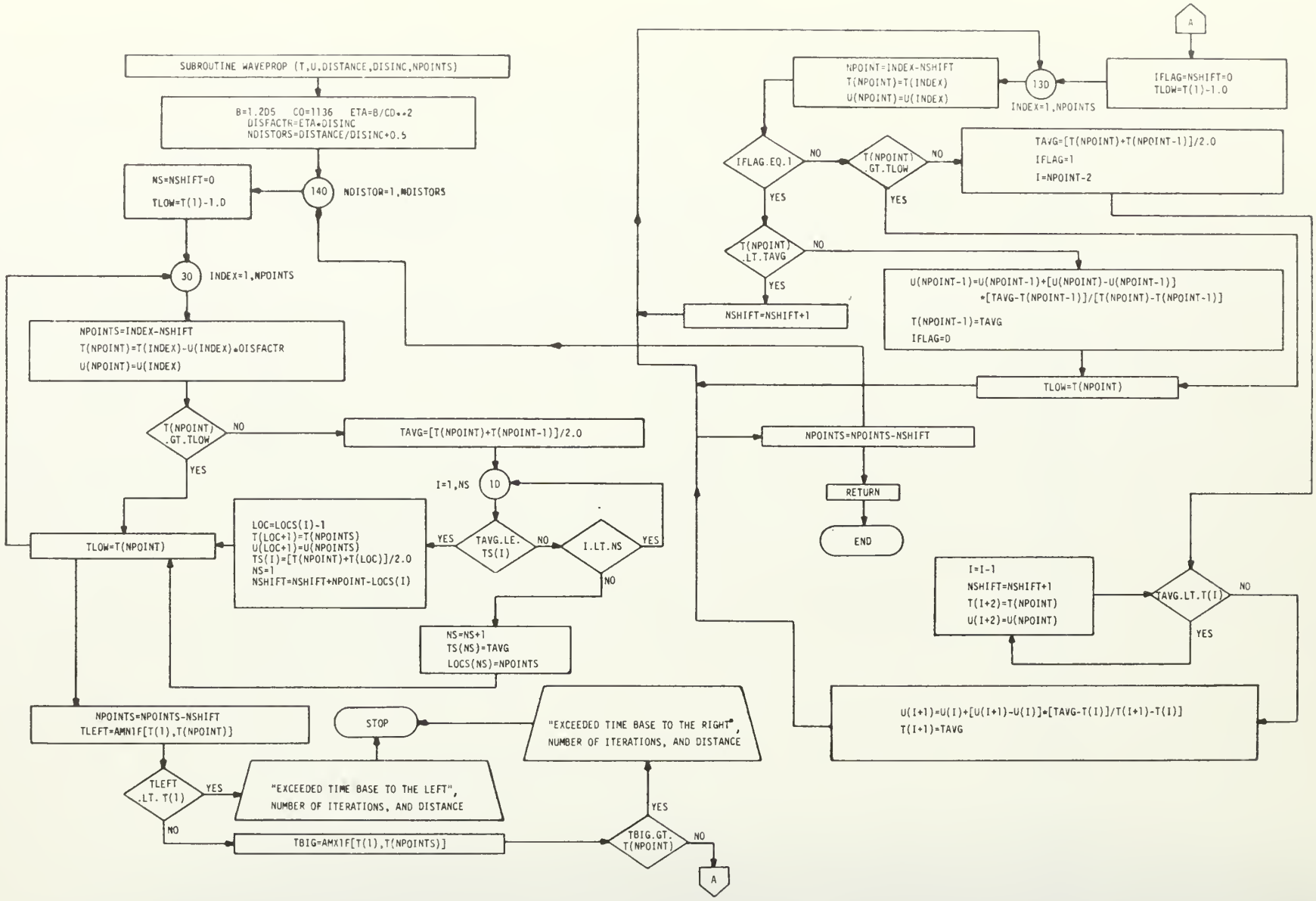

FIGURE A-1

FLOW CHART OF SUBROUTINE WAVEPROP

APPENDIX B

DRIVER PROGRAM LISTINGS AND FLOWCHARTS

The values assigned to the various program parameters in the cases shown are example values.

```
                                3200  FORTRAN    (2.1)          1970/7/3

      PROGRAM NSATDIS                                                    A    1
      DIMENSION U(515), UT(515), T(515), F(515)                          A    2
C                                                                        A    3
C     NSATDIS -- THIS PROGRAM CALCULATES WAVEFORMS OF RANDOM WAVES       A    4
C              AS A FUNCTION OF PROPAGATION DISTANCE.                    A    5
C                                                                        A    6
C     ***************************************************************  A    7
C                                                                        A    8
C     VARIABLES AND ARRAYS ---                                           A    9
C                                                                        A   10
C     DATAOT-- A REAL VARIABLE.  IT IS THE SAMPLING INTERVAL IN THE      A   11
C           ORIGIONAL DATA.                                              A   12
C                                                                        A   13
C     DT     -- A REAL VERIABLE.  IT IS THE TIME BETWEEN DATA SAMPLES    A   14
C                                                                        A   15
C     F      -- A REAL ONE-DIMENSIONAL SCRATCH ARRAY.                    A   16
C     ISW    -- AN INTEGER VARIABLE.  IT IS A SWITCH USED IN THE PLOTTING A   17
C           ROUTINE WAVEPLOT.  IT MAY HAVE VALUES 0 OR 1.                A   18
C                                                                        A   19
C     N      -- AN INTEGER VARIABLE.  THE ACTUAL PARAMETER USED IN       A   20
C           WAVEPROP CORRESPONDING TO THE FORMAL PARAMETER. NPOINTS       A   21
C                                                                        A   22
C     NEND   -- AN INTEGER VARIABLE.  IT IS THE NUMBER OF ZEROES AT THE  A   23
C           ENDS OF THE NOISE SAMPLE.                                    A   24
C                                                                        A   25
C     NEXP   -- AN INTEGER VARIABLE.  NN = 2**NEXP+1                     A   26
C                                                                        A   27
C     NN     -- AN INTEGER VARIABLE.  THE NUMBER OF POINTS IN THE INITAL A   28
C           WAVEFORM.                                                    A   29
C                                                                        A   30
C     NP     -- AN INTEGER VARIABLE.  IT IS THE NUMBER OF DATA POINTS IN A   31
C           THE ORTGINAL SAMPLED DATA.                                   A   32
C                                                                        A   33
C     PER    -- A REAL VARIABLE.  IT IS THE PERIOD OF THE INPUT SIGNAL.  A   34
C                                                                        A   35
C     SF     -- A REAL VARIABLE.  SF SCALES THE INPUT DATA INTO UNITS    A   36
C           OF FT/SEC.                                                   A   37
C                                                                        A   38
C     T      -- A REAL ONE-DEMINSIONAL ARRAY.  ITS ELEMENTS CONTAIN SAMPLE A   39
C           POINT TIMES.                                                 A   40
C                                                                        A   41
```

```
C     TAXIS -- A REAL VARIABLE.  IT IS THE LENGTH OF THE TIME AXIS USED    A  42
C           IN THE PLOTTING ROUTINE WAVEPLOT.                              A  43
C                                                                          A  44
C     U     -- A REAL ONE-DIMENSIONAL ARRAY.  IT CONTAINS VALUES OF        A  45
C           PARTICAL VELOCITY.                                             A  46
C                                                                          A  47
C     UAXIS -- A REAL VARIABLE.  IT IS THE LENGTH OF THE PARTICAL VELOCITY A  48
C           AXIS USED IN THE PLOTTING ROUTINE, WAVEPLOT.                   A  49
C                                                                          A  50
C     UI    -- A REAL ONE-DIMENSIONAL ARRAY USED IN THE FREQUENCY DOMAIN   A  51
C           HOLD THE IMAGINARY PORTION OF THE FOURIER COEFFICIENTS.        A  52
C                                                                          A  53
C     UA    -- A REAL VARIABLE.  IT IS USED IN THE PLOTTING ROUTINE.       A  54
C           WAVEPLOT. TO ACCOUNT FOR VERTICAL AMPLIFICATION.               A  55
C                                                                          A  56
C     XINC  -- A REAL VARIABLE.  THE ACTUAL PARAMETER USED IN WAVEPROP     A  57
C           CORRESPONDING TO THE FORMAL PARAMETER DISINC.                  A  58
C                                                                          A  59
C     XI    -- A REAL VARIABLE.  IT IS THE ACTUAL PARAMETER USED IN        A  60
C           WAVEPROP CORRESPONDING TO THE FORMAL PARAMETER DISTANCE.       A  61
C                                                                          A  62
C     XXX   -- A REAL VARIABLE.  IT IS A DISTANCE COUNTER.                 A  63
C                                                                          A  64
C  ********************************************************************  A  65
C                                                                          A  66
      N = NN = 513                                                         A  67
      NL = N-1                                                             A  68
      NEXP = 9                                                             A  69
      TAXIS = 5.23                                                         A  70
      UAXIS = 2.12                                                         A  71
      NP = 421                                                             A  72
C                                                                          A  73
C     THE DIMENSION OF U AND T MUST EXCEED THE NUMBER OF POINTS NEEDED     A  74
C     TO DESCRIBE THE WAVE BY AT LEAST 2.                                  A  75
C     THIS DATA IS NOISE 1                                                 A  76
C                                                                          A  77
      SLENGTH = 42.                                                        A  78
      IERR = 10                                                            A  79
      TSF = .0005/1.29                                                     A  80
      PER = SLENGTH*TSF                                                    A  81
      FO = 1./PER                                                          A  82
      DT = PER/NL                                                          A  83
      DATADT = PER/(NP-1)                                                  A  84
```

```
      XINC = 0.1                                                        A  85
      JSW = 1                                                           A  86
      SF = 8.931941407                                                  A  87
      READ 260, (U(I),I=1,NP)                                           A  88
      DO 10 I=1,NP                                                      A  89
         T(I) = DATADT*(I-1)                                            A  90
         UI(I) = 0.0                                                    A  91
10    U(I) = U(I)*SF                                                    A  92
      CALL RESAMPLE (U,T,NN,NP,DT)                                      A  93
      DO 20 K=1,NL                                                      A  94
20    U(K) = U(K)/NL                                                    A  95
      CALL FFTC (U,UT,NEXP)                                             A  96
      PRINT 270, U(1)                                                   A  97
      U(1) = 0.0                                                        A  98
      CALL FFTC (U,UT,NEXP)                                             A  99
      DO 30 I=1,NEND                                                    A 100
30    U(I) = 0.0                                                        A 101
      NC = NN-NEND                                                      A 102
      DO 40 I=NC,NN                                                     A 103
40    U(I) = 0.0                                                        A 104
      DO 50 K=1,N                                                       A 105
50    F(K) = U(K)                                                       A 106
      XL = 6.0                                                          A 107
      NSTEP = 84./XL                                                    A 108
      NN = NSTEP+1                                                      A 109
C                                                                       A 110
C     PROPAGATE THIS WAVE BY WEAK SHOCK THEORY                          A 111
C                                                                       A 112
      VA = 1.0                                                          A 113
      DO 120 I=1,NN                                                     A 114
         XXX = 1.0+XL*(I-1)                                             A 115
         IF (XXX.EQ.1.0) GO TO 110                                      A 116
         CALL WAVEPROP (U,T,XL,XINC,N)                                  A 117
         IF (XXX.EQ.13.0) 60,70                                         A 118
60       VA = 2.0                                                       A 119
         GO TO 110                                                      A 120
70       IF (XXX.EQ.37.) 80,90                                          A 121
80       VA = 4.0                                                       A 122
         GO TO 110                                                      A 123
90       IF (XXX.EQ.61.0.OR.XXX.EQ.85.0) 100,120                        A 124
100      CONTINUE                                                       A 125
110      CALL WAVEPLOT (U,T,XXX,N,ISW,TAXIS,UAXIS,VA)                   A 126
         PRINT 290, XXX                                                 A 127
```

```
  120  CONTINUE                                                          A 128
       N = NN                                                            A 129
       DO 130 KK=1,N                                                     A 130
          T(KK) = DT*(KK-1)                                              A 131
  130  U(KK) = F(KK)                                                     A 132
C                                                                        A 133
C      PROPAGATE THIS WAVE USING MODIFIED WEAK SHOCK THEORY              A 134
C                                                                        A 135
       VA = 1.                                                           A 136
       DO 250 I=1,NQ                                                     A 137
          XXX = 1.0+XL*(I-1)                                             A 138
          IF (XXX.EQ.1.0) GO TO 240                                      A 139
          CALL WAVEPROP (U,T,XL,XINC,N)                                  A 140
          CALL RESAMPLE (U,T,NN,N,DT)                                    A 141
          N = NN                                                         A 142
          CALL SET1 (UI(1),UI(NL),0.0)                                   A 143
          DO 140 J=1,NL                                                  A 144
  140     U(J) = U(J)/NL                                                 A 145
          CALL FFTC (U,UI,NEXP)                                          A 146
          NA = NL/2+1                                                    A 147
          KL = I-1                                                       A 148
          PRINT 280, KL,U(1)                                             A 149
          DO 150 K=2,NA                                                  A 150
             ARG = ALPHA(K-1,FO)*XI                                      A 151
             ZZ=U(K)                                                     A 151A
             U(K) = EXP(-ARG)*(U(K)*COSF(ARG)-UI(K)*SINF(ARG))           A 152
  150     UI(K)=EXP(-ARG)*(UI(K)*COSF(ARG)+ZZ*SINF(ARG))                 A 153
          NB = NA+1                                                      A 154
          DO 160 K=NB,NL                                                 A 155
             LL = N+1-K                                                  A 156
             U(K) = U(LL)                                                A 157
  160     UI(K) = -UI(LL)                                                A 158
          CALL FFTC (U,UI,NEXP)                                          A 159
          DO 170 K=1,NEND                                                A 160
             IF(ABSF(U(K)).LE..50)U(K) = 0.0                             A 161
  170     CONTINUE                                                       A 162
          DO 180 K=NC,NN                                                 A 163
             IF(ABSF(U(K)).LE..50)U(K) = 0.0                             A 164
  180     CONTINUE                                                       A 165
          IF (XXX.EQ.13.0) 190,200                                       A 166
  190     VA = 2.0                                                       A 167
          GO TO 240                                                      A 168
  200     IF (XXX.EQ.37.0) 210,220                                       A 169
```

```
  210       VA = 4.0                                                    A 170
            GO TO 240                                                   A 171
  220       IF (XXX.EQ.61.0.OR.XXX.EQ.85.0) 230,250                     A 172
  230       CONTINUE                                                    A 173
  240       CALL WAVEPLOT (D,T,XXX,NN,ISW,TAXIS,UAXIS,VA)               A 174
            PRINT 290, XXX                                              A 175
  250   CONTINUE                                                        A 176
      C                                                                 A 177
  260   FORMAT (8F10.5)                                                 A 178
  270   FORMAT (////,*    DC LEVEL=*,F10.7)                             A 179
  280   FORMAT (//,*  CYCLE NUMBER*,5X,I3,8X,*DC LEVEL*,F10.7)          A 180
  290   FORMAT (//,*  DISTANCE=*F7.3)                                   A 181
        END                                                             A 182-

NSATDIS    P   11327   C   00000   D   00000
```

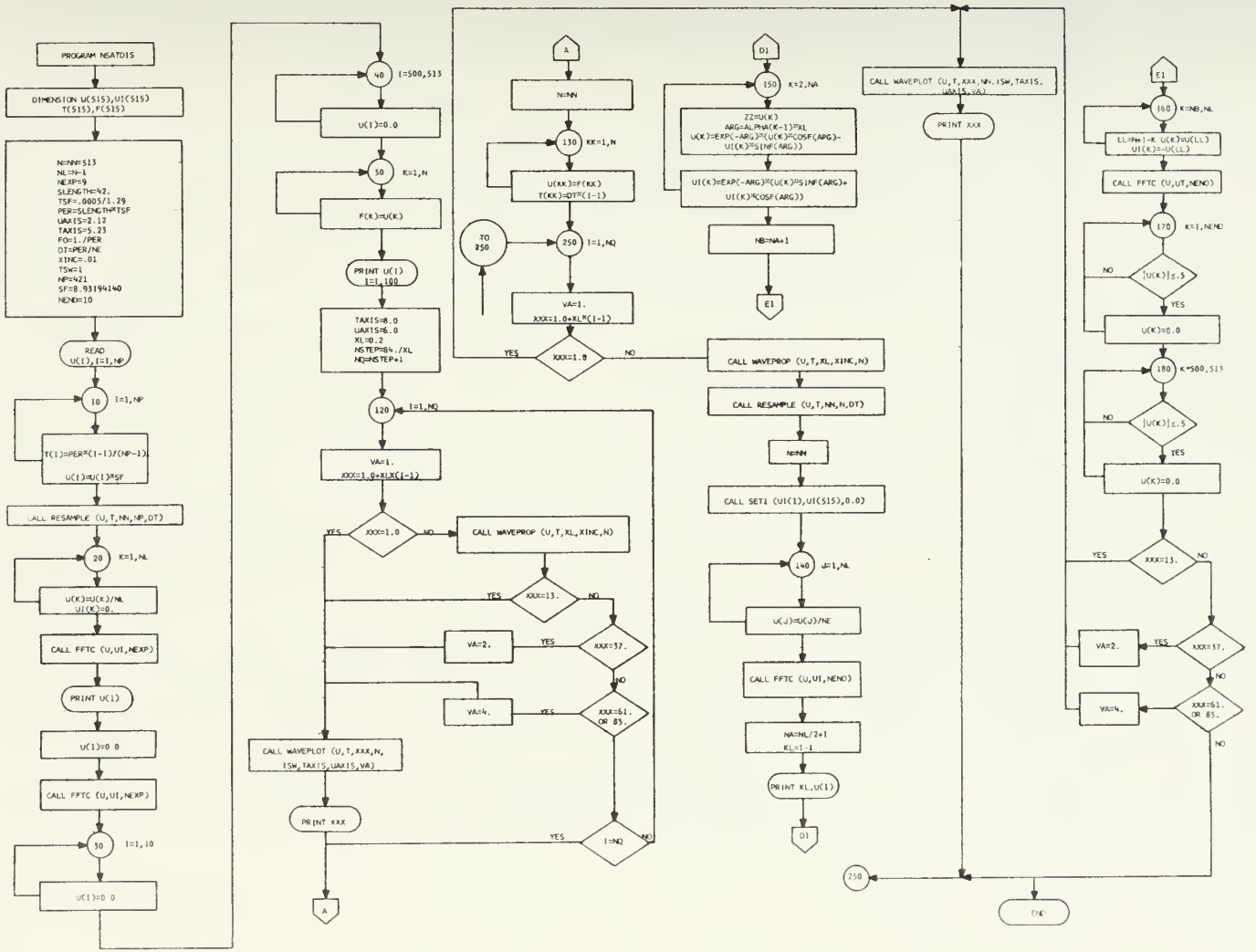

FIGURE B-1

FLOW CHART OF PROGRAM NSATDIS

3200 FORTRAN (2.1) 19/07/73

```
      PROGRAM ATENDIS5                                                    A   1
      DIMENSION U(515), T(515), UI(515), PHI(515), ACC(515), DIST(515),   A   2
     $F(515)                                                              A   3
C                                                                         A   4
C     ATENDIS 5 -- THIS PROGRAM CALCULATES WAVEFORMS OF DETERMINISTIC     A   5
C           WAVE AS A FUNCTION OF THE PROPAGATION DISTANCE.               A   6
C                                                                         A   7
C     THE DIMENSION OF U AND T MUST EXCEED THE NUMBER OF POINTS NEEDED    A   8
C     TO DESCRIBE THE WAVE BY AT LEAST TWO.                               A   9
C                                                                         A  10
C     THIS RUN INVESTIGATES A 3500 HZ SINUSOID.                           A  11
C ***************************************************************       A  12
C                                                                         A  13
C     VARIABLES AND ARRAYS ---                                            A  14
C                                                                         A  15
C     ACC   -- A REAL ONE DIMENSIONAL ARRAY.  IT CONTAINS THE ACCUMULATE  A  16
C           PHASE SHIFT.                                                  A  17
C                                                                         A  18
C     ALPHA -- A REAL VARIABLE.  IT IS AN EXPERIMENTALLY DETERMINED       A  19
C           ATTENUATION COEFFICIENT.                                      A  20
C                                                                         A  21
C     DIST  -- A REAL ONE DIMENSIONAL ARRAY.  ITS ELEMENTS CONTAIN THE    A  22
C           SEQUENCE OF DISTANCES AT WHICH THE ATTENUATION AND            A  23
C           DISPERSION CORRECTIONS ARE APPLIED.                           A  24
C                                                                         A  25
C     DT    -- A REAL VARIABLE.  IT IS THE TIME BETWEEN DATA SAMPLES      A  26
C                                                                         A  27
C     F     -- A REAL ONE-DIMENSIONAL SCRATCH ARRAY.                      A  28
C     ISW   -- AN INTEGER VARIABLE.  IT IS A SWITCH USED IN THE PLOTTING  A  29
C           ROUTINE WAVEPLOT.  IT MAY HAVE VALUES 0 OR 1.                 A  30
C                                                                         A  31
C     JSTEP -- AN INTEGER VARIABLE.  IT COUNTS THE NUMBER OF XL STEPS.    A  32
C           THAT IS, THE NUMBER OF TIMES THAT CORRECTION IS MADE FOR       A  33
C           ATTENUATION AND DISPERSION.                                   A  34
C                                                                         A  35
C     N     -- AN INTEGER VARIABLE.  THE ACTUAL PARAMETER USED IN         A  36
C           WAVEPROP CORROSPONDING TO THE FORMAL PARAMETER, NPOINTS.      A  37
C                                                                         A  38
C     NEXP  -- AN INTEGER VARIABLE.  NN = 2**NEXP+1                       A  39
C                                                                         A  40
```

```
C      NN     -- AN INTEGER VARIABLE.  THE NUMBER OF POINTS IN THE INITAL    A  41
C             WAVEFORM.                                                      A  42
C                                                                            A  43
C      NP     -- AN INTEGER VARIABLE.  IT IS THE NUMBER OF DATA POINTS IN    A  44
C             THE ORIGINAL SAMPLED DATA.                                     A  45
C                                                                            A  46
C      PER    -- A REAL VARIABLE.  IT IS THE PERIOD OF THE INPUT SIGNAL.     A  47
C                                                                            A  48
C      PHI    -- A REAL ONE-DIMENSIONAL ARRAY.  IT CONTAINS THE PHASE SHIFT A  49
C             SUFFERED BY THE WAVE AT EACH ATTENUATION AND DISPERSION        A  50
C             CORRECTION                                                     A  51
C                                                                            A  52
C      SF     -- A REAL VARIABLE.  SF SCALES THE INPUT DATA INTO UNITS       A  53
C             OF FT/SEC.                                                     A  54
C                                                                            A  55
C      T      -- A REAL ONE-DEMINSIONAL ARRAY.  ITS ELEMENTS CONTAIN SAMPLE A  56
C             POINT TIMES.                                                   A  57
C                                                                            A  58
C      TAXIS  -- A REAL VARIABLE.  IT IS THE LENGTH OF THE TIME AXIS USED    A  59
C             IN THE PLOTTING ROUTINE WAVEPLOT.                              A  60
C                                                                            A  61
C      U      -- A REAL ONE-DIMENSTONAL ARRAY.  IT CONTAINS VALUES OF        A  62
C             PARTICAL VELOCITY.                                             A  63
C                                                                            A  64
C      UAXIS  -- A REAL VARIABLE.  IT IS THE LENGTH OF THE PARTICAL          A  65
C             VELOCITY AXIS USED IN THE PLOTTING ROUTINE. WAVEPLOT.          A  66
C                                                                            A  67
C      UI     -- A REAL ONE-DIMENSIONAL ARRAY USED IN THE FREQUENCY DOMAIN   A  68
C             HOLD THE IMAGINARY PORTION OF THE FOURIER COEFFICIENTS.        A  69
C                                                                            A  70
C      UA     -- A REAL VARIABLE.  IT IS USED IN THE PLOTTING ROUTINE,       A  71
C             WAVEPLOT. TO ACCOUNT FOR VERTICAL AMPLIFICATION.               A  72
C                                                                            A  73
C      XINC   -- A REAL VARIABLE.  THE ACTUAL PARAMETER USED IN WAVEPROP     A  74
C             CORRESPONDING TO THE FORMAL PARAMETER DISINC.                  A  75
C                                                                            A  76
C      XL     -- A REAL VARIABLE.  IT IS THE ACTUAL PARAMETER USED IN        A  77
C             WAVEPROP CORRESPONDING TO THE FORMAL PARAMETER DISTANCE.       A  78
C                                                                            A  79
C      XX     -- A REAL VARIABLE.  XX IS UAED TO KEEP TRACK OF THE TOTAL     A  80
C             DISTANCE PROPAGATED.                                           A  81
C                                                                            A  82
C      XXX    -- A REAL VARIABLE.  IT IS A DISTANCE COUNTER.                 A  83
```

```
C                                                                       A  84
C      Y      -- A REAL VARIABLE.  IT IS THE REAL PARAMETER USED IN     A  85
C             WAVEPROF CORRESPONDING TO THE FORMAL PARAMETER DISTANCE, WHEN A  86
C             THE WAVE IS PROPAGATED BY WEAK-SHOCK THEORY.              A  87
C                                                                       A  88
C  ***********************************************************************A  89
C                                                                       A  90
      NF=42                                                             A  91
      NP = N = 513                                                      A  92
      NEXP = 9                                                          A  93
      NL = N-1                                                          A  94
      PER = 1./3500.                                                    A  95
      DT = PER/(N-1)                                                    A  96
      ALPHA = 0.02467024                                                A  97
      SF = 7.949980668                                                  A  98
      ISW = 0                                                           A  99
      XL = 0.2                                                          A 100
      XINC = 0.1                                                        A 101
      TAXIS = 8.0                                                       A 102
      UAXIS = 6.0                                                       A 103
      YA = 1.0                                                          A 104
      XX = 1.0                                                          A 105
      NSTEP = 84./XL                                                    A 106
      NG = NSTEP+1                                                      A 107
      READ 460, (U(I),I=1,NP)                                           A 108
      DO 310 I=1,NP                                                     A 109
         T(I) = PER*(I-1)/(NP-1)                                        A 110
  310 U(I) = U(I)*SF                                                    A 111
      CALL RESAMPLE (U,T,NN,NP,DT)                                      A 112
      DO 320 JJ=1,NL                                                    A 113
         U(JJ) = U(JJ)/NL                                               A 114
  320 UI(I) = 0.0                                                       A 115
      CALL FFTC (U,UI,NEXP)                                             A 116
      U(1) = 0                                                          A 117
      CALL FFTC (U,UT,NEXP)                                             A 118
      JSTEP = 1                                                         A 119
      CALL PTXER (U,T,PHI,N,JSTEP,PER)                                  A 120
      VELP = AMAX1F(U(1),U(NN))                                         A 121
      PRINT 470, VELP                                                   A 122
      DO 330 I=1,NN                                                     A 123
  330 F(I) = U(I)                                                       A 124
      Y = 12.0                                                          A 125
C                                                                       A 126
```

```
C      PROPAGATE USING WEAK SHOCK THEORY                                  A 127
C                                                                         A 128
       DO 350 I=1,8                                                       A 129
          XXX = 1.0+Y*(I-1)                                               A 130
          IF (XXX.EQ.1.0) GO TO 340                                       A 131
          CALL WAVEPROP (F,T,Y,XINC,N)                                    A 132
340       CALL WAVEPLOT(F,T,XXX,N,ISW,TAXIS,UAXIS,VA)                      A 133
 350   PRINT 500, XXX                                                     A 134
       DO 360 I=1,NN                                                      A 135
 360   T(I) = DT*(I-1)                                                    A 136
C                                                                         A 137
C      PROPAGATE USING MODIFIED WEAK SHOCK THEORY                         A 138
C                                                                         A 139
       N = NN                                                             A 140
       DO 410 J=1,NQ                                                      A 141
          XXX = 1.0+XL*(J-1)                                              A 142
          IF (XXX.EQ.1.0) GO TO 400                                       A 143
          CALL WAVEPROP (U,T,XL,XINC,N)                                   A 144
          CALL RESAMPLE (U,T,NN,N,DT)                                     A 145
          N = NN                                                          A 146
          DO 370 JJ=1,NL                                                  A 147
             U(JJ) = U(JJ)/NL                                             A 148
 370      UI(JJ) = UI(JJ)/NL                                              A 149
          CALL SET1 (UI(1),UI(515),0.0)                                   A 150
          CALL FFTC (U,UI,NEXP)                                           A 151
          NA = NL/2+1                                                     A 152
          DO 380 K=2,NA                                                   A 153
             ARG = SQRT(1.*(K-1))*ALPHA*XL                                A 154
             ZZ=U(K)                                                     A 154A
             U(K) = EXP(-ARG)*(U(K)*COSF(ARG)-UI(K)*SINF(ARG))            A 155
380       UI(K)=EXP(-ARG)*(UI(K)*COSF(ARG)+ZZ*SINF(ARG))                  A 156
          NB = NA+1                                                       A 157
          DO 390 K=NB,NL                                                  A 158
             LL = N+1-K                                                   A 159
             U(K) = U(LL)                                                 A 160
 390      UI(K) = -UI(LL)                                                 A 161
          CALL FFTC (U,UI,NEXP)                                           A 162
          JSTEP = J                                                       A 163
          CALL FIXER (U,T,PHI,N,JSTEP,PER)                                A 164
          IF ((XXX-XX).GE.0.0.OR.XXX.EQ.0.0) 400,410                      A 165
 400      CALL WAVEPLOT (U,T,XXX,NN,ISW,TAXIS,UAXIS,VA)                   A 166
          PRINT 500, XXX                                                  A 167
          XX = XX+12.                                                     A 168
```

```
 410  CONTINUE                                                          A 169
      PRINT 420                                                         A 170
      ACC(1) = PHI(1)                                                   A 171
      DO 420 I=2,NQ                                                     A 172
 420  ACC(I) = PHI(I)*ACC(I-1)                                          A 173
      DIST(1) = 1.0                                                     A 174
      DO 430 I=2,NQ                                                     A 175
 430  DIST(I) = 1.0+XL*(I-1)                                            A 176
      XX = 1.0                                                          A 177
      DO 450 I=1,NQ                                                     A 178
         IF (DIST(I).EQ.XX) 440,450                                     A 179
 440     PRINT 490, DIST(I),PHI(I),ACC(I)                               A 180
         XX = XX+12.0                                                   A 181
 450  CONTINUE                                                          A 182
C                                                                       A 183
 460  FORMAT (8F10.5)                                                   A 184
 470  FORMAT (5X,*MAXIMUM VELOCITY=*,F10.6)                             A 185
 480  FORMAT (/////,5X,*DISTANCE*,5X,*PHASE SHIFT*,5X,*ACCUMULATIVE PHAS  A 186
     *E SHIFT*)                                                         A 187
 490  FORMAT (8X,F5.2,5X,F12.7,7X,F12.7)                                A 188
 500  FORMAT (//,*  DISTANCE=*F7.3)                                     A 189
      END                                                               A 190-
```

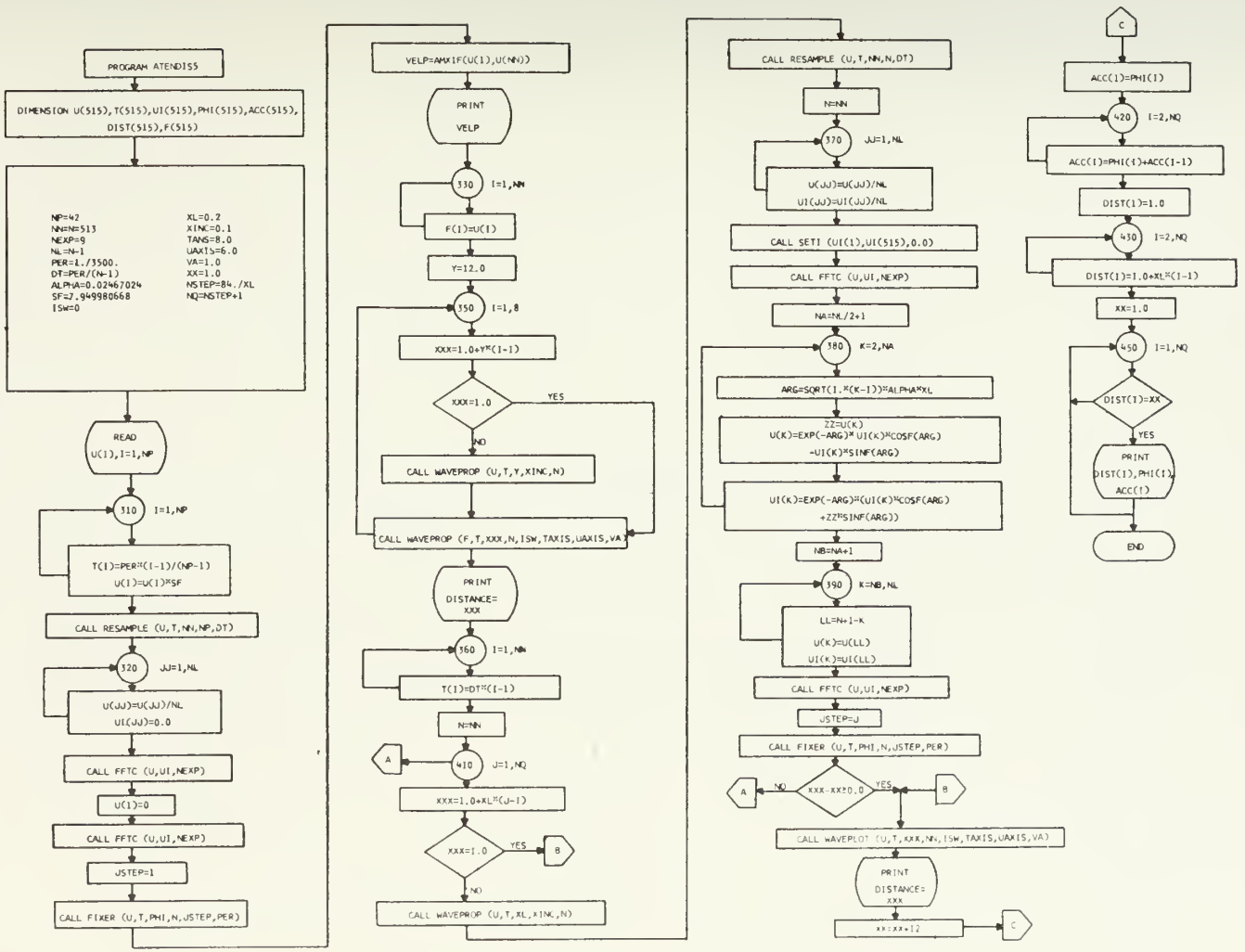

FIGURE B-2

FLOW CHART OF PROGRAM ATENDIS5

APPENDIX C

LISTINGS AND FLOWCHARTS OF SUBPROGRAMS OTHER THAN WAVEPROP

APPENDIX C,I SUBROUTINE RESAMPLE

3200 FORTRAN (2.1) 20/07/73

```
      SUBROUTINE RESAMPLE (U,T,N,NPOINTS,DT)                                    A   1
      DIMENSION U(1), T(1), FT(1200)                                            A   2
C                                                                               A   3
C ***************************************************************************** A   4
C                                                                               A   5
C     ARRAYS AND VARIABLES                                                      A   6
C                                                                               A   7
C ***************************************************************************** A   8
C                                                                               A   9
C     U        -- REAL ONE-DIMENSIONAL PARTICLE VELOCITY INPUT-OUTPUT           A  10
C              ARRAY                                                            A  11
C                                                                               A  12
C     T        -- REAL ONE-DIMENSIONAL TIME INPUT-OUTPUT ARRAY                  A  13
C                                                                               A  14
C     N        -- THE NUMBER OF OUTPUT DATA POINTS DESIRED.                     A  15
C     NPOINTS -- THE NUMBER OF INPUT DATA POINTS.                               A  16
C     DT       THE SAMPLING INTERVAL OF THE OUTPUT DATA POINTS.                 A  17
C     FT       -- A SCRATCH ARRAY                                               A  18
C ***************************************************************************** A  19
C                                                                               A  20
C     THE U AND T ARRAYS ENTER THE SUBROUTINE WITH NPOINTS AND ARE              A  21
C     RETURNED WITH N POINTS                                                    A  22
C     IF NN IS GREATER THAN NPOINTS INTERPOLATION HAS PROCEEDED                 A  23
C     BEYOND THE END OF THE USEFULL DATA IN THE U ARRAY.                        A  24
C     IF THE NUMBER OF SAMPLE POINTS EXCEEDS 1200, THE DIMENSION OF             A  25
C     FT MUST BE INCREASED.                                                     A  26
      NN = 2                                                                    A  27
      DO 30 I=1,N                                                               A  28
 10      TLIM = T(NN)                                                           A  29
         TT = (I-1)*DT                                                          A  30
         IF ((TT-TLIM).LE.1.0E-12) GO TO 20                                     A  31
         NN = NN+1                                                              A  32
         IF (NN.GT.NPOINTS) 50,10                                               A  33
 20      FT(I) = (TT-T(NN-1))*(U(NN)-U(NN-1))/(T(NN)-T(NN-1))+U(NN-1)           A  34
 30   CONTINUE                                                                  A  35
      DO 40 I=1,N                                                               A  36
         T(I) = (I-1)*DT                                                        A  37
 40   U(I) = FT(I)                                                              A  38
      GO TO 60                                                                  A  39
 50   PRINT 70                                                                  A  40
      STOP                                                                      A  41
```

```
      60    RETURN                                                    A  42
      C                                                               A  43
      C                                                               A  44
      70    FORMAT (1H1,19HNN EXCEEDED NPOINTS)                       A  45
            END                                                       A  46-

   RESAMPLE    P    05010    C    00000    D    00000
LOAD,56
RUN,,NM
```

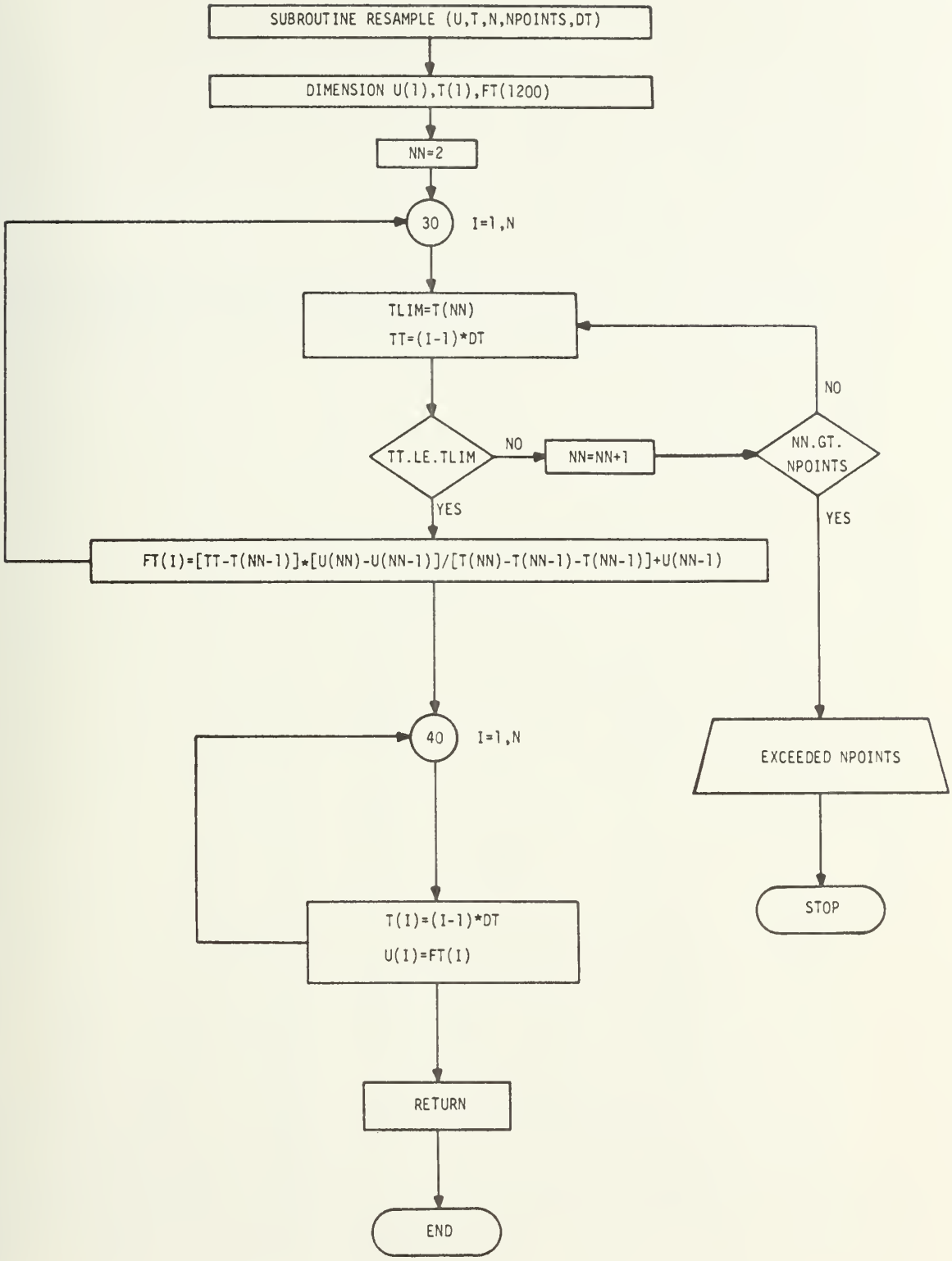

FIGURE C-1
FLOW CHART OF SUBROUTINE RESAMPLE

3200 FORTRAN (2.1) 18/04/73

```
      SUBROUTINE FIXER (U,T,PHI,N,ISTEP,PER)                                 D    1
      DIMENSION U(1), T(1), PHI(1), TEMP(513), TT(513)                       D    2
C                                                                            D    3
C  ***************************************************************************D    4
C                                                                            D    5
C     ARRAYS AND VARIABLES.                                                  D    6
C                                                                            D    7
C  ***************************************************************************D    8
C                                                                            D    9
C     U        -- REAL ONE-DIMENSIONAL PARTICLE VELOCITY INPUT-OUTPUT       D   10
C                 ARRAY.                                                     D   11
C                                                                            D   12
C     T        -- REAL ONE-DIMENSIONAL TIME INPUT-OUTPUT ARRAY              D   13
C                                                                            D   14
C     PHI      -- A REAL ONE-DIMENSIONAL ARRAY.  THE I-TH ELEMENT IN PHI    D   15
C                 IS THE PHASE SHIFT DETECTED IN THE I-TH CALL TO FIXER.     D   16
C                                                                            D   17
C     N        -- THE NUMBER OF POINTS IN THE U AND T ARRAY PLUS 1.         D   18
C                                                                            D   19
C     ISTEP    -- ISTEP COUNTS THE NUMMER OF CALLS TO FIXER.                D   20
C     PER      -- THE PERIOD OF THE WAVEFORM DESCRIBED BY U AND T           D   21
C  ***************************************************************************D   22
C                                                                            D   23
C     U AND T ENTER DESCRIBING THE WAVE PHASE SHIFTED DUE TO                 D   24
C     DISPERSION. THE ROUTINE DETECTS THE PHASE SHIFT AND RETURNS A          D   25
C     SINGLE CYCLE OF THE WAVE AND THE PHASE SHIFT.                          D   26
C                                                                            D   27
C        IF U AND T EXCEED 513 INCREASE TEMP AND TT ACCORDINGLY              D   28
      NM = N-1                                                               D   29
      PI = 6.28318308                                                        D   30
      IF (U(1).EQ.0.0) 10,20                                                 D   31
 10   PHI(ISTEP) = 0.0                                                       D   32
      GO TO 150                                                              D   33
 20   IF (U(1).GT.0.0) 30,80                                                 D   34
 30   DO 40 I=1,NM                                                           D   35
         IF (U(I).LE.0.0) 50,40                                              D   36
 40   CONTINUE                                                               D   37
 50   II = I                                                                 D   38
      T(II) = T(II-1)+(T(II)-T(II-1))/(U(II)-U(II-1))*(-U(II-1))             D   39
      T(II-1) = T(II)                                                        D   40
      U(II) = U(II-1) = 0.0                                                  D   41
```

```
      TSHIFT = T(II)                                                    D  42
      PHI(ISTEP) = TSHIFT*PI/PER                                        D  43
      MM = NM-II+1                                                      D  44
      DO 60 I=1,MM                                                      D  45
         JJ = II+I-1                                                    D  46
         TEMP(I) = U(JJ)                                                D  47
60    TT(I) = T(JJ)-TSHIFT                                              D  48
      IK = II-1                                                         D  49
      DO 70 I=1,IK                                                      D  50
         MA = I+MM                                                      D  51
         TEMP(MA) = U(I)                                                D  52
         TT(MA) = T(I)+PER-TSHIFT                                       D  53
70    CONTINUE                                                          D  54
      GO TO 130                                                         D  55
80    DO 90 J=1,NM                                                      D  56
         LL = NM+1-J                                                    D  57
         IF (LL.GE.0.0) 100,90                                          D  58
90    CONTINUE                                                          D  59
100   T(LL) = T(LL)+(T(LL+1)-T(LL))/(U(LL+1)-U(LL))*(-U(LL))            D  60
      T(LL+1) = T(LL)                                                   D  61
      U(LL) = U(LL+1) = 0.0                                             D  62
      JJ = LL                                                           D  63
      TSHIFT = T(JJ)-PER                                                D  64
      PHI(ISTEP) = TSHIFT*PI/PER                                        D  65
      MJ = NM-JJ                                                        D  66
      DO 110 J=1,JJ                                                     D  67
         MB = J+MJ                                                      D  68
         TEMP(MB) = U(J)                                                D  69
         TT(MB) = T(J)-TSHIFT                                           D  70
110   CONTINUE                                                          D  71
      DO 120 J=1,MJ                                                     D  72
         MC = J+JJ                                                      D  73
         TEMP(J) = U(MC)                                                D  74
         TT(J) = T(MC)-PER-TSHIFT                                       D  75
120   CONTINUE                                                          D  76
130   DO 140 I=1,NM                                                     D  77
         U(I) = TEMP(I)                                                 D  78
140   T(I) = TT(I)                                                      D  79
      DT = PER/(N-1)                                                    D  80
      CALL RESAMPLE (U,T,N,NM,DT)                                       D  81
150   RETURN                                                            D  82
      END                                                               D  83-
```

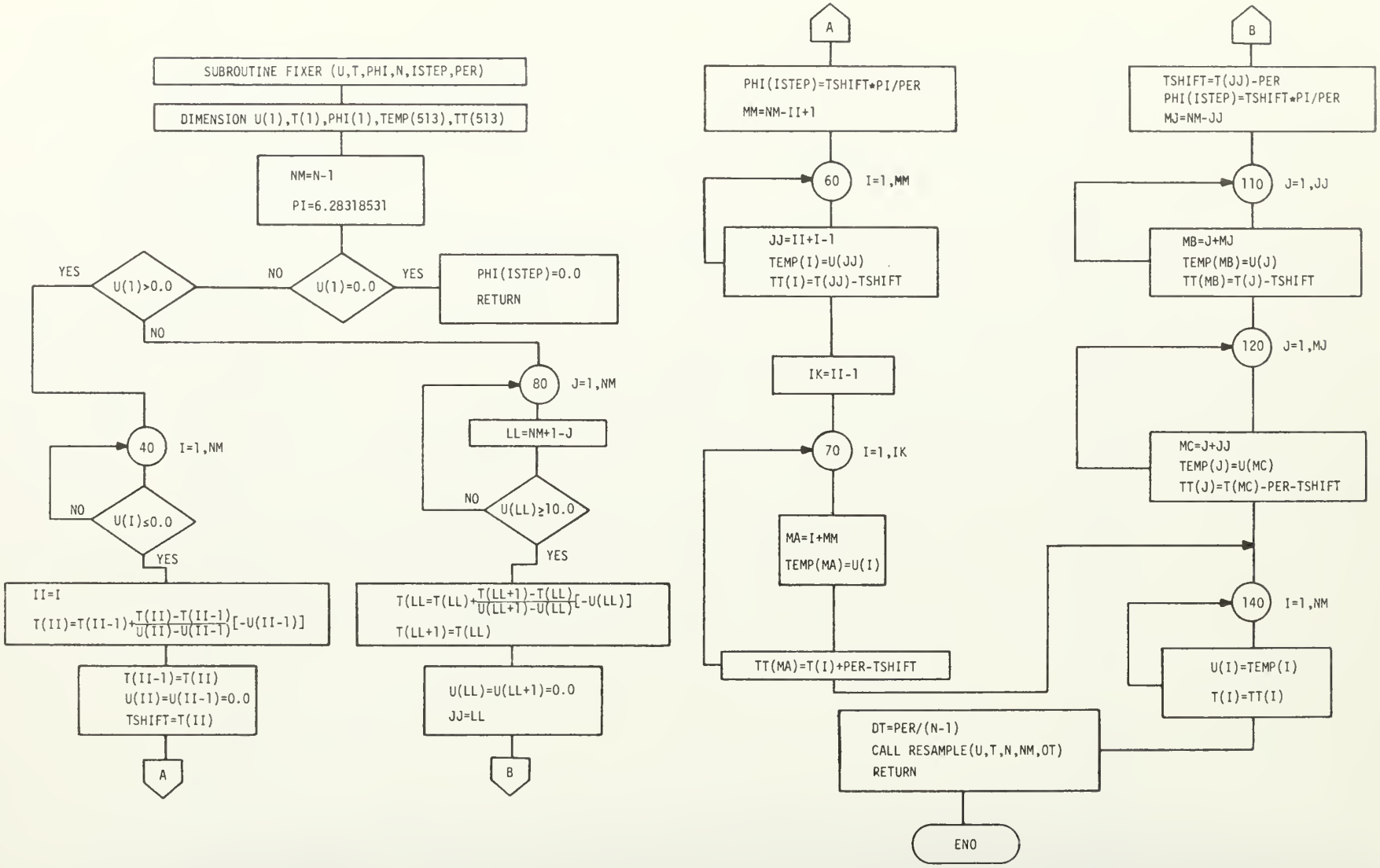

FIGURE C-2

FLOW CHART OF SUBROUTINE FIXER

3200 FORTRAN (2.1) 18/04/73

```
      SUBROUTINE WAVEPLOT (U,T,DISTANCE,NPOINTS,ISW,TAXIS,UAXIS,VA)          B   1
C     PLOTS THE WAVE WHOSE COMPONENTS ARE STORED IN T AND U AND              B   2
C     INDICATES THE DISTANCE AT WHICH THE WAVEFORM WAS COMPUTED              B   3
C     THE T COMPONENTS ARE SCALED TO A TAXIS INCH PLOT                       B   4
C     THE U COMPONENTS ARE SCALED TO A UAXIS INCH PLOT                       B   5
C     T         REAL ARRAY CONTAINING TIME COMPONENTS OF THE WAVE            B   6
C     U         REAL ARRAY CONTAINING VELOCITY COMPONENTS OF THE WAVE        B   7
C     DISTANCE REAL NUMBER GIVING DISTANCE AT WHICH THE WAVE WAS COMPUTE     B   8
C     NPOINTS   INTEGER GIVING NUMBER OF PAIRS OF COMPONENTS TO PLOT         B   9
C     ALL PARAMETERS ARE RETURNED UNCHANGED                                  B  10
C     ISW SETS THE PLOT VERTICAL SIZE. IF ISW=0 ALL PLOTS ARE UAXIS          B  11
C     INCHES VERTICALLY. IF ISW=1 THE FIRST PLOT IS UAXIS IN. AND THE        B  12
C     REST ARE PROPORTIONALLY SCALED.                                        B  13
C     VA      REAL VARIABLE ADJUSTS THE VERTICAL AXIS FOR                    B  14
C     OSCILLOSCOPE AMPLIFICATION. IT IS USED ONLY WHEN ISW=1.                B  15
C     IF ISW=0 SET VA=1.                                                     B  16
      INTEGER BCD                                                            B  17
      DIMENSION T(1), U(1)                                                   B  18
      COMMON /DATA/ BCD(6)                                                   B  19
      DATA (BCD=4HPART,4HICLE,4H VEL,4HTIME,4H(MSE,2HC))                     B  20
      IF (INIT.NE.1) CALL PLOTBUFF                                           B  21
      INIT = 1                                                               B  22
      CALL PLOT (4.0,-12.0,-3)                                               B  23
      CALL PLOT (0.0,2.5,-3)                                                 B  24
      IF (ISW) 10,20                                                         B  25
 10   IF (IFLAG.NE.1) 20,30                                                  B  26
 20   CALL SCALE (U,UAXIS,NPOINTS,1)                                         B  27
      UMINO = U(NPOINTS+1)                                                   B  28
      UDEL = U(NPOINTS+2)                                                    B  29
      GO TO 40                                                               B  30
 30   CALL SCALE (U,UAXIS,NPOINTS,1)                                         B  31
 40   IFLAG = 1                                                              B  32
      IF (ISW) 50,60                                                         B  33
 50   UMINO = UMINO/VA                                                       B  34
      UDEL = UDEL/VA                                                         B  35
 60   CONTINUE                                                               B  36
      CALL SCALE (T,TAXIS,NPOINTS,1)                                         B  37
      CALL AXIS (0.0,0.0,BCD,12,UAXIS,90.0,UMINO,UDEL,0.1,0.5,2)             B  38
      XJ = UAXIS+.1                                                          B  39
      CALL PLOTLINE (0.5,XJ,0.14,0.0)                                        B  40
      PRINT 100, DISTANCE                                                    B  41
```

```
      CALL AXIS (0.0,0.0,BCD(4),-10,TAXIS,0.0,T(NPOINTS+1)*1000.0,T      B  42
     $(NPOINTS+2)*1000.0,0.1,1.0,2)                                      B  43
      IF (U(NPOINTS+1).GE.0.0) GO TO 70                                  B  44
      ZERO = -UMINO/UDEL                                                 B  45
      IF (ZERO.GT.UAXIS) GO TO 70                                        B  46
      CALL PLOT (TAXIS,ZERO,3)                                           B  47
      CALL PLOT (0.0,ZERO,2)                                             B  48
   70 UMINO = UMINO*VA                                                   B  49
      UDEL = UDEL*VA                                                     B  50
      U(NPOINTS+1) = UMINO                                               B  51
      U(NPOINTS+2) = UDEL                                                B  52
      DO 80 J=1,NPOINTS                                                  B  53
   80 U(J) = VA*U(J)                                                     B  54
      CALL LINE (T,U,NPOINTS,1,0,0,0.08,1,0,0)                           B  55
      DO 90 J=1,NPOINTS                                                  B  56
   90 U(J) = U(J)/VA                                                     B  57
      NZK = TAXIS+3.0                                                    B  58
      ZK = NZK                                                           B  59
      CALL PLOT (ZK,0.0,-3)                                              B  60
      RETURN                                                             B  61
C                                                                        B  62
C                                                                        B  63
  100 FORMAT (* DISTANCE=*,F7.2)                                         B  64
      END                                                                B  65-

WAVEPLOT   P   00553   C   00000   D   00006
```

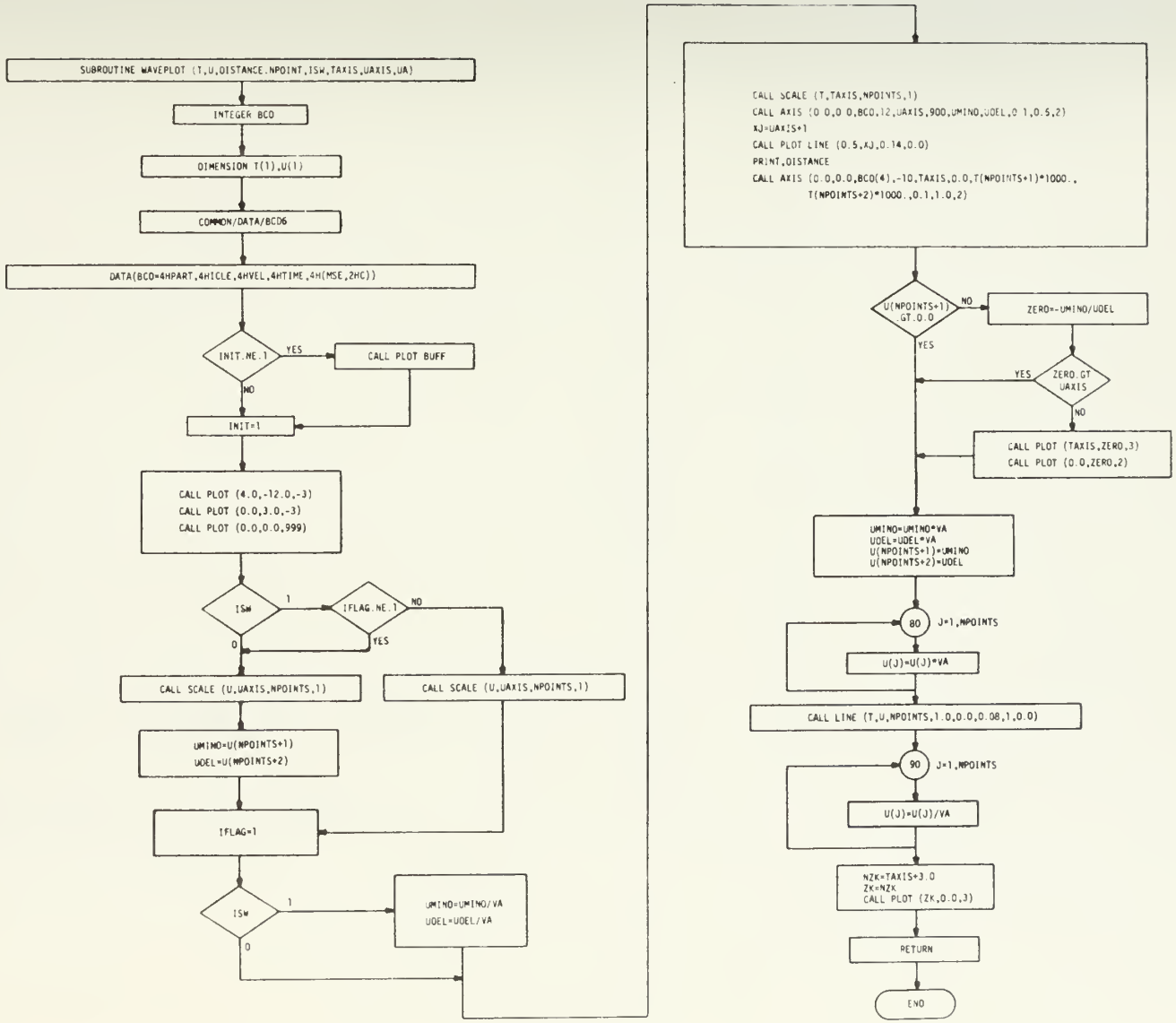

FIGURE C-3

FLOW CHART OF SUBROUTINE WAVEPLOT

APPENDIX C,IV FUNCTION ALPHA

```
                                3200  FORTRAN    (2.1)          20/07/73

          FUNCTION ALPHA (N,FO)                                          R   1
      C   R MUST BE SUPPLIED IN FEET
          R=0.0833                                                       R   2
          ALPHA=0.000029987/R*SQRT(FO*N)                                 R   3
          RETURN                                                         R   4
          END

   ALPHA      P   00061   C   00000   D   00000
LOAD.56
   *FIRST*    TR  00
```

APPENDIX D

LISTING AND FLOWCHART OF PROGRAM DOITALL3

The values assigned to various program parameters in this case are example values.

```
      PROGRAM DOITAL3                                                    A    1
      DIMENSION U(1025), T(1025), UA(1025), UB(1025), IUA(2050), UI(256)  A    2
      EQUIVALENCE (UA,IUA)                                               A    3
C                                                                        A    4
C     DOITALL3 CALCULATES POWER SPECTRA.  THE INITIAL WAVEFORM IS        A    5
C     PROPAGATED BY WEAK SHOCK THEORY ONLY.  THERE IS NO DISSIPATION     A    6
C     CORRECTION.  PROVISION IS MADE FOR ENSEMBLE AVERAGING OF           A    7
C     SPECTRA OF NOISE SAMPLE RECORDS.                                   A    8
C                                                                        A    9
C     U       REAL ARRAY.  STORES PARTICLE VELOCITY VALUES               A   10
C     T       REAL ARRAY.  STORES TIME VALUES IN THE FIRST HALF OF THE   A   11
C         PROGRAM AND AVERAGE POWER VALUES IN THE SECOND HALF            A   12
C     UA      REAL ARRAY USED IN POWER SPECTRA CALCULATIONS              A   13
C     UB      REAL USED IN POWER SPECTRA CALCULATIONS AND LATER AS       A   14
C         AN ARRAY OF FREQUENCIES.                                       A   15
C     UI      REAL ARRAY USED IN FFTC TO STORE IMAGINARY PART OF THE     A   16
C         INPUT/OUTPUT ARRAY.                                            A   17
C     IUA     INTEGER ARRAY USED TO BUFFER POWER SPECTRA VALUES          A   18
C         ONTO AND OFF OF TAPE.                                          A   19
C     LAGS    INTEGER VARIABLE. IT IS THE NUMBER OF CORRELATION          A   20
C         FUNCTION LAGS TO BE TRANSFORMED.                               A   21
C     MFFTCOR INTEGER VARIABLE.  THE NUMBER OF CORRELATION FUNCTION      A   22
C         POINTS CALCULATED=2**MFFTCOR.                                  A   23
C     MFFTC   INTEGER VARIABLE.  THE NUMBER OF POINTS IN THE POWER       A   24
C         SPECTRUM=2**MFFTC.                                             A   25
C     ZPROP  REAL VARIABLE.  IT IS THE DISTANCE OF PROPAGATION USED      A   26
C         IN WAVEPROP.                                                   A   27
C     ZINC    REAL VARIABLE.  IT IS THE INCREMENTAL STEP SIZE IN WAVEPROP A   28
C     NA      INTEGER VARIABLE.  NUMBER OF INITIAL WAVEFORM POINTS.      A   29
C     NN      INTEGER VARIABLE.  NUMBER OF POINTS PROPAGATED BY WAVEPROP. A   30
C     NLOC    INTEGER VARIABLE.  NUMBER OF LOCATIONS THAT PLOTS ARE DRAWN A   31
C     WL      REAL VARIABLE.  IT IS THE PERIOD OF THE INPUT SAMPLE.      A   32
C     NP      INTEGER VARIABLE. NUMBER OF SAMPLED DATA POINTS BEFORE     A   33
C         RESAMPLING.                                                    A   34
C     NW      INTEGER VARIABLE.  IT IS USED WITH NOISE SAMPLES TO ENSEMBLE A   35
C         AVERAGE THE POWER SPECTRA. FOR DETERMINISTIC WAVES NW=1        A   36
C     SF      REAL VARIABLE. SCALES INPUT DATA TO FEET/SEC.              A   37
C     DATADT REAL VARIABLE.  IT IS THE SAMPLE INCREMENT IN THE NP DATA.  A   38
C                                                                        A   39
C     THE POWER SPECTRA ARE PLOTTED ON IN A SEMI-LOG FORMAT USING        A   40
C     PLOT SUBROUTINE LOGPLOT                                            A   41
```

```
C                                                                       A  42
C     IN THIS RUN 5.23 MSEC OF NOISE 1 ARE INVESTIGATED. THE FUNDAMENTAL A  43
C     FREQUENCY IS 764 HZ.                                              A  44
      LAGS = 128                                                        A  45
      MEETCOR = 10                                                      A  46
      MEETC = 8                                                         A  47
      ZPROP = 12.0                                                      A  48
      ZINC = 0.1                                                        A  49
      NA = NN = 1025                                                    A  50
      NLOC = 3                                                          A  51
      NW = 1                                                            A  52
      SF = 8.93194141                                                   A  53
      DATADT = 5.0E-05/1.29                                             A  54
      NP = 136                                                          A  55
      WL = DATADT*(NP-1)                                                A  56
      LFOLD = LAGS+1                                                    A  57
      LAGSTWO = LAGS*2                                                  A  58
      NNTO = LFOLD                                                      A  59
      DT = WL/(NA-1)                                                    A  60
      S = 1./DT                                                         A  61
      PRINT 280, S                                                      A  62
      INNTO = NNTO*2                                                    A  63
      NPLOT = LAGS                                                      A  64
      NLOCSKP = NLOC-1                                                  A  65
      PRINT 290                                                         A  66
      DO 140 I1=1,NW                                                    A  67
         NN = NA                                                        A  68
         READ 300, (U(I),I=1,NP)                                        A  69
         DO 10 I=1,NP                                                   A  70
            T(I) = (I-1)*DATADT                                         A  71
10       U(I) = U(I)*SF                                                 A  72
         CALL RESAMPLE (U,T,NA,NP,DT)                                   A  73
         IZPIPE = 1                                                     A  74
         GO TO 40                                                       A  75
20       CONTINUE                                                       A  76
         CALL WAVEPROP (U,T,ZPROP,ZINC,NN)                              A  77
         IZPIPE = IZPIPE+12                                             A  78
         IF (IZPIPE.EQ.49) 40,30                                        A  79
30       IF (IZPIPE.EQ.73) 40,20                                        A  80
40       DO 50 JJ=1,NN                                                  A  81
            UR(JJ) = T(JJ)                                              A  82
50       UA(JJ) = U(JJ)                                                 A  83
         IF (IZPIPE.EQ.1) 70,60                                         A  84
```

```
60      CALL RESAMPLE (UA,UB,NA,NN,DT)                                  A  85
70      CONTINUE                                                        A  86
        DO 80 I3=1,NA                                                   A  87
           UB(I3) = UA(I3)                                              A  88
80      CONTINUE                                                        A  89
        CALL FFTCOR (UA,UB,MFFTCOR)                                     A  90
        DO 90 K=LFOLD,LAGSTWO                                           A  91
           J = NA-1-LAGSTWO+K                                           A  92
90      UA(K) = UA(J)                                                   A  93
        CALL SET1 (UI(1),UI(LAGSTWO),0.0)                               A  94
        CALL FFTC (UA,UI,MFFTC)                                         A  95
        CALL HANGEN1 (LAGSTWO,UA,1,1.0)                                 A  96
100     BUFFER OUT (1,1) (IUA(1),IUA(INNIQ))                            A  97
110     GO TO (110,130,130,120), UNITSTF(1)                             A  98
120     CALL SPACER (1)                                                 A  99
        GO TO 100                                                       A 100
130     CONTINUE                                                        A 101
        PRINT 310, I1,IZPIPE                                            A 102
        IF (IZPIPE.EQ.73) 140,20                                        A 103
140  CONTINUE                                                           A 104
     PRINT 320,                                                         A 105
     END FILE 1                                                         A 106
     NL = 0                                                             A 107
     DO 150 K=1,LAGSTWO                                                 A 108
150  UB(K) = K/(WL/4.)                                                  A 109
     DO 260 I5=1,NLOC                                                   A 110
        REWIND 1                                                        A 111
        CALL SKIPPER (1,0,NL)                                           A 112
        CALL SET1 (T(1),T(NNIQ),0.0)                                    A 113
        DO 200 I6=1,NW                                                  A 114
           BUFFER IN (1,1) (IUA(1),IUA(INNIQ))                          A 115
160        GO TO (160,180,180,170), UNITSTF(1)                          A 116
170        PRINT 330, (I6,I5)                                           A 117
           GO TO 270                                                    A 118
180        CONTINUE                                                     A 119
           DO 190 I7=2,NNIQ                                             A 120
190        T(I7-1) = T(I7-1)+UA(I7)                                     A 121
           CALL SKIPPER (1,0,NLOCSKP)                                   A 122
200     CONTINUE                                                        A 123
        DO 210 I9=1,NNIQ                                                A 124
210     T(I9) = T(I9)/NW                                                A 125
        PRINT 370, (T(I),T(I+32),T(I+64),T(I+96),I=1,32)                A 126
        IF (I5.EQ.1) 220,230                                            A 127
```

```
      220      BIG = AMX1F(T(1),T(NNIQ-1))                                    A 128
      230      CONTINUE                                                       A 129
               PRINT 360, BIG                                                 A 130
               DO 250 IB=1,NPLOT                                              A 131
                  T(IB) = 10.*ALOG10(ABSF(T(IB))/BIG)                         A 132
                  IF (T(IB).LT.-65.) 240,250                                  A 133
      240         T(IB) = -65.                                                A 134
      250      CONTINUE                                                       A 135
               PRINT 370, (T(I),T(I+32),T(I+64),T(I+96),I=1,32)               A 136
               CALL PLOT (2.0,-12.0,-3)                                       A 137
               CALL PLOT (0.0,2.0,-3)                                         A 138
               CALL LOGPLOT (1,UB,T,NPLOT,1.12.,7.0.3,1.4,.1,.150000.,5.,150.,  A 139
           $   -65.,-2,.05,4)                                                 A 140
               CALL PLOTLINE (0.5,0.3,0.14,0.0)                               A 141
               PRINT 340, IS                                                  A 142
               CALL PLOT (15.,-12.,-3)                                        A 143
               CALL PLOT (0.0,2.0,-3)                                         A 144
               PRINT 350, IS                                                  A 145
      260   NL = NL+1                                                         A 146
      270   CONTINUE                                                          A 147
            C                                                                 A 148
            C                                                                 A 149
      280   FORMAT (/////,10X,* SAMPLE RATE = *,E15.8)                        A 150
      290   FORMAT (///////,10X,*SAMPLE STATIONS*,10X,*FEET*,//,15X,1H1,21X,  A 151
           $1H1,//,15X,1H2,21X,2H49,//,15X,1H3,21X,2H73)                      A 152
      300   FORMAT (8E10.5)                                                   A 153
      310   FORMAT (///* WAVE NO. *,I2,* AT *,I2,* FEET IS BUFFERED OUT.*)    A 154
      320   FORMAT (///,* BUFFERING OUT COMPLETED*,1H1)                       A 155
      330   FORMAT (1H1,* BUFFERING IN ERROR AT WAVE NO. *,I2,* LOCATION NO. *  A 156
           $,I2)                                                              A 157
      340   FORMAT (* PIPE STATION NO. *,I2)                                  A 158
      350   FORMAT (////,* PLOT ON TAPE FOR PIPE LOCATION*,I2)                A 159
      360   FORMAT (///,*   BIG=*,F20.10)                                     A 160
      370   FORMAT (1H1,(4(10X,E15.7)))                                       A 161
            END                                                               A 162-

DOITAL3     P   22560    C   00000    D   00000
```

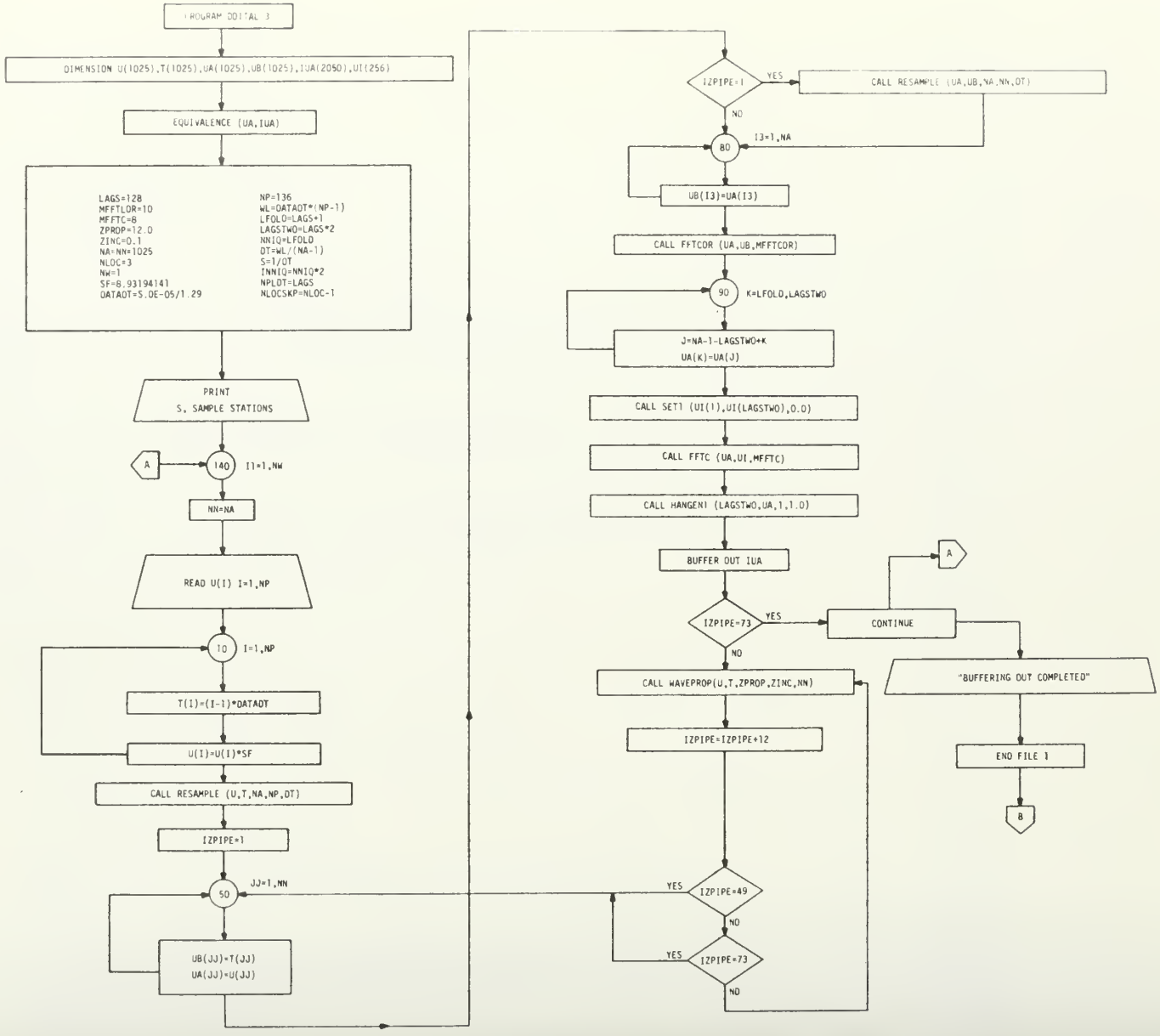

FIGURE D-1

FLOW CHART OF PROGRAM DOITALL3

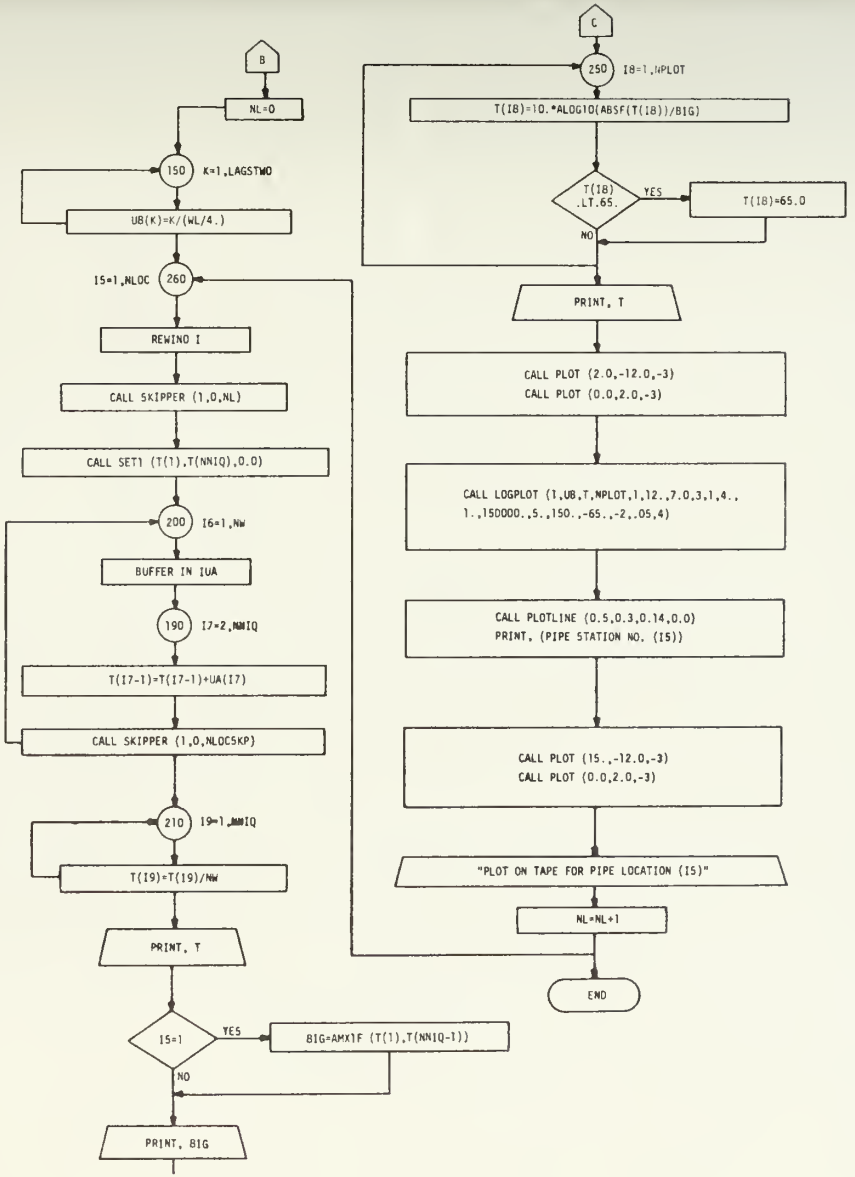

FIGURE D-1 (Cont'd)

FLOW CHART OF PROGRAM DOITALL3

APPENDIX E

The Limitation on the Strength of the Waves that may be Considered using Weak-Shock Theory

Previous researchers [see, for example, Rudnick (1952, Blackstock (1964) and Temkin (1969)] have used a variety of upper bounds for the strength of the waves that may be considered using weak-shock theory. In this appendix we shall analyze the limit using entropy considerations. Our analysis will basically follow Rudnick's (1952).* In Rudnick's derivation and in ours the implicit assumption of simple wave flow is made. For waves of high-intensity, however, reflections from the shocks may be large enough to invalidate the simple wave assumption, even as an approximation. Therefore, we should not regard the results obtained here as a tool for calculating the attenuation of very intense waves, but rather as an estimate useful in establishing the limits of weak-shock theory. Our results may be used in problems concerning very intense waves if

1) further analysis shows that the reflected waves may be ignored, or

2) they are used in conjunction with the Riemann invariants [see, for example, Thompson (1972)].

In Rudnick's derivation of the weak-shock propagation of sawtooth waves use is made of the approximate relation

$$s_2 - s_1 \doteq \frac{\beta R}{6\gamma^2}\,\delta^3 \quad . \tag{E-1}$$

*A brief but more accessible form of this derivation appears in the paper by Rudnick (1953).

Equation (E-1) is numbered (3-17) in Chapter III. Use of Eq. (E-1) leads to the weak-shock relation

$$\frac{d(1/\delta)}{d(x/\lambda)} = \frac{\gamma + 1}{2\gamma} \quad . \tag{E-2}$$

The solution of Eq. (E-2) subject to the boundary condition $\delta = \delta_o$ at $x = 0$ is

$$\frac{1}{\delta} - \frac{1}{\delta_o} = \frac{\gamma + 1}{2\gamma} \frac{x}{\lambda} \quad . \tag{E-3}$$

If we use the exact expression for the entropy change across the shock, an improvement is obtained. The exact entropy change across any shock in a perfect gas, is given by*

$$\Delta s = C_v \, \ell n \left[(1 + \delta)(\rho_2/\rho_1)^{-\gamma} \right] \quad , \tag{E-4}$$

where C_v is the specific heat at constant volume. The absolute density ratio ρ_2/ρ_1 is obtained from Eq. (3-13). Use of the perfect gas relations and inversion at the resulting equation yields the desired relation

$$\frac{\rho_2}{\rho_1} = \frac{\delta(\gamma + 1) + 2\gamma}{\delta(\gamma - 1) + 2\gamma} \quad . \tag{E-5}$$

---

*Equation (E-4) is derived, for example, by Lindsay (1960).

Following Rudnick's procedure and using Eqs. (E-4) and (E-5) in lieu of Eq. (E-1) we obtain the differential equation

$$\frac{d(1/\delta)}{d(x/\lambda)} = \frac{6\gamma}{(\gamma - 1)\delta^3} \ln \left[(1 + \delta) \left[\frac{\delta(\gamma + 1) + 2\gamma}{\delta(\gamma - 1) + 2\gamma} \right]^{-\gamma} \right] , \tag{E-6}$$

in place of Eq. (E-2).

We have obtained approximate solutions of Eq. (E-6) by two different methods. In the first method the right hand side of Eq. (E-6) was expanded in a power series and terms through the fifth order in δ retained. The final result is

$$\frac{d(1/\delta)}{d(x/\lambda)} \doteq \frac{\gamma + 1}{2\gamma} - \frac{3(\gamma + 1)\delta}{4\gamma} + \frac{3(11\gamma^2 + 1)(\gamma + 1)\delta^2}{40\gamma^3} . \tag{E-7}$$

Solution of Eq. (E-7) subject to the boundary condition $\delta = \delta_o$ at $x = 0$ yields the result

$$\frac{1}{\delta} - \frac{1}{\delta_o} = \frac{\gamma + 1}{2\gamma} \frac{x}{\lambda} - F(\delta) + F(\delta_o) \tag{E-8}$$

where

$$F(\delta) = \frac{3}{4\gamma} \ln \left(\frac{20\gamma^2}{\delta^2} + \frac{30\gamma^2(\delta - 1)}{\delta} + 3 \right) - \frac{132\gamma^2 + 15}{[1740\gamma^2 + 240]^{1/2}} \tan^{-1} \left(\frac{\frac{40\gamma}{\delta} - 30\gamma}{[1740\gamma^2 + 240]^{1/2}} \right) .$$

Note that Eq. (E-8) is an implicit result, since we have not obtained an explicit solution for the quantity $\delta(x)$.

In our second solution Eq. (E-6) was numerically integrated by means of Simpson's rule. In Fig. (E-1) we have plotted the quantity $1/\delta$ versus x/λ for $\gamma = 1.41$ using Eqs. (E-3), (E-8) and the results of the numerical integration. Three values of δ_o^{-1} have been used, $\delta_o^{-1} = 2$, 10 and 15. For each value of δ_o^{-1} the top curve is the ordinary weak-shock result Eq. (E-2), the middle curve is the three-term result Eq. (E-8), and the bottom curve is the result of the numerical integration. In each case the three curves shown appear to be diverging. In reality if the plots are extended to larger values of x/λ the three curves become parallel with the common slope given by the quantity $(\gamma + 1)/2\gamma$.

Note that the bottom curve in the set for $\delta_o^{-1} = 2$ has considerable curvature for small values of x/λ. This curvature indicates that very intense waves will attenuate at a rate considerably less than that predicted by use of weak-shock theory.

The upper limit of applicability of weak-shock theory was obtained by evaluating the right sides of Eq. (E-2) and (E-6) as functions of δ and calculating the percentage difference between the two results. The percentage differences along with results obtained by evaluating the right sides of Eqs. (E-2), (E-6) and (E-7) are shown in Table (E-1). The results obtained using Eq. (E-7) are included for the purpose of comparison with the results obtained using Eq. (E-6).

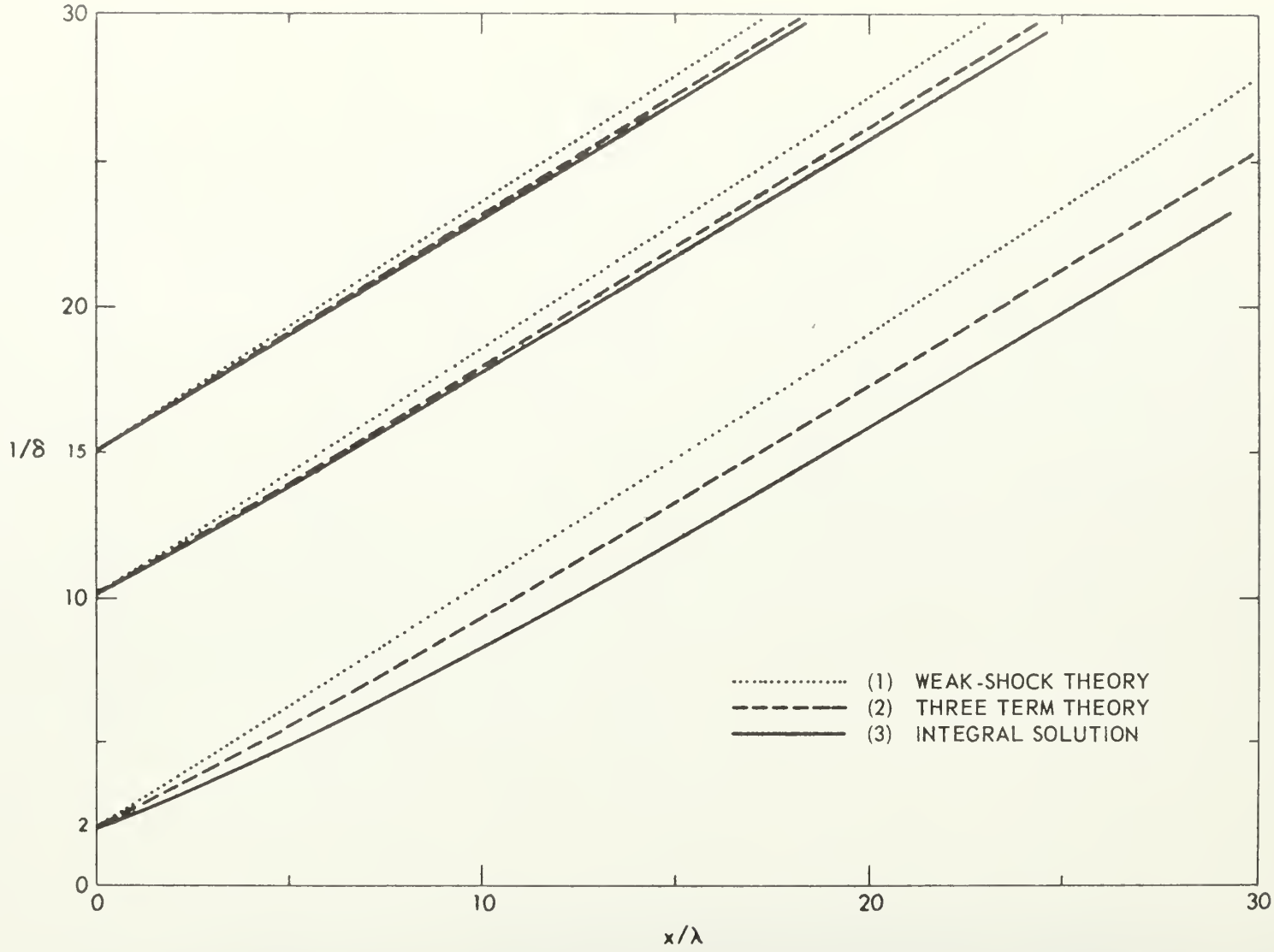

FIGURE E-1
δ^{-1} VERSUS x/λ

TABLE E-1

Analysis of the Upper Strength Limit of Weak-Shock Theory

δ	A	B	C	D
	Weak Shock Theory	Eq. (E-7)	Eq. (E-6)	% Error
0.5	0.855	0.582	0.7938	88.32
0.2	0.855	0.658	0.647	32.14
0.1	0.855	0.741	0.740	15.54
0.0667	0.855	0.776	0.775	10.32
0.05	0.855	0.7942	0.7938	7.71
0.01	0.855	0.8419	0.8418	1.65

Notes: 1) $\gamma = 1.41$

2) $D = (A - C)/C \times 100$

We see from Table E-1 that the error involved in using the weak-shock result when $\delta = 0.01$ is less than 2% whereas the error when $\delta = 0.1$ is 15.5%. Clearly, the use of weak-shock theory will produce results of doubtful validity for values of δ_o larger than 0.1. The value $\delta_o^{-1} = 10$ corresponds to a source SPL of about 165 dB. For waves stronger than 165 dB improved versions of weak-shock theory based upon Eq. (E-6) in conjunction with the Riemann invariants should be used.

BIBLIOGRAPHY

Applied Research Laboratories 3200 Plot Routines (1973). Applied Research Laboratories, The University of Texas at Austin, Austin, Texas.

Baird, D. C. (1964). An Introduction to Measurement Theory and Experimental Design (Prentice-Hall Book Company, Englewood Cliffs, N. J.), 4th printing, p. 182.

Beyer, R. T. (1960). "Parameter of Nonlinearity in Fluids," J. Acoust. Soc. Amer. 32, 719-721.

Bingham, C., Godfrey, M. D., and Tukey, J. W. (1967). "Modern Techniques of Power Spectrum Estimation," IEEE Trans. on Audio and Electroacoustics AU-15, pp. 56-66.

Blackman, R. B., and Tukey, J. W. (1959). The Measurement of Power Spectra, (Dover Publications Inc., New York), pp. 120-124.

Blackstock, D. T. (1962a). "Propagation of Plane Sound Waves of Finite Amplitude in Nondissipative Fluids," J. Acoust. Soc. Amer. 34, 9-30.

Blackstock, D. T. (1962b). "Dissipative Propagation of Finite-Amplitude Waves in a Tube," Paper 0-15 in Congress Rep. I, Fourth International Congress on Acoustics, Copenhagen, Denmark.

Blackstock, D. T. (1964). "On Plane, Spherical, and Cylindrical Sound Waves of Finite Amplitudes in Lossless Fluids," J. Acoust. Soc. Amer. 36, 217-219.

Blackstock, D. T. (1966). "Connection Between the Fay and Fubini Solutions of Plane Sound Waves of Finite Amplitude," J. Acoust. Soc. Amer. 39, 1019-1026.

Blackstock, D. T. (1969). "History of Nonlinear Acoustics and a Survey of Burgers' and Related Equations," in Nonlinear Acoustics, T. G. Muir, Ed. (Applied Research Laboratories, The University of Texas at Austin, Austin, Texas), pp. 1-28.

Blackstock, D. T. (1972). "Nonlinear Acoustics (Theoretical)," in Amer. Inst. Phys. Handbook, D. Gray Ed. (McGraw-Hill Book Co., Inc., New York), ch. 3n, pp. 3-183 through 3-205.

Burgers, J. M. (1948). "A Mathematical Model Illustrating the Theory of Turbulence," in Advances in Applied Mechanics, R. von Mises and T. von Karman Eds. (Academic Press Inc., New York), pp. 171-199.

Burgers, J. M. (1972). "Statistical Problems Connected with Asymptotic Solutions to the One-Dimensional Nonlinear Diffusion Equation," in Statistical Models of Turbulence, M. Rosenblatt and C. van Atta Eds. (Springer-Verlag, Berlin), pp. 41-60.

Burnett, W. A., and Ackerman, E. (1960). "Propagation Distortion of Large Amplitude Acoustic Noise," WADD Tech. Rep. 60-232, Wright-Patterson Air Force Base, Ohio.

Burns, S. H. (1966a). "Finite-Amplitude Traveling Waves with Boundary Dissipation," Tech. Mem. No. 60, Acoust. Res. Lab, Harvard University, Cambridge, Mass.(AD 628-671).

Burns, S. H. (1966b). "Finite-Amplitude Distortion in Air at High Acoustic Pressures," J. Acoust. Soc. Amer. 41, 1157-1169.

Burns, S. H. (1971). "Rational Design of Matched Abosrbing Terminations for Tubes," J. Acoust. Soc. Amer. 49, 1693-1697.

Cook, B. D. (1962). "New Procedure for Computing Finite-Amplitude Distortion," J. Acoust. Soc. Amer. 34, 941-946.

Coppens, A. B. (1971). "Theoretical Study of Finite-Amplitude Traveling Waves in Rigid-Walled Ducts: Behavior for Strengths Precluding Shock Formation," J. Acoust. Soc. Amer. 49, 306-318.

Coppens, A. B., and Sanders, J. V. (1968). "Finite-Amplitude Standing Waves in Rigid-Walled Tubes," J. Acoust. Soc. Amer. 43, 516-529.

Courant, R., and Friedrichs, K. O. (1948). Supersonic Flow and Shock Waves (John Wiley & Sons, Inc., New York)

Crow, S. C., and Canavan, G. H. (1970). "Relationship Between a Wiener-Hermite Expansion and an Energy Cascade," J. Fluid Mech. 41, 387-403.

Cruikshank, D. B., Jr. (1966). "Growth of Distortion in a Finite-Amplitude Sound Wave in Air," J. Acoust. Soc. Amer. 40, 731-733(L).

Earnshaw, S. (1860). "On the Mathematical Theory of Sound," Phil. Trans. Roy. Soc. London 150, 133-148.

Evans, L. B., Bass, H. E., and Sutherland, L. C. (1972). "Atmospheric Absorption of Sound: Theoretical Predictions," J. Acoust. Soc. Amer. 51, 1565-1574.

Fay, R. D. (1956). "Successful Method of Attack on Plane Progressive Finite Waves," J. Acoust. Soc. Amer. 28, 910-914.

Fay, R. D. (1962). "Corrected Analysis of Plane Finite Waves," J. Acoust. Soc. Amer. 34, 1269-1271.

Ffowcs Williams, J. E. (1965), Personal Communication, J. E. Ffowcs Williams to D. T. Blackstock.

Fox, F. E., and Wallace, W. A. (1954). "Absorption of Finite Amplitude Sound Waves," J. Acoust. Soc. Amer. 26, 494-510.

Friedrichs, K. O. (1948). "Formation and Decay of Shock Waves," Commun. Pure Appl. Math. 1, 211-245.

Geertsen, O. N. (1951). "A Study of Finite Amplitude Distortion of Sound Waves in Air," Technical Report No. III, Department of Physics, University of California, Los Angeles, Calif.

Hawkings, D. (1970). "Multiple Tone Generation by Transonic Compressors," J. Sound Vib. 17, 241-250.

Horton, C. W., Sr. (1969). Signal Processing of Underwater Acoustic Waves (U. S. Govt. Printing Office, Washington D. C.), pp. 94-97.

Jones, I. S. F. (1971). "Finite Amplitude Waves from a Supersonic Jet," Paper No. 71-151, AIAA Ninth Aerospace Sciences Meeting, New York, New York.

Kinsler, L. E., and Frey, A. R. (1950). Fundamentals of Acoustics (John Wiley and Sons, Inc., New York), 2nd Ed., chap. 7, pp. 169-172.

Kirchhoff, G. (1868). "Ueber der Einfluss der Warmeleitungs in Gase auf die Schallbewegung," Ann. Physik 134, 177-193.

Kraichnan, R. H. (1968). "Lagrangian-History Statistical Theory for Burgers' Equation," Phys. Fluids 11, 265-277.

Kuznetsov, V. P. (1970). "On the Spectra of High-Intensity Noise," Soviet Phys. - Acoust. 16, 129-130.

Landau, L. (1945). "On Shock Waves at Large Distances from the Place of their Origins," Journal of Physics (USSR) 9, 496-500.

Landau, L. D., and Lifshitz, E. M. (1959). Fluid Mechanics (Pergamon Press, London), pp. 372-378.

Leonard, R. W., and Wilson, O. B., Jr. (1952). "Instrumentation and Apparatus for a High Amplitude Sound Research Program," Technical Report No. 2, Soundrive Engine Co., Los Angeles, California.

Lighthill, M. J. (1956). "Viscosity Effects in Sound Waves of Finite Amplitude," in Surveys in Mechanics G. K. Batchelor and R. M. Davies Eds.(Cambridge Univ. Press, Cambridge, England), pp. 250-352.

Lindsay, R. B. (1960). Mechanical Radiation (McGraw-Hill Book Company, Inc., New York), pp. 290-292.

Mariens, P. (1957). "Kirchhoff-Helmholtz Absorption in Wide and in Capillary Tubes at Audible Frequencies," J. Acoust. Soc. Amer. 29, 442-445.

McKittrick, J. L., Blackstock, D. T., and Wright, W. M. (1967). "Profile of Repeated Shock Waves in a Tube," J. Acoust. Soc. Amer. 42, 1153(A).

Medwin, H. (1964). "Attenuation of Guided, Repeated Shock Waves in Gases," J. Acoust. Soc. Amer. 36, 870-877.

Morfey, C. L. (1973). Private Communication, C. L. Morfey to D. T. Blackstock.

Oda, F., and Ackerman, E. (1960). "Propagation of Finite Amplitude Acoustic Noise," WADD Tech. Rep. 60-232, Wright-Patterson Air Force Base, Ohio.

Ogata, K. (1967). State Space Analysis of Control Systems (Prentice-Hall Book Company, Englewood Cliffs, N. J.), pp. 336-340.

Papoulis, A. (1965). Probability, Random Variables and Stochastic Processes (McGraw-Hill Book Co., Inc., New York), p. 475.

Pelinovskii, E. N., and Fridman, V. E. (1973). "Statistical Effects in the Generation of Shock Waves," Soviet Phys. - Acoust. 18, 482-484.

Pernet, D. F., and Payne, R. C. (1969). "Propagation of Finite Amplitude Sound Waves in Tubes," AERO Report Ac 43, National Physical Laboratory, Teddington, England.

Pernet, D. F., and Payne, R. C. (1971a). "Nonlinear Propagation of Signals in Air," J. Sound Vib. 17, 383-396.

Pernet, D. F., and Payne, R. C. (1971b). "Propagation of Finite Amplitude Noise in Tubes," AERO Report Ac 48, National Physical Laboratory, Teddington, England.

Pestorius, F. M., and Blackstock, D. T. (1972). "A Computer Algorithm for Predicting Propagation of Intense Acoustical Signals of Arbitrary Waveform," J. Acoust. Soc. Amer. 53, 383(A).

Pestorius, F. M., and Blackstock, D. T. (1973a). "Nonlinear Distortion in the Propagation of Intense Acoustic Noise," Proceedings of the Interagency Symposium on University Research in Transportation Noise, Standford Univ., Stanford, Calif., vol. II, pp. 565-577.

Pestorius, F. M., and Blackstock D. T. (1973b). "Experimental and Theoretical Study of Propagation of Finite-Amplitude Noise in a Pipe," J. Acoust. Soc. Amer. 53, 7th Issue(A).

Pickett, G. F., (1971). "The Prediction of the Spectral Content of Combination Tone Noise," AIAA Paper No. 71-730, AIAA/SAE Seventh Propulsion Joint Specialist Conference, Salt Lake City, Utah.

Poisson, S. D. (1808). "Mémoire sur la Théorie du Son," J. École Polytech. (Paris) 7, 319-370.

Rayleigh, J. W. S. (1910). "Aerial Plane Waves of Finite Amplitude," Proc. Roy. Soc. (London) A84, 247-284.

Ribner, H. S. (1969). "Jets and Noise," in Aerodynamic Noise H. S. Ribner Ed. (University of Toronto Press, Toronto, Ontario, Canada), pp. 3-42.

Rudnick, I. (1952). "Theory of Attenuation of Very High Amplitude Sound Waves," Tech. Rep. No. 1, Soundrive Engine Co., Los Angeles, Calif.

Rudnick, I. (1953). "On the Attenuation of a Repeated Sawtooth Shock Wave," J. Acoust. Soc. Am. 25, 1012-1013(L).

Shin, Y. (1963). "Attenuation of Repeated Spherical Shock Waves," Technical Report No. 22, Department of Physics, University of California, Los Angeles, Calif. (AD 413 346).

Standard Mathematical Tables (1956). (Chemical Rubber Co., Cleveland, Ohio) 4th ed., p. 406.

Stein, S., and Jones, J. J. (1967). Modern Communication Principles (McGraw-Hill Book Company, Inc., New York), pp. 188-190.

Tatsumi, T., and Kida, S. (1972). "Statistical Mechanics of the Burgers Model of Turbulence," J. Fluid Mech. 55, 659-675.

Temkin, S. (1969). "Attenuation of Guided, Weak Sawtooth Waves," J. Acoust. Soc. Amer. 46, 267-271.

Thompson, P. A. (1972). Compressible-Fluid Dynamics (McGraw-Hill Book Company, Inc., New York).

Thuras, A. L., Jenkins, R. T., and O'Neil, H. T. (1935). "Extraneous Frequencies Generated in Air Carrying Intense Sound Waves," J. Acoust. Soc. Amer. 6, 173-180.

Van Buren, A. L., and Breazeale, M. A. (1968). "Reflection of Finite-Amplitude Ultrasonic Waves, II. Propagation," J. Acoust. Soc. Amer. 44, 1021-1027.

Webster, J. C. (1971). "Noise Levels on Aircraft-Carrier Flight Decks, and Their Effects," NELC/TR 1762, Naval Electronics Laboratory Center, San Diego, Calif.

Welch, P. D. (1967). "The Use of Fast Fourier Transform for the Estimation of Power Spectra: a Method Based on Time Averaging over Short, Modified Periodograms," IEEE Trans. of Audio and Electro-Acoustics AU-15, pp. 70-73.

Werth, G. C., and Delsasso, L. P. (1954). "Attenuation of Repeated Shock Waves in Tubes," J. Acoust. Soc. Amer. 26, 59-64.

Westervelt, P. J. (1960). "Self Scattering of High Intensity Sound" in Proceedings of the Third International Congress on Acoustics Stuttgart 1959 L. Cremer Ed. (Elsevier Publishing Co., Amsterdam), vol. I, pp. 316-321.

Weston, D. E. (1953). "The Theory of the Propagation of Plane Sound Waves in a Tube," Proc. Phys. Soc. (London) B66, 645-709.

Whitham, G. B. (1952). "The Flow Pattern of a Supersonic Projectile," Commun. Pure Appl. Math. 5, 301-348.

Whitham, G. B. (1956). "On the Propagation of Weak Shock Waves," J. Fluid. Mech. 1, 290-318.

Wilks, S. S. (1963). Mathematical Statistics (John Wiley and Sons, Inc., New York), 2nd ed., p. 265.

August 1973

DISTRIBUTION LIST FOR
ARL-TR-73-23
UNDER OFFICE OF NAVAL RESEARCH CONTRACT N00014-70-A-0166-0004
and
UNDER AIR FORCE OFFICE OF SCIENTIFIC RESEARCH CONTRACT F44620-71-C-0015

uropean Office of Aerospace Research
ox 14, FPO
ew York, NY 09510

FOSR/NAM
400 Wilson Boulevard
16) rlington, VA 22209

rnold AFS, TN 37389
ttn: Library/Documents
AEDC
ARO, Inc.

ommander
AMSO
os Angeles AFS, CA 90045

Wright-Patterson AFB, OH 45433
Attn: AFFDL (Library)
AFIT Library (AU)
AFML (Library)
ARL (Library)
6570 AMRL (BB)
Dr. H. E. von Gierke
J. N. Cole
AFPL

Commander
Aeronautical Systems Division
Wright-Patterson AFB, OH 45433
Attn: Library

Air Force Avionics Laboratory
Air Force Systems Command
Wright-Patterson AFB
Dayton, OH 45433
Attn: Technical Library

Air University Library
(SE) 63-578
Maxwell AFB, AL 36112

Frank J. Seiler Research Laboratories
USAFA, CO 80840

L. G. Hanscom Field
Bedford, MA 01731
Attn: AFCRL (Library)

Kirtland AFB, NM 98117
Attn: AFWL (Library)

USAFA, CO 80840
Attn: USAFA (Library)

(Air Force Office of Scientific Research
Department of the Air Force
Washington, D C 20333

NASA Langley Research Center
Langley AFB, VA 23365
Attn: Library
I. E. Garrick

NASA Langley Research Center
Langley Station
Hampton, VA 23365
Attn: Dr. R. L. Barger,
Full-Scale Analysis Branch
H. H. Hubbard,
Acoustics Branch, MS 239

NASA Lewis Research Center
21000 Brookpark Road
Cleveland, OH 44135
Attn: Library M. S. 60-3

NASA
600 Independence Avenue, SW
Washington, DC 20546

Ames Laboratory
NASA
Moffett Field, CA 94035

George C. Marshall Space Fight Center
NASA
Huntsville, AL 35812
Attn: Library

Goddard Space Flight Center
NASA
Greenbelt, MD 20771

John F. Kennedy Space Center
NASA
Kennedy Space Center, FL 32899

Office of Naval Research
Department of the Navy
Arlington, VA 22217
Attn: Mechanics Branch (Code 439)
(2) N. Prohaska (Code 412)

Commanding Officer
Office of Naval Research
Branch Office Chicago
536 South Clark Street
Chicago, IL 60605

Commanding Officer
Office of Naval Research
Branch Office Pasadena
Department of the Navy
1030 East Green Street
Pasadena, CA 91106

Commanding Officer
Office of Naval Research
Branch Office Boston
495 Summer Street
Boston, MA 02210

Commanding Officer
Office of Naval Research
San Francisco Area Office
Department of the Navy
760 Market Street
San Francisco, CA 94102

Commanding Officer
Office of Naval Research
New York Area Office
Department of the Navy
207 West 24th Street
New York, NY 10011

(2) Commander
Naval Ship Systems Command
Department of the Navy
Washington, DC 20362
Attn: RDT&E Planning Division

(2) Research and Technology
Naval Air Systems Command
Department of the Navy
Washington, DC 20360

(3) Office of the Director of
Defense Research and Engineering
Room 3E 1063, The Pentagon
Washington, DC 20301
Attn: Information Office Library Branch

(2) Research and Technology Directorate
Naval Electronics Systems Command
Department of the Navy
Washington, DC 20360

(2) Research and Technology Directorate
Naval Ordnance Systems Command
Department of the Navy
Washington, DC 20360

Director
Advanced Research Projects Agency
The Pentagon
Washington, DC 20301
(3) Attn: Technical Library
CAPT W. J. Hipple, USN

Office of Noise Abatement, TST-52
Department of Transportation
400 7th St., SW
Washington, DC 20590
Attn: Dr. G. Banerian

Naval Research Laboratory
Underwater Sound Reference Division
P. O. Box 8337
Orlando, FL 32806
Attn: Technical Library

Officer-in-Charge
Naval Undersea Center
Department of the Navy
3202 East Foothill Boulevard
Pasadena, CA 91107
Attn: Technical Library

Director
Naval Research Laboratory
Department of the Navy
Washington, DC 20390
(3) Attn: Technical Information Division
(5) Library (Code 2029 (ONRL))
A. L. van Buren (Code 8153)

Commander
Naval Undersea Center
San Diego, CA 92132
Attn: Technical Library

Commanding Officer and Director
Naval Ship Research and Development Center
Department of the Navy
Washington, DC 20034
Attn: Central Library (Code 5643)
Library, Aerodynamics Laboratory

Officer-in-Charge
Newport Laboratory
Naval Underwater Systems Center
Department of the Navy
Newport, RI 02840
Attn: Technical Library

Commander
Naval Weapons Laboratory
Department of the Navy
Dahlgren, VA 22448
Attn: Library

Commander
Naval Command Control Communications
Laboratory Center
Department of the Navy
San Diego, CA 92152

Commander
Naval Ordnance Laboratory
Department of the Navy
White Oak
Silver Spring, MD 20910
Attn: Library
Acoustics Division

Officer-in-Charge
New London Laboratory
Naval Underwater Systems Center
New London, CT 06320
Attn: Technical Library
D. G. Browning
W. L. Konrad

Commanding Officer
Naval Coastal Systems Laboratory
Panama City, FL 32401

Commander
Naval Weapons Center
China Lake, CA 93555
Attn: Technical Library

Commanding Officer
Naval Air Development Center
Johnsville, Warminster, PA 18974
Attn: Library

Naval Academy
Annapolis, MD 21401
Attn: Library, Serials, and
Binding Department
Engineering Department
Prof. S. H. Burns

Superintendent
Naval Postgraduate School
Monterey, CA 93940
Attn: Technical Library
J. V. Sanders
H. Medwin
A. B. Coppens
A. I. Eller

(2) Commanding Officer
Army Research Office
Department of the Army
Box CM, Duke Station
Durham, NC 27706
Attn: Library

Commanding Officer
Department of the Army
Army Advanced Materials Concept Laboratory
2461 Eisenhower Avenue
Alexandria, VA 22314

Commanding Officer
Ballistic Research Laboratory
I. S. Aberdeen Research and Development
Center
Aberdeen Proving Ground, MD 21005
Attn: STEAP-TL,
(Technical Library Division)

Commanding Officer
Harry Diamond Laboratories
Connecticut Avenue and Van Nes Street
Washinton, DC 20438
Attn: Library

Director
National Science Foundation
1951 Constitution Avenue, NW
Washington, DC 20550
Attn: Engineering Sciences Division

NOaa Environmental Research Laboratories
Wave Propagation Laboratory
Boulder, CO 80302
Attn: Dr. F. F. Hall, Jr.

National Bureau of Standards
Department of Commerce
Washington, DC 20234
(2) Attn: Technical Library
Technical Reports Section

American Institute of Aeronautics and
Astronautics
1290 Avenue of the Americas
New York, NY 10019
Attn: Mr. John Newbauer,
Editor-in-Chief

Battelle Memorial Institute
505 King Avenue
Columbus, OH 43201
Attn: Defense Metals Information Center

Los Alamos Scientific Laboratory
P. O. Box 1665
Los Alamos, NM 87544
Attn: Report Library

Aeronautical Research Associates
of Princeton, Inc.
50 Washington Road
Princeton, NJ 08540

Advanced Technology Laboratories, Inc.
400 Jericho Turnpike
Jericho, NY 11753

The Martin Company
RIAS Division
1450 South Rolling Road
Baltimore, MD 21227
Attn: Dr. S. H. Maslen

North American Rockwell Corporation
Science Center/Aerospace and Systems Group
1049 Camino Dos Rios
Thousand Oaks, CA 91360
Attn: Dr. N. D. Malmuth

AMETEK/STRAZA
P. O. Box 666
El Cajon, CA 92022
Attn: Dr. J. C. Lockwood

Airesearch Manufacturing Co. of
Arizona
Sky Harbor Airport
402 S. 36th Street
Phoenix, AZ 85034
Attn: R. N. Tedrick

(2) Aerospace Corporation
P. O. Box 95085
Los Angeles, CA 90045
Attn: Library

Bolt, Beranek, and Newman, Inc.
50 Moulton Street
Cambridge, MA 02138
Attn: Dr. C. H. Allen

Mitre Corporation
Bedford, MA 02138
Attn: Library

Hydronautics, Inc.
Pindell School Road
Laurel, MD 20810

Stanford Research Institute
Menlo Park, CA 94025
Attn: Dr. G. M. Muller

Westinghouse Electric Corporation
Research and Development Center
Beulah Road
Pittsburg, PA 15235
Attn: Dr. F. H. Fenlon
J. B. Moreland

Department of Engineering Sciences
Harvard University
Cambridge, MA 02138
Attn: Professor B. Budiansky

Lincoln Laboratory
Massachusetts Institute of Technology
P. O. Box 73
Lexington, MA 02173
Attn: Library

Physics Department
Massachusetts Institute of Technology
Cambridge, MA 02139
Attn: Professor U. Ingard

Mechanical Engineering Department
Massachusetts Institute of Technology
Cambridge, MA 02139
Attn: Professor R. H. Lyon

Gas Dynamics Laboratory
Forrestal Research Center
Princeton University
Princeton, NJ 08540

Department of Engineering Mechanics
Virginia Polytechnic Institute and
State University
Blacksburg, VA 24061
Attn: Dr. D. P. Telionis

Department of Aeronautical Engineering
University of Notre Dame
Notre Dame, IN 46556

)epartment of Aeronautics and Astronautics
tanford University
tanford, CA 94305
ttn: Professor Nicholas J. Hoff

epartment of Mechanical Engineering
tanford University
tanford, CA 94305

epartment of Aerospace Engineering
and Applied Mechanics
olytechnic Institute of Brooklyn
oute 110
armingdale, NY 11735

epartment of Engineering and Applied
Science
alifornia Institute of Technology
asadena, CA 91109

ivision of Aeronautical Sciences
niversity of California
erkeley, CA 94720
ttn: Professor Maurice Holt

chool of Engineering
ase Western Reserve University
niversity Circle
leveland, OH 44106

ollege of Engineering
ornell University
thaca, NY 14850
ttn: Professor E. L. Resler
Professor R. Seabass

ornell Aeronautical Laboratory, Inc.
455 Genesee Street
P. O. Box 235
uffalo, NY 14221

Department of Mechanical and
Aerospace Engineering
Illinois Institute of Technology
Chicago, IL 60610

Department of Mechanical Engineering
Georgia Institute of Technology
Atlanta, GA 30332
Attn: Professor A. D. Pierce
Professor Novak Zuber

Department of Oceanography
University of Washington
Seattle, WA 98105
Attn: Professor William O. Criminale

Department of Aeronautical Engineering
Princeton University
Princeton, NJ 08540

Department of Mechanical and
Aerospace Engineering
Rutgers--The State University
New Brunswick, NJ 08903

Department of Aeronautics and Astronautics
Massachusetts Institute of Technology
Cambridge, MA 02139

Department of Meteorology
Massachusetts Institute of Technology
Cambridge, MA 02139
Attn: Professor Erik Mollo-Christensen

Department of Aeronautics and Astronautics
New York University
University Heights
Bronx, NY 10453

Department of Aerospace Engineering
Virginia Polytechnic Institute
and State University
Blacksburg, VA 24061
Attn: Dr. G. R. Inger
Dr. H. Nayfeh

Department of Mechanics
The Johns Hopkins University
Baltimore, MD 21218
Attn: Professor Carl Kaplan
Dr. Ho, Chih-ming

Department of Aerospace Engineering
University of Southern California
University Park
Los Angeles, CA 90007
Attn: Professor J. Laufer
Professor W. Chu

Department of Electrical Engineering
The University of Texas at Austin
Austin, TX 78712
Attn: Professor E. L. Hixson

Department of Mechanical Engineering
The University of Texas at Austin
Austin, TX 78712
Attn: A. J. Healey
R. L. Panton

Department of Physics
The University of Texas at Austin
Austin, TX 78712
Attn: Professor C. W. Horton, Sr.

Department of Civil Engineering
The University of Texas at Austin
Austin, TX 78712
Attn: Professor D. D. Reynolds

Department of Physics
Brown University
Providence, RI 02912
Attn: Professor R. T. Beyer
Professor P. J. Westervelt
Professor A. O. Williams, Jr.

Department of Mechanical Engineering
University of Houston
Houston, TX 77004
Attn: Professor B. D. Cook

Department of Physics
Kalamazoo College
Kalamazoo, MI 49001
Attn: Professor W. M. Wright

Department of Ocean Engineering
University of Rhode Island
Kingston, RI 02881
Attn: Professor M. B. Moffett

Department of Physics
University of Tennessee
Knoxsville, TN 37916
Attn: Professor M. A. Breazeale

Department of Physics
University of Vermont
Burlington, VT 05401
Attn: Professor W. L. Nyborg

Department of Physics
Anderson College
Anderson, IN 46011
Attn: Professor D. B. Cruikshank, Jr.

Department of Space Science
Rice University
Houston, TX 77001
Attn: Professor A. A. Few

Osaka University
Institute of Scientific and Industrial
Research
Yamadakami, Suita, Osaka
JAPAN
Attn: Dr. A. Nakamura

Department of Aerodynamics
Tel Aviv University
Tel Aviv, ISRAEL
Attn: Professor I. J. Wygnanski

Department of Aeronautical Engineering
Technion Research and Development
Foundation
Haifa, ISRAEL
Attn: Professor J. Rom

Hypersonic Laboratory
Von Kármán Institute for Fluid Dynamics
Rhode-Saint-Genese, BELGIUM
Attn: Dr. J. J. Ginoux

Institut de Mecanique Statistique
de la Turbulence
12, Avenue General Leclerc
13-Marseille (3e)-FRANCE
Attn: Professor A. Favre

Department of Mechanical Engineering
University of Toronto
Toronto, Ontario
CANADA
Attn: Professor D. S. Scott

Institute for Aerospace Studies
University of Toronto
Toronto 5, O
CANADA
Attn: Professor H. S. Ribner

Department of Electronic and
Electrical Engineering
University of Birmingham
P. O. Box 363
Birmingham B15 2TT, ENGLAND
Attn: Dr. H. O. Berktay
Professor D. G. Tucker

Department of Physics
Chelsea College
London, ENGLAND
Attn: Dr. R. W. B. Stephens

Department of Fluid Mechanics
Technical University of Denmark
DK-2800 Lyngby, DENMARK
Attn: Dr. L. Bjørnø

University of Bergen
Bergen
NORWAY
Attn: Professor S. Tjötta, Mathematics Dept.
Dr. H. Hobaek, Physics Dept.

Department of Engineering
Cambridge University
Trumpington Street
Cambridge CB2 1PZ
ENGLAND
Attn: Professor J. E. Ffowcs Williams

Defence Research Establishment Atlantic
Dartmouth, Nova Scotia
CANADA
Attn: H. M. Merklinger

Department of Theoretical Mechanics
University of Nottingham
University Park, Nottingham
ENGLAND
Attn: Dr. D. F. Parker

UNCLASSIFIED

SECURITY CLASSIFICATION OF THIS PAGE *(When Data Entered)*

REPORT DOCUMENTATION PAGE

READ INSTRUCTIONS BEFORE COMPLETING FORM

1. REPORT NUMBER: ARL-TR-73-23	2. GOVT ACCESSION NO.
3. RECIPIENT'S CATALOG NUMBER	
4. TITLE *(and Subtitle)*: PROPAGATION OF PLANE ACOUSTIC NOISE OF FINITE AMPLITUDE	5. TYPE OF REPORT & PERIOD COVERED: technical report
6. PERFORMING ORG. REPORT NUMBER	
7. AUTHOR(s): Frederick M. Pestorius	8. CONTRACT OR GRANT NUMBER(s): AFSOR F44620-71-C-0015; ONR N00014-70-A-0166 Task 0004
9. PERFORMING ORGANIZATION NAME AND ADDRESS: Applied Research Laboratories, The University of Texas at Austin, Austin, Texas 78712	10. PROGRAM ELEMENT, PROJECT, TASK AREA & WORK UNIT NUMBERS: 9781-02, 61102F, 681307
11. CONTROLLING OFFICE NAME AND ADDRESS: AFOSR, 1400 Wilson Blvd., Arlington, VA 22209; Office of Naval Research, Department of the Navy, Arlington, VA 22217	12. REPORT DATE: August 1973
	13. NUMBER OF PAGES: 238
	15. SECURITY CLASS. *(of this report)*
	15a. DECLASSIFICATION/DOWNGRADING SCHEDULE

16. DISTRIBUTION STATEMENT *(of this Report)*

Approved for public release; distribution unlimited.

17. DISTRIBUTION STATEMENT *(of the abstract entered in Block 20, if different from Report)*

18. SUPPLEMENTARY NOTES

19. KEY WORDS *(Continue on reverse side if necessary and identify by block number)*

Noise
High-intensity sound
Shock waves
Weak-shock theory
Distortion
Attenuation and dispersion
Computer algorithm

20. ABSTRACT *(Continue on reverse side if necessary and identify by block number)*

(U)Theoretical and experimental work on propagation of plane, finite-amplitude waves in air is reported. The emphasis is on finite-amplitude noise but periodic signals, mainly sawtooth waves, are also considered. The theoretical model is basically weak-shock theory, implemented by means of a computer algorithm and modified to take account of Kirchhoff tube wall attenuation and dispersion. Inclusion of tube wall effects was necessary because the experimental work was done in a pipe. The pipe was a 96 ft long, 2 in. i.d. (cont'd)

DD FORM 1 JAN 73 1473 EDITION OF 1 NOV 65 IS OBSOLETE S/N 0102-014-6601

UNCLASSIFIED

SECURITY CLASSIFICATION OF THIS PAGE *(When Data Entered)*

plane wave tube, terminated to prevent reflections. The horn driver source had a passband of roughly 500 to 3500 Hz and was capable of producing a sound pressure level of 160 dB (re 0.0002 μbar) in the central region of the passband. Asymmetrical sawtooth waves form when the source excitation is sinusoidal; the asymmetry is due to dispersion caused by the tube wall boundary layer. With regard to both waveform and decay of the sawtooth, excellent agreement is found between theory and experiment. Excellent agreement is also found when the source excitation is noise (initial bandwidth approximately equal to the passband of the horn driver). Distortion of the noise waveforms is qualitatively different, however. Because shocks form at irregular places in the waveform, their position in the waveform is not fixed. As they move they sweep up other shocks and minor irregularities in the waveform. Thus the noise waveform simplifies with increasing propagation distance. In terms of frequency, shock formation and waveform simplification give rise to a redistribution of energy, the high- and low-frequency parts of the spectrum growing at the expense of the middle.

APPLIED RESEARCH LABORATORIES

THE UNIVERSITY OF TEXAS AT AUSTIN